Intramuscular lipid droplets in type 2 diabetes and obesity: effects of exercise and training on subcellular distribution, morphology, and mitochondrial contact

de Almeida, Martin Eisemann

DOI:
10.21996/khw1-7d60

Publication date:
2023

Document version:
Final published version

SDU
Syddansk Universitet

The research unit of Muscle Physiology and Biomechanics,
Department of Sports Science and Clinical Biomechanics,
Faculty of Health Sciences, University of Southern Denmark

Steno Diabetes Center Odense, Odense University Hospital

PhD Thesis

Martin Eisemann de Almeida

Intramuscular lipid droplets in type 2 diabetes and obesity: effects of exercise and training on subcellular distribution, morphology, and mitochondrial contact

A dissertation submitted for the degree of Doctor of Philosophy

February 2023

Intramuscular lipid droplets in type 2 diabetes and obesity: effects of exercise and training on subcellular distribution, morphology, and mitochondrial contact

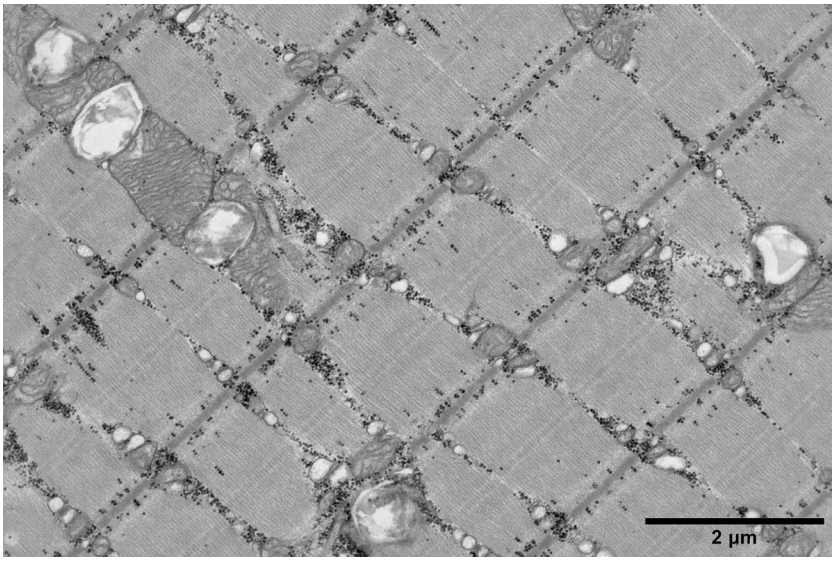

Supervisors

NIELS ØRTENBLAD (Main supervisor)
Professor, MSc, PhD
Department of Sports Science and Clinical Biomechanics
Faculty of Health Science
University of Southern Denmark
Odense, Denmark

KURT HØJLUND (Co-supervisor)
Professor, Dr.Med, PhD
Steno Diabetes Center Odense
Odense University Hospital
Odense, Denmark

Assessment committee

MICHAELA DEVRIES-ABOUD
Associate Professor
Department of Kinesiology and Health Sciences
University of Waterloo
Waterloo, Canada

LASSE GLIEMANN
Associate Professor
The August Krogh Section for Human Physiology
Department of Nutrition, Exercise and Sports
University of Copenhagen
Copenhagen, Denmark

ANDERS GRØNTVED (Chair)
Professor, MSc, PhD
Department of Sports Science and Clinical Biomechanics
Faculty of Health Science
University of Southern Denmark
Odense, Denmark

Papers

Study I
Petersen MH, **de Almeida ME**, Wentorf EK, Jensen K, Ørtenblad N & Højlund K. (2022). High-intensity interval training combining rowing and cycling efficiently improves insulin sensitivity, body composition and VO2max in men with obesity and type 2 diabetes. *Frontiers in Endocrinology* **13**, 1032235.

Study II
de Almeida ME, Nielsen J, Petersen MH, Wentorf EK, Pedersen NB, Jensen K, Højlund K & Ørtenblad N. (2023). Altered intramuscular network of lipid droplets and mitochondria in type 2 diabetes. *Am J Physiol Cell Physiol* **324**, C39-C57.

Study III
de Almeida ME, Ørtenblad N, Petersen MH, Schjerning ASN, Wentorf EK, Jensen K, Højlund K & Nielsen J. Acute exercise increases the contact between lipid droplets and mitochondria independently of obesity and type 2 diabetes. In Review, *J Physiol*, February 2023.

Funding

The work in this thesis was supported by grants from:

Region of Southern Denmark (19/37137)
Steno Diabetes Center Odense, which is funded by the Novo Nordisk Foundation
University of Southern Denmark
Novo Nordisk Foundation (NNF150C0015986)
Christenson-Cesons Family Fund
Sawmill Owner Jeppe Juhl and wife Ovita Juhl Memorial Fund

Acknowledgements

First, I would like to express my sincere gratitude to my principal supervisor Prof. **Niels Ørtenblad**. Thank you, Niels, for your effort in securing funding to start as a Ph.D. candidate, for endless hours of supervision, for constantly pushing me forward in Academia, and for showing interest in my life besides work. Niels, I am grateful for having been allowed to take the first steps as a researcher in an ambitious, emphatic, and inspiring research environment.

Thanks to my co-supervisor Prof. **Kurt Højlund** at the Steno Diabetes Center Odense (SDCO) for valuable feedback and for making this project possible. A special thanks to Assoc. Prof. **Joachim Nielsen** for introducing me to the world of stereology. I admire your curiosity and dedication to any aspect of scientific research. Together with Niels, you have provided invaluable support during this whole journey.

I want to thank everyone in the research unit of Muscle Physiology and Biomechanics (MoB) for inspiring scientific presentations and discussions and creating a friendly, helpful atmosphere and exciting social events. Thanks to fellow colleagues **Camilla Tvede Schytz** and **Rasmus Jensen** for sharing office, projects, and ups and downs.

My heartfelt thanks to Laboratory Technologists **Aleksandra Maria Rojek** and **Sandra Holm Riggelsen** at the Dept. of Pathology (OUH) for their excellent technical assistance in transmission electron microscopy. Also, a huge thanks to Laboratory Technologists **Lone Hansen** and **Charlotte Bøtchiær Olsen** at SDCO (OUH) for their work during the testing days. Thanks to former pre-graduate student **Ann-Sofie Nybøle Schjerning** and master student **Niklas Bigum Pedersen** for putting a massive effort into the stereological analyses.

Many thanks go to all collaborators for graciously sharing research materials and to co-authors for giving much help when I was preparing manuscripts for publication. Thanks to fellow colleague **Maria Houborg Petersen** for superb collaboration in this project. Also, thanks to my friend and former colleague, **Emil Kleis Wentorf**, for outstanding teamwork during our pre-graduate research year back in 2018, which provided the base for this Ph.D.

Last but not least, ultimate thanks to my family and friends. Although I have been largely absent for the past few years, you are still there for me. Thank you, mum **Charlotte**, dad **René**, and sisters **Linnea** and **Katrine**, for your unconditional love and faith in me. Because of you, my life has a meaningful purpose and a goal. **Stine**, no words can ever be strong enough to thank you. You have been on this journey with me since the beginning and never doubted my abilities, even when I did. I am amazed by the person you are and what I can accomplish because of you. Without you, I would not have made it this far.

ABSTRACT

In the skeletal muscle, the excessive storage of lipids, deposited as lipid droplets (LDs), has multiple detrimental effects on cellular functions and systems and is associated with the development of type 2 diabetes. However, LD morphology, subcellular distribution, and mitochondrial contact display a high level of heterogeneity, which may impede the current understanding of lipid-induced insulin resistance. By employing transmission electron microscopy (TEM), this thesis aimed to provide a comprehensive analysis to investigate intramuscular LDs and mitochondria and associations with insulin sensitivity in patients with type 2 diabetes and glucose-tolerant obese and lean controls. We further aimed to investigate the effects of 1) eight weeks of high-intensity interval training (HIIT) targeting major muscle groups and 2) 60 min acute exercise on the morphological characteristics of LDs.

In study I, insulin-stimulated glucose disposal rate (GDR), as assessed by the hyperinsulinemic-euglycemic clamp, was ~40% lower in the patients with type 2 diabetes than in the obese and lean controls at baseline. After HIIT, insulin-stimulated GDR increased by ~30–40% in all three groups, accompanied by a clinically relevant decrease in HbA1c (4 ± 2 mmol/mol) and fasting plasma glucose (1.0 ± 0.4 mmol/l) in patients with type 2 diabetes. HIIT also increased $\dot{V}O_2$max (~8–15%), decreased total fat mass, and increased lean body in all three groups. There were no correlations between these training adaptions nor group-specific differences in these responses.

In study II, the excess storage of intramuscular lipids in patients with type 2 diabetes was present as extremely large individual LDs situated in single muscle fibers poor of subsarcolemmal mitochondria. HIIT improved this intramuscular deficiency by redistributing LD size and subcellular distribution while increasing mitochondrial volumetric content. Morphological shape analysis further showed that individual LDs were better described as ellipsoids than spheres. Moreover, analysis of contact between LDs and mitochondria revealed an altered interaction between organelles in insulin-resistant conditions. However, there were no robust correlations between morphological LD analysis and insulin sensitivity.

In study III, acute exercise did not mediate changes in LD volumetric content, numerical density, or profile size. However, when evaluating the fraction of LDs touching mitochondria and the magnitude of inter-organelle contact, exercise increased the LD-mitochondrial contact irrespective of obesity or type 2 diabetes. This effect was profound in the subsarcolemmal region of type 1 fibers with an increased contact length from ~275 to ~420 nm. Interestingly, the absolute contact length before exercise (ranging from ~140 to ~430 nm) was positively associated with fat oxidation rates during exercise.

Together, results from study I, II, and III demonstrates that type 2 diabetes displays cellular heterogeneity in intramuscular LD storage, highlighting the relevance of single-cell modalities in clinical research. HIIT changed this muscle LD storage toward non-diabetic characteristics while efficiently improving insulin sensitivity with intact responses in all three groups. Although this is too early to state, our data further suggest that the increased contact between LDs and mitochondria with acute exercise is not disturbed in obesity or type 2 diabetes.

RESUMÉ IN DANISH

I skeletmuskulaturen lagres lipider som lipid dråber (LD) og en forøget mængde af disse har en række skadelige virkninger på cellulære funktioner og systemer, og er også forbundet med udviklingen af type 2 diabetes. LD'er er dog heterogene i deres morfologi, subcellulære lokalisering og kontakt med mitokondrier og tager man ikke højde for disse faktorer, kan det hæmme forståelsen af lipid-induceret insulin resistens. Ved anvendelse af transmission elektron mikroskopi (TEM), er formålet med denne afhandling at udføre en dybdegående analyse af de intramuskulære LD'er og mitokondrier og undersøge sammenhængen med insulinfølsomhed hos patienter med type 2 diabetes og glukosetolerante overvægtige og normalvægtige kontroller. Vi vil ligeledes undersøge effekterne af 1) otte ugers højintens intervaltræning (HIIT) målrettet flere muskelgrupper samt 2) 60 min akut arbejde på disse muskelspecifikke LD-karakteristika.

I studie I var den insulin-stimulerede glukoseoptagelse, som evalueret ved en hyperinsulin-euglykæmisk clamp, ~40% lavere hos patienterne med type 2 diabetes sammenlignet med de overvægtige og normalvægtige kontroller ved baseline. HIIT forbedrede den insulin-stimulerede glukoseoptagelse med ~30–40 % hos alle tre grupper, hvilket blev ledsaget af et klinisk relevant fald i både HbA1c (4 ± 2 mmol/mol) og fastende plasma glukose (1,0 ± 0,4 mmol/l) hos patienterne med type 2 diabetes. HIIT forbedrede også $\dot{V}O_2$max (~8–15%), reducerede fedtmassen og øgede den fedtfrie masse hos alle tre grupper. Vi fandt ingen sammenhænge mellem disse træningsadaptationer eller gruppeforskelle i ændringerne.

I studie II kunne nogle ekstremt store individuelle LD'er forklare den forøgede mængde af lipider hos patienterne med type 2 diabetes. Disse LD'er var lokaliseret i specifikke muskelfibre med et lavt indhold af subsarcolemmal mitokondrier. HIIT forbedrede disse intramuskulære forhold ved at redistribuere LD'ernes størrelse og subcellulære lokalisering, samtidig med at mitokondrie volumen også blev øget. En morfologisk analyse viste ydermere at LD'er bedre kunne beskrives som ellipsoider end kugleformede organeller. Desuden tydede vores data på, at patienterne med type 2 diabetes havde et ændret interaktionsforhold mellem LD'er og mitokondrier. Vi fandt dog ingen robuste korrelationer med insulinfølsomhed.

I studie III observerede vi ingen ændringer i volumen, antal eller størrelse af LD'er efter akut arbejde. På trods af dette, øgedes både andelen af LD'er som rører mitokondrierne og også den absolutte længde for fysisk kontakt mellem organellerne efter arbejde. Denne effekt var størst i subsarcolemmal regionen hos type 1 fibrene, hvor den absolutte kontaktlængde i gennemsnit øgedes fra ~275 til ~420 nm. Den absolutte kontaktlængde før arbejde (fra ~140 til ~430 nm) var ligeledes positivt forbundet med fedtoxidationshastigheder under arbejde.

Som konklusion viser resultater fra studie I, II og III at type 2 diabetes har cellulær heterogenitet i den intramuskulære LD-lagring, hvilket understreger betydningen af enkeltfiber teknologier i klinisk forskning. HIIT ændrede denne LD-lagring mod glukosetolerante forhold samtidig med at træningsformen også havde en effektiv virkning på insulinfølsomhed hos alle tre grupper. Selvom dette er tidligt at konkludere, tyder vores data ligeledes på, at den øgede LD-mitokondrie kontakt med akut arbejde ikke er påvirket af enten fedme eller type 2 diabetes.

Content

Abbreviations

ACSL	Long-chain acyl-CoA synthetase
ATGL	Adipose triglyceride lipase
BMI	Body mass index
CE_{est}	Coefficient of error in estimates
CHOox	Carbohydrate oxidation
CV_{group}	Group coefficient of variation
ECG	Electrocardiogram
FATmax	The relative exercise intensity (%$\dot{V}O_2$max) needed to elicit MFO
FATox	Fat oxidation
GDR	Glucose disposal rate
GIR	Glucose infusion rate
HE clamp	Hyperinsulinemic-euglycemic clamp
HIIT	High-intensity interval training
IPAQ–SF	International Physical Activity Questionnaire–Short Form
LD	Lipid droplet
MFO	Maximal fat oxidation rate
NEFA	Non-esterified fatty acids
NOX	Non-oxidative glucose metabolism
OGTT	Oral glucose tolerance test
PLIN	Perilipin
P:A ratio	Perimeter-to-area ratio
RER	Respiratory exchange ratio
TAG	Triacylglycerol
TEM	Transmission electron microscopy
WHR	Waist-to-hip ratio

01 Background

01.01 Introduction

Obesity and sedentary behavior are major risk factors contributing to the prevalence of severe metabolic diseases, including type 2 diabetes (Fletcher *et al.*, 2002). Type 2 diabetes is characterized by an inability to maintain glucose homeostasis due to an insulin deficiency and insulin resistance in several tissues, including the skeletal muscle (DeFronzo, 1988). The skeletal muscle is one of the largest tissues in the human body and serves as the predominant site for insulin-stimulated glucose uptake and is, therefore, essential for maintaining glucose homeostasis (DeFronzo *et al.*, 1981). However, it is well-known that excessive storage of lipids in the skeletal muscle, deposited as lipid droplets (LDs), is inversely associated with insulin action (Pan *et al.*, 1997; Krssak *et al.*, 1999). Furthermore, when intramuscular LD stores are changed with diet-induced weight loss or lipid infusions, concurrent alterations in insulin sensitivity are observed (Hoeks *et al.*, 2006; Toledo *et al.*, 2008), suggesting a causal relationship between LD content and insulin resistance.

LDs are not static energy stores but display a high heterogeneity in their morphology, subcellular localization, mitochondrial contact, and composition of LD-associated proteins, and exercise induces changes in these properties (Gemmink *et al.*, 2020). While recent studies suggest that big LDs stored in the subsarcolemmal region could be the reason for lipid-induced insulin resistance in type 2 diabetes (Nielsen *et al.*, 2017; Daemen *et al.*, 2018), there is an unmet need for more detailed investigations into the characteristics of LDs and how these are affected by exercise and training in glucose-tolerant individuals and patients with type 2 diabetes. In the skeletal muscle, thousands of fibers, organized in motor units, are non-uniformly recruited during muscle contractions (Heckman & Enoka, 2012). This diversity may correspond with a considerable variation in single-fiber characteristics of mitochondrial content and mechanical power outputs (Schiaffino & Reggiani, 2011). While the volumetric content of LDs and mitochondria is closely linked in healthy lean and active individuals (Hoppeler *et al.*, 1973), this might be disturbed in patients with type 2 diabetes, who, to a greater extent, accumulate LDs in glycolytic type 2 fibers expected to have low mitochondrial content (Daemen *et al.*, 2018; Koh *et al.*, 2018). As only some fibers may be affected, there needs to be more knowledge on how LDs accumulate at the single-fiber level.

Both acute and chronic aerobic exercise are well-established models to improve insulin sensitivity and glycemic control (O'Hagan *et al.*, 2013; Colberg *et al.*, 2016), often coinciding

with a remodeling of intramuscular LDs and mitochondria (Nielsen *et al.*, 2010; Devries *et al.*, 2013; Samjoo *et al.*, 2013; Li *et al.*, 2014; Koh *et al.*, 2018). High-intensity interval training (HIIT) has recently earned attention, demonstrating the same or even better effects on insulin sensitivity and glucose tolerance as compared with endurance training in healthy lean individuals (Robinson *et al.*, 2017; Søgaard *et al.*, 2018) and in obese individuals with and without type 2 diabetes (De Nardi *et al.*, 2018; Winding *et al.*, 2018; Ryan *et al.*, 2020). While these effects might be related to the high recruitment of all muscle fibers during HIIT (Gollnick *et al.*, 1973), a recent study suggests that activating several muscle groups is necessary to take full advantage of the insulin-sensitizing effects of exercise (Steenberg *et al.*, 2020). Thus, the combination of several exercise modalities in a HIIT protocol may enhance the favorable effects of exercise on insulin sensitivity and intramuscular LDs and mitochondria.

01.02 Lipid droplet biogenesis, growth, and degradation

Over the past decades, it has become clear that LDs are multifunctional organelles essential for cell metabolism with an active biogenesis and consumption cycle (Farese & Walther, 2009; Pol *et al.*, 2014; Wilfling *et al.*, 2014; Welte, 2015; Walther *et al.*, 2017). LDs are found in most eukaryotic cells, primarily in the cytoplasm, and span a wide range of sizes (diameter) from 0.1–5 µm in non-adipocytes while reaching 100 µm or above in white adipocytes. LDs specialize in storing neutral lipids (nonpolar, hydrophobic lipids), predominantly triacylglycerols (TAGs) and sterol esters, which serve as a reservoir for energy generation or membrane synthesis. A phospholipid monolayer surrounds these neutral lipids and comprises a composition of mainly phosphatidylcholine and phosphatidylethanolamine (Tauchi-Sato *et al.*, 2002), highly relevant for regulating LD size and interacting with other LDs or interacting with partner organelles such as the endoplasmic reticulum.

LDs can either form *de novo* or be derived from existing LDs by fission. It is believed that *de novo* formation occurs from the endoplasmic reticulum (Jacquier *et al.*, 2011; Jacquier *et al.*, 2013), where neutral lipids are synthesized (Buhman *et al.*, 2001), but knowledge of the precise mechanisms for this process is still unclear. Based on previous reviews (Pol *et al.*, 2014; Wilfling *et al.*, 2014; Walther *et al.*, 2017), the process of LD formation can be described in three discrete stages (**Figure 1**): (1) Neutral lipids are synthesized in the endoplasmic reticulum and accumulate within the bilayer. Essentially, TAGs generate by an elaborate biosynthetic pathway whose final step is catalyzed by diacylglycerol acyltransferases DGAT1 and DGAT2, converting diacylglycerol (DAG) and fatty acids into TAGs. (2) Neutral lipids accumulate between leaflets of the endoplasmic reticulum, and as the concentration rises, lipid lenses will form. (3) Above a certain size, dependent on the neutral lipids and phospholipid composition, a nascent LD will form and either remain attached to the endoplasmic reticulum or be unstable and separate (budding).

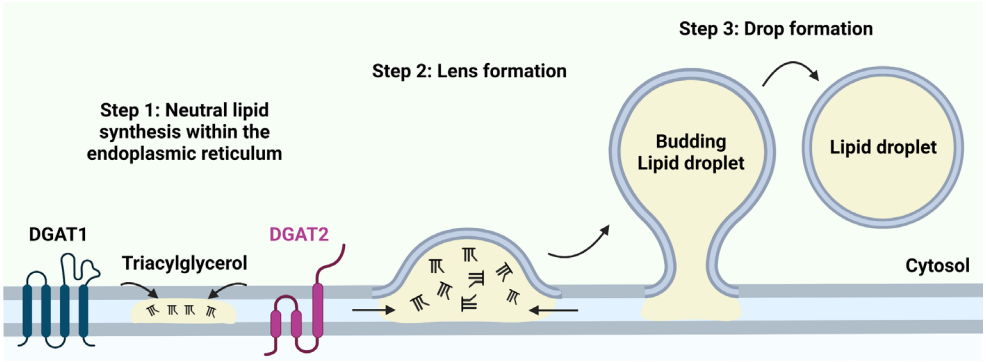

Figure 1. Lipid droplets form in three steps, from synthesizing neutral lipids within the endoplasmic reticulum to a nascent lipid droplet bud into the cytoplasm. The figure was designed using BioRender.

Nascent LDs are relatively small compared with the large LDs seen in various cells, indicative of LD growth. LD growth occurs via the local synthesis of TAGs at the LD surface or the fusion of smaller LDs through permeation or coalescence processes (Pol *et al.*, 2014; Wilfling *et al.*, 2014; Walther *et al.*, 2017). Local droplet growth requires a cellular trafficking pathway that delivers the enzymes for TAG synthesis to the LDs. On the LD surface, coatamer (COP)-I proteins act by removing phospholipids, which increases LD surface tension and facilitates interaction with the endoplasmic reticulum. Once connected, TAG synthesis enzymes re-localize to the LD surface to produce TAG locally, which, in turn, triggers the growth of LDs. Regarding fusion processes, LDs can grow via a ripening process called permeation, where neutral lipids transfer from a smaller LD to an adjacent larger LD. Under certain conditions, when phosphatidylcholine is limited, and the surface tension is high, large LDs can grow by coalescence/fusion of two or more LDs.

Lipids in LDs are released when demands exist to produce energy or synthesize membranes (Farese & Walther, 2009). This process is known as lipolysis, which is the mobilization of individual fatty acyl chains sequentially cleaved from the glycerol backbone of TAGs by a string of lipases such as adipose triglyceride lipase (ATGL), hormone sensitive lipase (HSL), and monoacylglycerol lipase (MGL). On the other hand, macroautophagy has also been shown to mediate the degradation of LDs. Under this process, LDs are engulfed whole or partially (autophagosomes) and transported to lysosomes, which contain acidic lipases that will assist in releasing fatty acids from TAGs. In post-absorptive healthy male individuals, the turnover of intramuscular LD stores is a fast process, taking about 29 hours (Sacchetti *et al.*, 2004). During resting, ~50% of the fatty acids taken up by the skeletal muscle from the circulation are esterified into TAGs, presumably as LDs (Sacchetti *et al.*, 2002). However, this number decreases during muscle contractions as more fatty acids are oxidized.

LDs at different stages of formation, growth, and degradation seem diverse in number, size, and composition (Thiam & Beller, 2017). In epithelial cells (CHO K2), subgroup fractioning of LDs into various size categories recently demonstrated that larger LDs were connected with the endoplasmic reticulum while smaller LDs were not, suggesting that the morphology of individual LDs may be related to differential functions (Zhang *et al.*, 2016).

01.03 Comparison of assessment methods for intramuscular lipid droplets

Various techniques exist for assessing intramuscular LDs, including biochemical extraction and quantification, magnetic resonance spectroscopy (^{1}H-MRS), and the imaging techniques such as transmission electron microscopy (TEM) and light microscopy combined with histochemical staining of lipids. While ^{1}H-MRS is non-invasive, biochemical extraction and imaging techniques require the sampling of muscle biopsies. In general, biochemical analysis quantifies freed fatty acids or glycerol from the hydrolysis of TAGs extracted from freeze-dried muscle specimens. In the histochemical analysis, thinly sectioned muscle specimens are stained with the lipid-target antibodies BODIBY 493/503 or Oil Red O before visualization in a fluorescence microscope, often combined with stains targeting myosin heavy chains or specific proteins involved in lipid metabolism. In contrast, TEM visualizes LDs and other organelles in chemically fixed ultra-thin muscle sections. Finally, ^{1}H-MRS measures lipid content in the skeletal muscle by differentiating the resonance frequency of intramuscular LDs from frequencies of adipocytes and intermuscular lipids. This latter method can be conducted at the same site and repeated over time without discomfort to the participant. While biochemical analysis correlates poorly with the other methods, there are solid correlations between ^{1}H-MRS and TEM in assessing intramuscular lipid content (Howald *et al.*, 2002; De Bock *et al.*, 2007).

Studies are debating the suitability of these techniques to discriminate between intra- and intermuscular lipid pools (Watt *et al.*, 2002; Kiens, 2006). Especially the biochemical analysis has been criticized for having a high variability (Wendling *et al.*, 1996), potentially ascribed to the invisible contamination of the muscle fibers with intermuscular lipids. Since the TAG content in adipocytes is enormous compared with the content inside the muscle fibers, contamination with a few adipocytes will greatly influence TAG measurements in muscle tissue. While this might not be a problem in muscle samples from healthy young participants displaying infrequent intermuscular lipid storage (van Loon, 2004), caution must be taken when working with muscle samples from patients with obesity and type 2 diabetes. Studies using ^{1}H-MRS or imaging techniques do not have this contamination issue with intermuscular lipids. Furthermore, imaging techniques can perform fiber-type specific analysis of LDs, albeit the results are considered semi-quantitative.

In ultrastructural TEM investigations of the muscle cell, lipids, compared to those found in membranes, appear as LDs composed of a neutral lipid core and a phospholipid monolayer (Tauchi-Sato *et al.*, 2002). Generally, intramuscular LDs appear as white-greyish circular organelles with a fuzzy border (Fujimoto & Parton, 2011) and are often found close to mitochondria (Hoppeler, 1999; Shaw *et al.*, 2008). Especially Hans Hoppeler and his group at the University of Bern in Switzerland pioneered the stereological analysis of skeletal muscle ultrastructure using TEM. One of the earliest publications of detailed cross-sectional morphometry in human skeletal muscle is dated 1973 (Hoppeler *et al.*, 1973). The group followed with a series of studies exploring the effects of acute and chronic exercise training on these ultrastructural aspects (Hoppeler *et al.*, 1985; Howald *et al.*, 1985; Kayar *et al.*, 1986; Suter *et al.*, 1995).

01.04 Subcellular distribution of lipid droplets and mitochondria

LDs and mitochondria are located in two subcellular regions: (1) the subsarcolemmal region, which is the space just beneath the plasma membrane (sarcolemma) where other organelles such as Golgi apparatus and nuclei are found, and (2) the intermyofibrillar region, which is the space between myofibrils and close to the sarcoplasmic reticulum. In healthy individuals, intermyofibrillar LDs and mitochondria contribute to ~80% of total stores. However, the relative distribution of LDs and mitochondria depends on fiber types, training status, and disease state. Importantly, in tissues like the skeletal muscle, where structures are orderly and tightly arranged in a limited volume, energy metabolism might be compartmentalized to overcome macromolecular overcrowding and hampered substrate diffusions (Ovadi & Saks, 2004; Saks *et al.*, 2008). Thus, LDs and mitochondria located in the subsarcolemmal or intermyofibrillar regions may have differential roles in skeletal muscle cells due to the inter-region distance *per se*. Besides subcellular localization, lipid metabolism also depends on fiber type-specific localization of LDs.

01.05 Insulin-stimulated glucose uptake in skeletal muscle

The translocation of GLUT4-containing vesicles to the cell surface is activated when circulating insulin binds to the insulin receptor located in the plasma membrane (**Figure 2**). After the binding of insulin to the extracellular α-subunit of the receptor, it undergoes a conformational change resulting in autophosphorylation of the intracellular β-subunit, which, in turn, increases the tyrosine kinase activity of the receptor (Lee & Pilch, 1994). Muscle-specific knockout of the insulin receptor is shown to ultimately compromise insulin-stimulated glucose uptake (Wojtaszewski *et al.*, 1999), underlining the crucial role of the insulin receptor in insulin signaling. Increased tyrosine kinase activity recruits and phosphorylates the key

insulin receptor substrate 1 (IRS1) (Yamauchi *et al.*, 1996; Higaki *et al.*, 1999). Upon tyrosine phosphorylation, IRS1 acts as a docking site for signaling molecules having an Src-homology-2 (SH2) domain. This process involves the p85 regulatory subunit of phosphoinositide 3-kinase (P13K) (Myers *et al.*, 1992). Once activated, the catalytic subunit of P13K, p110, catalyzes the synthesis of phosphatidylinositol 3,4,5-triphosphate (PIP3) from phosphatidylinositol 4,5-biphosphate (PIP2) (Leto & Saltiel, 2012). PIP3 acts as a docking site for the pleckstrin-homology activation loops of serine/threonine kinases, including phosphoinositide-dependent kinase-1 (PDK1) and Akt (previously known as PKB). PDK1 phosphorylates Akt on the site of Thr308, while mTORC2 phosphorylates the site of Ser473 (Alessi *et al.*, 1997; Sarbassov *et al.*, 2005).

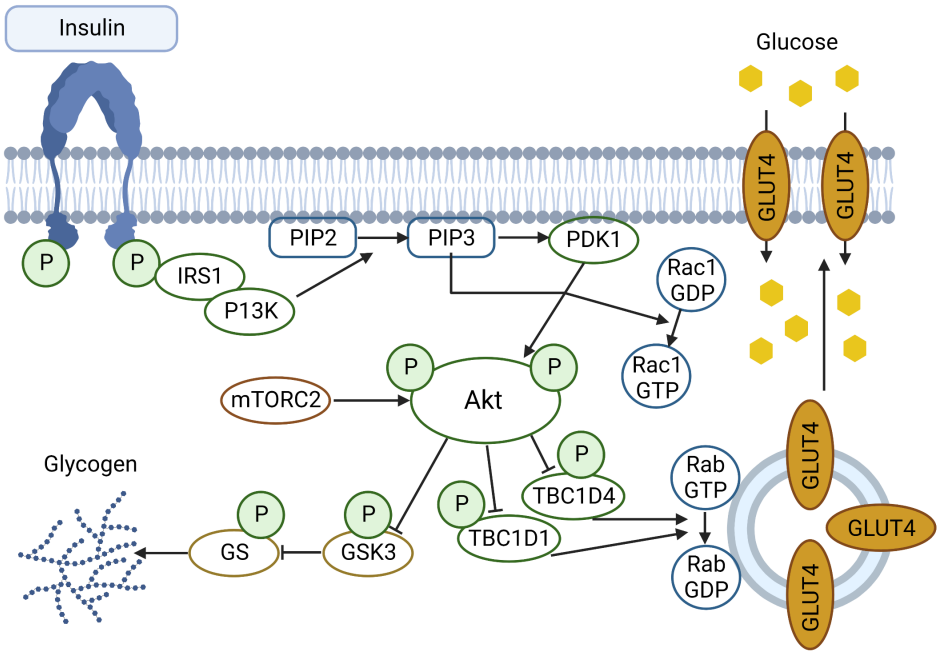

Figure 2. Overview of the insulin signaling resulting in GLUT4 translocation. When insulin binds to its receptor, it initiates a signaling cascade leading to the translocation of GLUT4-containing vesicles to the plasma membrane. As a result, GLUT4 transporters fuse with the membrane, and glucose is transported into the muscle cell. The figure was designed using BioRender.

Akt has multiple downstream targets involved in various cellular processes. Glycogen synthase kinase 3 (GSK3) was the first identified target for Akt (Cross *et al.*, 1995). In response to insulin stimulation, the Akt-mediated phosphorylation (and inactivation) of GSK3

increases glycogen synthase (GS) activity and thereby enhances glycogen synthesis. Akt is further suggested to regulate various proteins involved in GLUT4 translocation, including the Rab-GTPase activating proteins TBC1D4 and TBC1D1 (Sakamoto & Holman, 2008). TBC1D4 comprises a GAP (GTPase activating protein) domain, which converts GTP to GDP under basal states, inhibiting GLUT4-containing vesicles. Thus, under insulin stimulation, Akt phosphorylates (and inactivates) TBC1D4 and, as a result, GTP is not converted to GDP, promoting GLUT4-vesicle translocation to the plasma membrane. Another pathway by which insulin stimulates GLUT4-vesicle translocation is through Rac1. Rac1 is a Rho GTPase that is activated (GTP-bound) in response to insulin (Sylow *et al.*, 2013). In incubated mouse muscles with P13K, Rac1, and Akt inhibitors, Sylow and colleagues demonstrated that Rac1, and not Akt, was a downstream target for P13K (Sylow *et al.*, 2014). Furthermore, when muscles were incubated with both Rac1 and Akt inhibitors, insulin-stimulated glucose uptake was blunted, suggesting the roles of Akt and Rac1 signaling in insulin-stimulated glucose uptake.

01.06 Lipid droplets and insulin sensitivity

Although various studies have reported that elevated levels of intramuscular lipid content are negatively associated with insulin sensitivity, this proposed relationship is inconclusive as neither causality has been shown (Pan *et al.*, 1997; Krssak *et al.*, 1999) nor does it extend to endurance-trained individuals who also store increased levels of lipids despite being markedly insulin sensitive (Goodpaster *et al.*, 2001; van Loon *et al.*, 2004). This phenomenon is known as the athlete's paradox, indicating that other factors than lipid content *per se* may be responsible for the compromised insulin action in insulin-resistant conditions. While little is still known, we and others have shown that big LDs stored in the subsarcolemmal region could be the reason for lipid-induced insulin resistance (Nielsen *et al.*, 2010; Nielsen *et al.*, 2017; Daemen *et al.*, 2018). In addition, recent insight into the subtype specificity of bioactive lipids suggests a role for subsarcolemmal ceramides, specifically the C16 and C18 chain lengths, in insulin resistance (Chung *et al.*, 2017; Perreault *et al.*, 2018; Bergman & Goodpaster, 2020). Nevertheless, much more research is warranted to elucidate the role of LD morphology and subcellular localization in muscle insulin sensitivity.

02 Aim and hypothesis

Using quantitative TEM, this thesis aimed to investigate LDs and mitochondria, and the relation to insulin sensitivity, in the skeletal muscle of overweight-to-obese patients with type 2 diabetes and glucose-tolerant overweight-to-obese and lean controls. We also aimed to investigate the effects of exercise and training in these participants.

02.01 Objectives of the studies

Study I

This study aimed to investigate the effects of HIIT on insulin sensitivity, as determined by the hyperinsulinemic-euglycemic clamp, $\dot{V}O_2max$, body composition, glycemic control, and substrate oxidation in overweight-to-obese patients with type 2 diabetes, and whether these effects are attenuated, as compared with glucose-tolerant overweight-to-obese and lean controls.

Study II

This study aimed to provide a comprehensive single-fiber analysis of intramuscular LDs and mitochondria in overweight-to-obese patients with type 2 diabetes and glucose-tolerant overweight-to-obese and lean controls. The study also aimed to investigate the effects of HIIT on these muscle properties. We hypothesized that patients with type 2 diabetes display larger intramuscular LDs and deficient mitochondrial networks, specifically in the subsarcolemmal region of type 2 fibers. Furthermore, we hypothesized that HIIT would improve these properties.

Study III

This study aimed to investigate changes in LD volume fractions, morphology, subcellular distribution, and contact with mitochondria in overweight-to-obese patients with type 2 diabetes and glucose-tolerant overweight-to-obese and lean controls in response to 1-hour ergometer cycling. We hypothesized that acute exercise would utilize intramuscular LDs, specifically in the intermyofibrillar space of lean controls, with reduced net changes in the overweight-to-obese groups. We further hypothesize that contact between LDs and mitochondria would 1) reflect the exercise-mediated decrease in intramuscular LDs in the lean controls and 2) be compromised in the overweight-to-obese groups during exercise.

03 Methodology

03.01 Research ethics and data protection

The study was approved by the Regional Committees on Health Research Ethics for Southern Denmark (Project ID: S-20170142) and conducted following the principles outlined in the Declaration of Helsinki II. The participants were fully informed about the study and any potential risks or discomfort associated with the experiments before giving written informed consent, which they could freely withdraw from at any time during the study. REDCap, a secure web-based database hosted by Odense Patient Data Explorative Network (OPEN), was used to store and manage research data. Storage of personal and sensitive data, trial material, and case report forms were treated in accordance with the general guidelines and rules set by the Danish Data Protection Agency (Journal No.: 17/31977).

03.02 Study population

Middle-aged (40–65 years) overweight to obese (BMI 27–36) males with type 2 diabetes (n=15) and glucose-tolerant overweight to obese (BMI 27–36; n=15) and lean (BMI 27–36; n=18) males were included in this study (**Table 3**). All participants were Caucasian, non-smokers, and matched according to age, while the obese participants with and without type 2 diabetes were matched according to BMI. In addition, the physical activity level for the participants had to be low (defined as <2 hours of moderate activity per week) as evaluated by the International Physical Activity Questionnaire–Short Form (IPAQ–SF). Patients with type 2 diabetes were all GAD65-antibody negative, had no signs of micro- or macrovascular complications, except for one with mild retinopathy, and were treated with anti-diabetic medications: metformin (n=14), DPP4-inhibitors (n=4) and sulphonylureas (n=1), either as a monotherapy (n=11) or a two-drug combination (n=4). Most of the participants with type 2 diabetes were also treated with cholesterol-lowering (n=11) and antihypertensive (n=12) medication. The lean and obese controls had normal glucose tolerance, as evaluated by a 75 g oral glucose tolerance test (OGTT), no family record of diabetes, and were not taking any medications. All participants had normal blood test screening for renal, hepatic, and hematological function and normal resting electrocardiogram (ECG).

03.03 Experimental protocol

Recruitment, intervention, and experimental testing took place at the Department of Sports Science and Clinical Biomechanics, University of Southern Denmark (SDU), and Steno Diabetes Center Odense (SDCO), Odense University Hospital (OUH), in the period from January 2018 and December 2019. The participants reported to the laboratory on three experimental days (Day 1, 2, and 3), separated by at least 48 hours (**Fig. 3**). Day 1 and 2 were repeated after eight weeks of HIIT, while Day 3 (Acute exercise test) was performed only once as a separate study. On experimental days, participants arrived at the laboratory facilities at 7:30 AM after 12 hours of overnight fasting while refraining from caffeine and alcohol for at least 24 hours and physically demanding activities (e.g., bicycling, jogging, gardening) for at least 48 hours. In addition, patients with type 2 diabetes were instructed to withdraw from taking any medications (anti-diabetic, cholesterol-lowering, and anti-hypertensive) for one week prior to the experimental days and then resume. The participants were instructed to eat a meal of similar size in the two evenings before Day 3.

On Experimental Day 1, total body weight and body composition were determined by Dual-energy X-ray Absorptiometry (DXA) scans (Prodigy Advance, GE Healthcare, Chicago, US), followed by assessments of substrate oxidation rates and maximal oxygen uptake ($\dot{V}O_2max$) during a graded exercise test. Approximately two hours before the start of the exercise test, the participants consumed a standardized mixed breakfast meal (64% carbohydrate, 22% fat, and 14% protein) consisting of oatmeal (2.4 kcal/kg body weight), almonds (1.3 kcal/kg body weight), skimmed milk (0.9 kcal/kg body weight), and apple juice (1.4 kcal/kg body weight).

On Experimental Day 2, a resting skeletal muscle biopsy was taken in the m. vastus lateralis before assessing insulin sensitivity by a three-hour hyperinsulinemic-euglycemic clamp (HE clamp) combined with indirect calorimetry measurements. At baseline, biochemical blood samples were drawn and analyzed for plasma glucose, HbA1c, serum insulin, C-peptides, and lipids. the participants were instructed to eat a meal of similar size and macronutrient content in the evenings before pre and post testing.

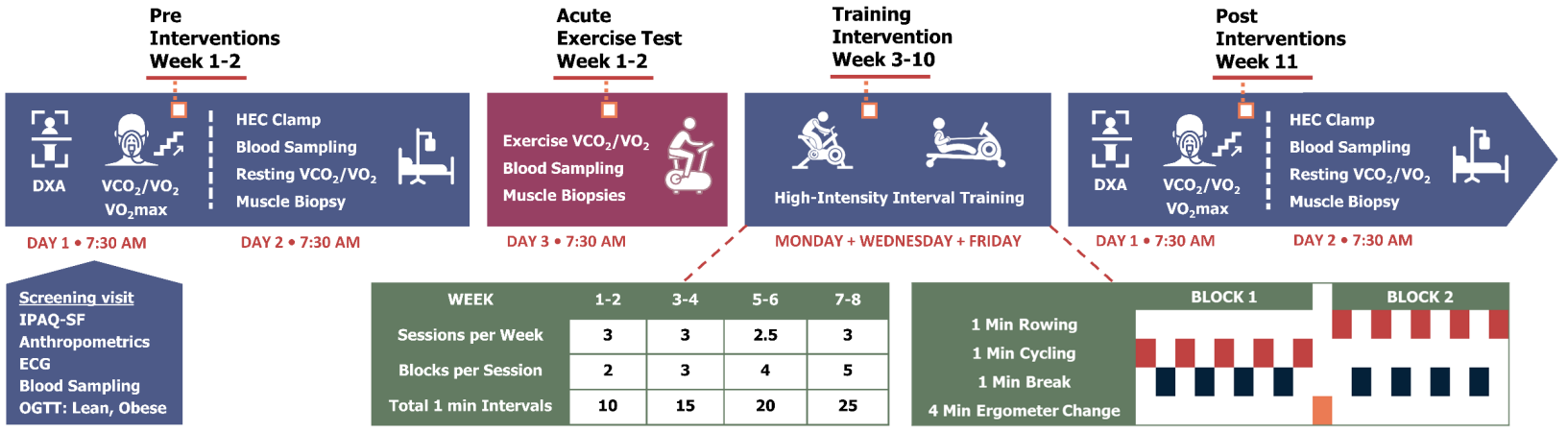

Figure 3. Experimental protocol. DXA, Dual-energy X-ray Absorptiometry; HEC, hyperinsulinemic-euglycemic clamp; IPAQ-SF, International Physical Activity Questionnaire Short Form; ECG, electrocardiogram; OGTT, oral glucose tolerance test.

.

03.03.01 Deviations from the protocol

Some participants from the original cohort (patients with type 2 diabetes: n=15, obese controls: n=15, and lean controls: n=18) were excluded from the eligible studies (I–III):

In studies I and II, four participants did not complete the intervention: one lean control and two lean patients with type 2 diabetes withdrew their consent to continue training due to lack of time, and one lean control never started training because of a knee injury. The baseline characteristics of the four participants were included in the analysis. Furthermore, in study II, pre- training samples from three lean controls, one obese control, and one patient with type 2 diabetes were missing due to a technical mistake during the fixation procedure of biopsies. These five participants were excluded from this study. Thus, Study I ended up with patients with type 2 diabetes (Pre: n=15; Post: n=13), obese controls (Pre and Post: n=15), and lean controls (Pre: n=18; Post: n=16). Study II ended up with patients with type 2 diabetes (Pre: n=14; Post: n=12), obese controls (Pre and Post: n=14), and lean controls (Pre: n=15; Post: n=13).

In study III, two lean controls never started the acute exercise test: one withdrew consent due to a lack of time, while another had a knee injury. Furthermore, pre- and post-exercise samples from three lean controls, one obese control, and one patient with type 2 diabetes were lost due to a technical mistake during the fixation procedure of muscle biopsies. Additionally, two lean controls, two obese controls, and three patients with type 2 diabetes declined to have biopsies taken. Finally, one lean and two obese controls did not manage to perform the exercise with a constant intensity, and two participants from each group could not be matched (matching is described in the Acute exercise test section). These participants were excluded from this study, and the analysis ended up with patients with type 2 diabetes (n=9), obese controls (n=8), and lean controls (n=8).

03.04 Acute exercise test (Study III)

The participants performed a 60 min acute submaximal exercise test on a cycle ergometer (Monark 828E, Monark Exercise, SE) (**Fig. 4**). Participants were familiarized with the equipment and rested for 30 min in a supine position before testing. Indirect calorimetry (Jaeger Oxycon Pro, Viasys Healthcare GmbH, Höchberg, DE) and heart rate (Polar T31, Polar Electro, Kempele, FI) was measured continuously during the test. Data from min 6-60 was used in the analysis. A paired design ensured equal exercise intensities in matched triplets or twins (**Fig. 26A**). Criteria for matched pairs were a variation of ≤ 3%-point in average %$\dot{V}O_2$max and ≤ 9%-point in average %HRmax during the 60 min exercise. On average, the matched pairs exercised at an intensity of 62% (range: 51 to 75%) of $\dot{V}O_2$max and 73% (range: 63 to 84%) of HRmax. We calculated energy expenditure (kJ/min) using the equation

by Weir (1949) ($total\ kcal = 3.941 \cdot \dot{V}O_2 + 1.11 \cdot \dot{V}CO_2$) and rates of fat and carbohydrate oxidation (FATox and CHOox, g/min) using the stoichiometric equations by Frayn (1983), assuming that the urinary nitrogen excretion was negligible. A muscle biopsy was taken in the m. vastus lateralis at baseline (pre) and immediately after (post) the 60 min exercise test, while blood samples were drawn and analyzed for plasma glucose and lactate at baseline, midway (30 min), and post the test.

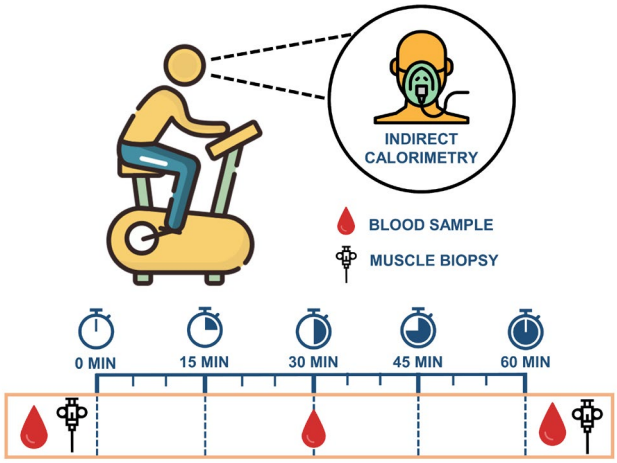

Figure 4. Schematics of the 60 min acute exercise test protocol, including measurements of indirect calorimetry and timed collections of blood samples and muscle biopsies. The figure was designed using resources from Flaticon.com.

03.05 Training intervention (Study I and II)

The training intervention consisted of eight weeks, three sessions per week, of supervised HIIT combining rowing (Concept 2 Model E, Vermont, US) and cycling (WattBike Pro/Trainer, Nottingham, UK) ergometry (**Fig. 5**). During the 24 sessions (23 HIIT sessions and one midway test), there was a progression in the training volume. Participants from the three groups trained together in one group of up to ten participants with a continuous run-in and completion. Most of the HIIT sessions (>95%) occurred in the afternoon between 4:00 pm and 6:00 pm. Each HIIT session began with a 10-min warm-up involving technique fundamentals in rowing and increasing workload. The HIIT protocol then consisted of HIIT blocks, each comprised of 5 × 1-min intervals interspersed by a 1-min break. Between HIIT blocks, participants had a 4-min break in which they changed between ergometers (i.e., from rowing to cycling or vice versa). Starting ergometer changed from session to session. The amount of HIIT blocks per session gradually increased by adding an extra HIIT block after every second week completed, progressing from two HIIT blocks per session in *weeks 1* and *2* to a total of five HIIT blocks per session in *weeks 7* and *8*. Cycling intervals were carried out at 100–110% maximal cycling capacity (MCC), while the obtained heart rate (86–88% of max)

was similar during rowing and cycling. MCC was reassessed at the beginning of week 5 to maintain the relative workload throughout the eight weeks of training. Before each session, we calibrated rowing ergometers with a drag factor of 105–110 (numerical value describing the rate at which the flywheel is decelerating). Participants were given continuous feedback during the HIIT sessions to achieve a mean power output supramaximal to their measured MCC. Participants were further encouraged by social engagement, supervisor feedback, high-energy music, and awareness of concurrent relative heart rate (Polar H7, Polar Team, Kempele, FI). Energy expenditure (kJ) was calculated from the obtained watts during exercise and gross mechanical efficiency (22.1% on Wattbike and 18.1% on Concept 2), based on Lindenthaler *et al.* (2018).

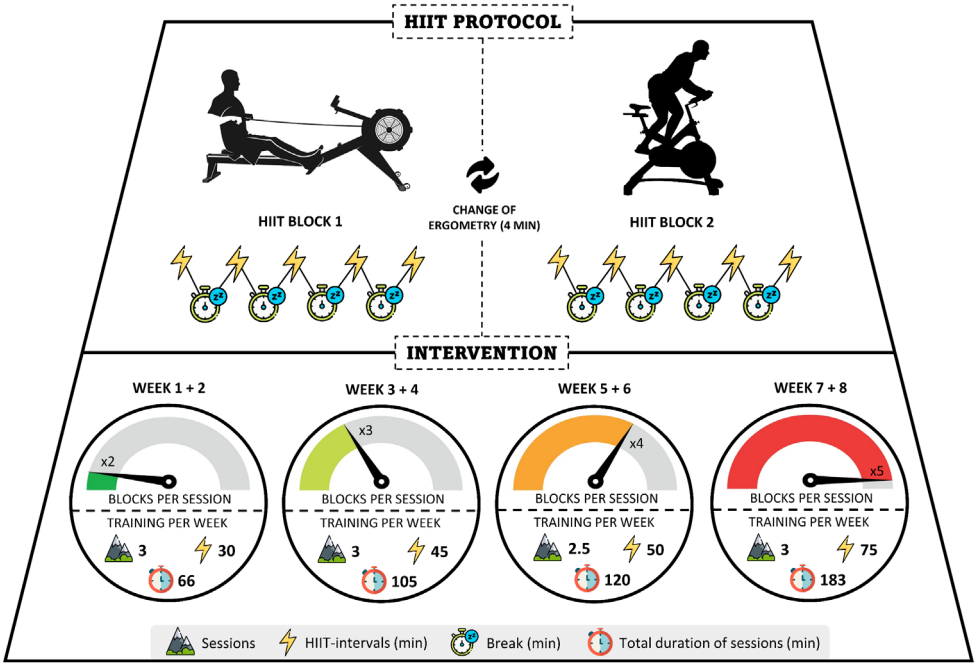

Figure 5. Schematic overview of the high-intensity interval training (HIIT) protocol. Over the eight weeks intervention, a total of 23 sessions were performed as combined rowing and cycling on ergometers. The HIIT protocol consisted of HIIT blocks, each comprised of 5 × 1-min intervals interspersed by a 1-min break. Between blocks, subjects shifted from rowing to cycling (4-min ergometer change) or vice versa. Blocks per session gradually increased with an extra block added after every second week done Thus, HIIT intervals increased from 30 to 75 × 1 min per week while total workout time increased from 66 to 183 min per week. The figure was designed using resources from Flaticon.com, Kpdmedia (no. 250221461), grate_art (no. 478415214), and Hary (no. 317299591) from stock.adobe.com.

03.06 Method details

03.06.01 Graded exercise test

The graded exercise test was adopted from earlier described and validated protocols (Achten *et al.*, 2002; Venables *et al.*, 2005) with some modifications for participants with low physical fitness. Testing was conducted on an electromagnetically braked cycle ergometer (SRM Ergometer System, SRM GmbH, Jülich, DE) with adjustable saddle and handlebars. Participants used the hyperbolic ergometer mode to determine their optimum, individual cadence at specific workloads. Respiratory gas exchange ($\dot{V}O_2$ and $\dot{V}CO_2$) was monitored in 10 s averages throughout the test using a mixing chamber cardiopulmonary exercise analyzer (Oxigraf O2CPX, California, US), which was warmed up for one hour before testing. O_2 and CO_2 analyzers were calibrated immediately before testing using a two-point calibration with two high-precision ($\pm$0.03% accuracy) certified gas mixtures from Air Liquid Danmark A/S (Taastrup, DK) and Strandmøllen A/S (Ejby, DK). Pneumotach (the flow rate of gases during breathing) was calibrated using a 3-liter spirometer syringe (Hans Rudolph, inc., Kansas, US) in a five-pump series. Participants wore a mouthpiece and nose-clip while heart rate was monitored (Polar H7, Polar, Kempele, FI).

The exercise protocol started with an initial workload of 40/60 watts and was increased every fourth min by 20 watts until the respiratory exchange ratio (RER: $\dot{V}CO_2/\dot{V}O_2$) reached 1.0. Following a 5-min break, the workload was lowered by 20 watts and followed by increments every min until volitional exhaustion. $\dot{V}O_2$max was reached when at least two of the following three criteria were achieved: 1) plateau in $\dot{V}O_2$ (increment of <2.1 mL/kg/min) despite further increases in workload (Taylor *et al.*, 1955), 2) RER >1.1, and 3) blood lactate levels >8.0 mmol/L as measured 2 min post-exercise (Lactate Scout+, EKF Diagnostics, Wales, UK). $\dot{V}O_2$max was not reached on two occasions. In these participants, testing was repeated 4–6 days after the original test.

Estimation of substrate oxidation curves

For each participant, raw data for $\dot{V}O_2$ and $\dot{V}CO_2$ (L/min) were averaged over the final 60 sec of each 4–min exercise increment. FATox and CHOox (g/min) were calculated using the equations by Frayn (1983), with the assumption that the urinary excretion was negligible:

$$FATox\ \left(\frac{g}{min}\right) = 1.67 \cdot \dot{V}O_2\ \left(\frac{L}{min}\right) - 1.67 \cdot \dot{V}CO_2 \left(\frac{L}{min}\right)$$

$$CHOox\ \left(\frac{g}{min}\right) = 4.55 \cdot \dot{V}CO_2\ \left(\frac{L}{min}\right) - 3.21 \cdot \dot{V}O_2 \left(\frac{L}{min}\right)$$

The calculated values for FATox and CHOox were plotted graphically as a function of exercise intensity, expressed in absolute (watt) and relative (%$\dot{V}O_2$max) terms, to construct a 2nd polynomial curve ($y = ax^2 + bx + c$). The constants a, b, and c were extracted from a curve-fitting analysis and used to determine the relative exercise intensity ($FATmax = \%\dot{V}O_2max = x = \frac{-b}{2a}$) needed to elicit the maximal fat oxidation rate ($MFO = \frac{g}{min} = y = -0.25\left(\frac{b^2}{a}\right) + c$). FATox and CHOox during specific absolute (20, 100, 160, and 220 watts) and relative (20, 40, 60, and 80 % $\dot{V}O_2$max) intensities were used in the statistical analysis to evaluate group differences and training effects.

03.06.02 Hyperinsulinemic-euglycemic clamp and biochemical analysis

Insulin sensitivity was examined by a HE clamp (**Fig. 6**), as previously reported in detail (Hother-Nielsen *et al.*, 1996; Højlund *et al.*, 2006; Højlund *et al.*, 2009). Two catheters were inserted, one in the antecubital vein for infusion of insulin, glucose, and tracer, and another in the contralateral dorsal hand vein for collection of blood samples. A primed-constant infusion of [3-^{3}H]-glucose was started and continued throughout the clamp. After two hours of basal tracer equilibration to assess basal glucose turnover, insulin was infused at a rate of 40 mU/min/m^2 over 3 hours while plasma glucose levels were maintained (clamped) at basal levels using a variable infusion of glucose. [3-^{3}H]-glucose was added to the glucose infusates to maintain plasma-specific activity constant at baseline levels during the clamp (Hother-Nielsen *et al.*, 1996). Blood samples were collected at baseline and at timed 10–20 min intervals throughout the clamp to determine plasma glucose and plasma [3-^{3}H]-glucose activity. In patients with type 2 diabetes, plasma glucose was allowed to decline to ~5.5 mmol/L before the infusion of glucose was initiated. Total glucose disposal rate (GDR) and hepatic glucose production (HGP) were determined using Steele's non-steady-state equations during the final 40 min of the basal and insulin-stimulated periods (Hother-Nielsen *et al.*, 1996). The distribution volume of glucose was taken as 200 ml/kg BM and the pool fraction as 0.65.

The clamp studies were combined with indirect calorimetry measurements using a ventilated hood system (Jaeger Oxycon Pro, Viasys Healthcare GmbH, Höchberg, DE). FATox and CHOox (g/min) were calculated during the last 30 min of the basal and insulin-stimulated periods using the equations by Frayn (1983). Protein oxidation rates were estimated from urinary nitrogen excretion and corrected for changes in the pool size as described (Tappy *et al.*, 1988). Rates of non-oxidative glucose metabolism (NOX) were calculated as the difference between GDR and CHOox.

Blood samples were measured for plasma glucose on a Radiometer ABL800 FLEX Blood Gas Analyzer (Radiometer Medical ApS, Brønshøj, DK). Serum insulin and C-peptides were

measured on a Cobra e 411 analyzer (Roche Diagnostics International AG, Rotkreuz, CH). Plasma cholesterol and triglycerides were measured on heparinized plasma with absorption photometry on a Cobas 8000 analyzer (Roche Diagnostics International AG, Rotkreuz, CH).

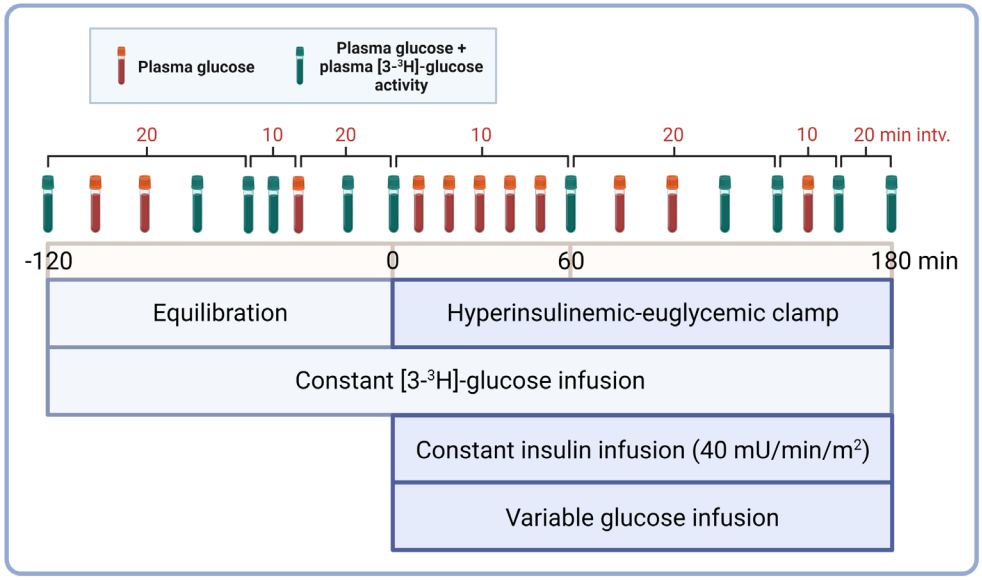

Figure 6. Protocol for the hyperinsulinemic-euglycemic clamp. A primed-constant infusion of [3-^{3}H]-glucose was started and continued throughout the clamp. After 2 hours of equilibration, insulin was infused at a constant rate (40 mU/min/m^2) over 3 hours, while glucose was infused at a variable rate to maintain euglycemia. Blood samples were obtained in 10–20 min intervals to assess plasma glucose and plasma [3-^{3}H]-glucose activity. Glucose disposal rate and hepatic glucose production were determined during the last 40 min of the basal and clamp periods. The figure was designed using BioRender.

03.06.03 Muscle biopsies

The same physician collected all skeletal muscle biopsies in the m. vastus lateralis under local anesthesia (5 mL 2% lidocaine) using a modified Bergström needle with suction. Biopsies were obtained from the same location and depth in the right leg. However, during the acute exercise test, incisions were separated by ~3–4 cm to avoid damage from multiple biopsies. Biopsy specimens were dissected free of blood and visible connective tissue before partitioning into multiple blocks for different purposes, including one block (~1 mm^3) being prepared for TEM analysis.

03.07 Transmission electron microscopy

03.07.01 Fixation of muscle specimens

Specimens were fixed with glutaraldehyde to stabilize surfaces and intracellular structures. With this approach, proteins are cross-linked when the amino residues react with the aldehyde fixatives (Hayat, 1986). However, as aldehyde fixatives do not react avidly with most lipid molecules, preserving the LD structure, which consists of a high lipid-protein ratio, can be an issue in microscopy. Indeed, artifactual formation and fusion of adjacent LDs have been shown in cultured cells (Fukumoto & Fujimoto, 2002). Thus, as part of the sample preparation for TEM, treatment with osmium tetroxide reacts with lipid molecules, making them insoluble and resistant to extraction when exposed to inorganic solvents used in tissue dehydration (Riemersma, 1968).

03.07.02 Basic principles of TEM

TEM employs a high-voltage electron beam to create an image (**Fig. 7**) (Graham & Orenstein, 2007). An electron gun emits electrons that travel through the microscope tube under a vacuum. Rather than having glass lenses focusing the light (as in the case of light microscopy), TEM uses electromagnetic lenses to focus the electrons into a fine beam. This beam transmits through a thinly sectioned (<100 nm) specimen whose tissue and cellular components are usually treated in fixatives or stains of osmium and the heavy metals uranyl and lead, which impede the beam in proportion to their respective degrees of electron density. The differential transmission of electrons creates an image projected on a fluorescent screen or, more frequently used in modern instruments, an electron imaging device such as a CCD (charge-coupled device) camera.

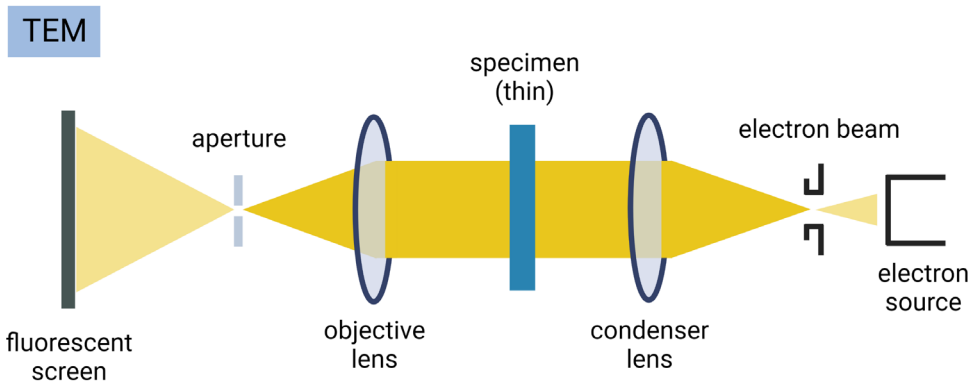

Figure 7. The transmission electron microscope (TEM). The figure was designed using BioRender.

03.07.03 Stereological-based analysis of LD and mitochondrial morphometry in the skeletal muscle

Sampling and morphometric analysis of intramuscular LDs and mitochondria are based on stereological principles (Hoppeler *et al.*, 1973; Weibel, 1979). Efficient acquisition of unbiased stereological estimates requires 1) random and systematic sampling of sections and 2) a test probe system to explore the specific parameters of interest. The latter employs mathematical relationship equations to extract quantitative descriptions of three-dimensional (3D) geometric structures from measurements made on two-dimensional (2D) images or sections (**Fig. 8**). Delesse (1847) came up with proof for the first principle, showing that the area fraction of a sectional profile of an object (A_A) is proportional to the volume fraction of the object (V_V). Other researchers extended this model with additional mathematical relationship equations between probes of various dimensions and a sectional profile of an object – one of these employed test points as a probe. Here, the ratio of points that touch the sectional profile of an object to the total number of points on the section (P_P) will, on average, be equal to the ratio of the volume of the object to the volume of the embedded structure (V_V) (West, 2012).

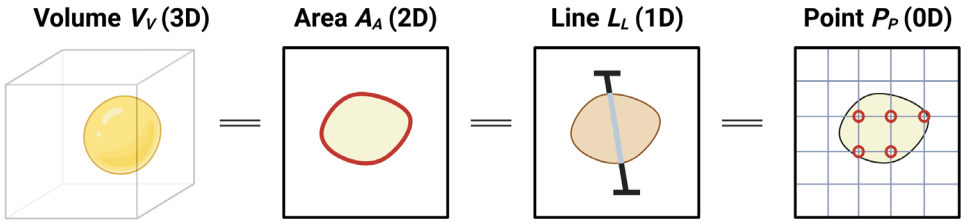

Figure 8. Relationship equations between probes of various dimensions and a sectional profile of an object. (*V*) Volume, (*A*) area, (*L*) length, and (*P*) points. The figure was designed using BioRender.

Sectioning of specimens

At the sectioning level, stereological sampling of geometrical probes is sensitive to the structural features of interest. For example, surfaces and lines uniformly oriented in all directions (in 3D space) have isotropic orientations (West, 2012). That said, most biological structures are anisotropic, as they have a preferred direction or orientation rather than being randomly organized. A skeletal muscle is no exception. Bundles of elongated muscle fibers and alternate sequential arrangements of actin and myosin filaments in sarcomeres organize these fasciculate and periodic structures. As the components in the skeletal muscle are not randomly and uniformly distributed, the structure of interest must be sectioned with an appropriate angle so that all parts of the structure have equal probabilities of being present in the sections. Of note, as point-counting probes are not direction sensitive, the tissue to be

analyzed with these probes can be cut in any direction. This is only sometimes the case for surface-area probes. Skeletal muscle fibers are typically sectioned in the longitudinally or transverse orientation. Sectioning in the longitudinal orientation has the advantages of 1) overcoming spatial inhomogeneities of LDs and mitochondria, as these often are distributed near the I-bands rather than the A-bands of the myofibrils, and 2) enabling measurements of the Z-disc width, which is in the present project used to categorize fiber types at the ultrastructural level. However, the diameter of a fiber cannot be determined in a longitudinal section. As such, muscle fibers are assumed to have a diameter of 80 µm for the derivation of total values and relative contributions of subcellular LDs. Transverse sections, on the other hand, have the main advantage of permitting quantitative analysis of diffusion pathways in energy metabolism (e.g., capillaries to mitochondria). Furthermore, the muscle fiber composition is also better reflected in this plan than in longitudinal sections.

Sampling hierarchy

When designing a stereological study, selecting sections, and selecting the positions in the section to be probed must be performed in a statistically representative manner, meaning that all parts of the structure have an equal probability of being sampled. Systematic random sampling is one way to achieve this in stereological investigations of histological structures (Weibel *et al.*, 1966). This means that the set of sections to be collected for analysis is spaced at equal intervals throughout the entire region of interest, with the first section randomly positioned. In the present project, sectioning of the specimen block are performed randomly and independently, while the acquisition of 2D electron micrographs corresponded to the principles of systematic sampling. Here, micrographs are obtained in a coordinate system (equal intervals between micrographs) with a random start (**Fig. 9b**). Experimentally, systematic random sampling is more efficient than simple random sampling because it yields smaller errors (Ebbesson & Tang, 1965).

Volume estimation by point counting

The practical procedure (steps 1–6) to determine the number of test points required in electron micrographs was based on stereological principles described in **Table 1** (Weibel, 1979). However, based on Nielsen *et al.* (2017), satisfactorily estimates in the volume fractions of intermyofibrillar and subsarcolemmal LDs are achieved after analyzing 2,500 µm^2 of the myofibrillar space and 400 µm of the fiber length, respectively. This corresponded to a total of ~12 micrographs from the subsarcolemmal space and ~6 from both the superficial and central region of the myofibrillar space.

Table 1. Practical procedure to select a test point system

Procedure	Implementation
1. Determine the number of test points needed to meet the specified precision in a representative sample (P_T) (e.g., muscle fiber, biopsy). This is obtained by the means of a nomogram (*Fig. 4.7*) in Weibel (1979).	When the expected volume fraction of LDs in IMF is 0.003, and the relative standard error is 25% (based on Nielsen *et al.* (2010)), P_T is estimated to be 6,000.
↓	↓
2. Determine the optimal magnification (M) at which the measurements will be performed. This will define the micrograph area (A_{T1}) available for analysis.	$A_{T1} = 9.6\ \mu m \times 6.4\ \mu m = 61.4\ \mu m^2$.
↓	↓
3. With a chosen M, measure approximately the area (a_m) of the largest profiles of interest.	If a mean LD diameter of 0.6 µm is chosen (based on Koh *et al.* (2018)), a_m (area of a circle with radius 0.3 µm) will be 0.28 µm^2.
↓	↓
4. Decide a value for the spacing of test points (d_1), such that the condition $(d_1)^2 > a_m$ is met. However, $(d_1)^2 < a_m$ if the object of interest is rare.	If we consider LDs as rare adopt ($(d_1)^2 < a_m$), the spacing between test point (d_1) can be 0.5 µm. Then $(d_1)^2$ will be 0.25 µm^2.
↓	↓
5. The number of test points applied to each micrograph will be: $$P_{T1} = \frac{A_{T1}}{(d_1)^2}$$	$$P_{T1} = \frac{61.4\ \mu m^2}{0.25\ \mu m^2} = 245.6 \approx 246\ points.$$
↓	↓
6. Finally, the number of micrographs required to form a representative sample will be: $$\frac{sample\ P_T}{P_{T1}}$$	The required number of micrographs (from 3 muscle fibers) in the IMF will be: $$\frac{6000}{246\ points} = 24.3 \approx 24\ micrographs.$$

Precision of estimates

The group coefficient of variation (CV_{group}) is related to biological variability and stereological noise sources. While biological variability is inherent in any biological experiment and beyond the control of investigators, stereological noise is calculated by the coefficient of error in estimates (CE_{est}) (Howard & Reed, 2005). CE_{est} describes the method (itself) and how far the obtained estimates are from the true value. The combination of variability within and between sections influences CE_{est}. An optimal sampling scheme involves minimum sampling while providing enough precision to conclude with a predetermined confidence level. If biological variability is the primary contributor to CV_{group}, it is efficient to sample more individuals from the respective population. However, if stereological noise is the primary contributor to CV_{group}, it is recommended to sample more blocks and sections and increase the field of view in probes.

The TEM and stereological-based analyses conducted in studies II and III are outlined in **Table 2** and **Figs. 9 and 10**.

03.08 Statistics

Quantitative electron microscopy analyses were based on estimates from 3 fibers for each observation. All interactions or main effects were tested using a simple linear mixed-effects model with participants (study I–III) and matched triplets or twins (study III) as random effects and time, groups, and fiber types as fixed effects. The Bonferroni correction was applied in study II to counteract the multiple comparisons on the same dependent variable. Data on self-reported physical activity levels were compared between the groups by linear regression analysis. Variables with a skewed distribution were transformed before analysis. The assumption of data normality was tested by Q–Q plots, the Shapiro-Wilk test, and the Skewness-Kurtosis All test, and the assumption of data heteroscedasticity was tested by residual plots. Interactions and main effects were tested by the Wald X^2-test. The Pearson correlation coefficient was applied to test the associations between variables. With the assumption of an even (50:50) fiber type distribution in m. vastus lateralis, the fiber type-weighted volume fractions, morphological characteristics and numbers of LDs were computed by averaging values from type 1 and 2 fibers for each biopsy. This was done before the analysis of associations between GDR, fat oxidation, and fiber type-weighted LD variables. The significance level was accepted as $P<0.05$. Data are presented as means ± standard error of the mean (SEM) in study I and medians ± interquartile range (IQR) in study II and III unless otherwise stated. Statistical analyses were performed using Stata 16/17 (StataCorp LLC, Texas, US) and Prism (GraphPad Software, inc., California, US).

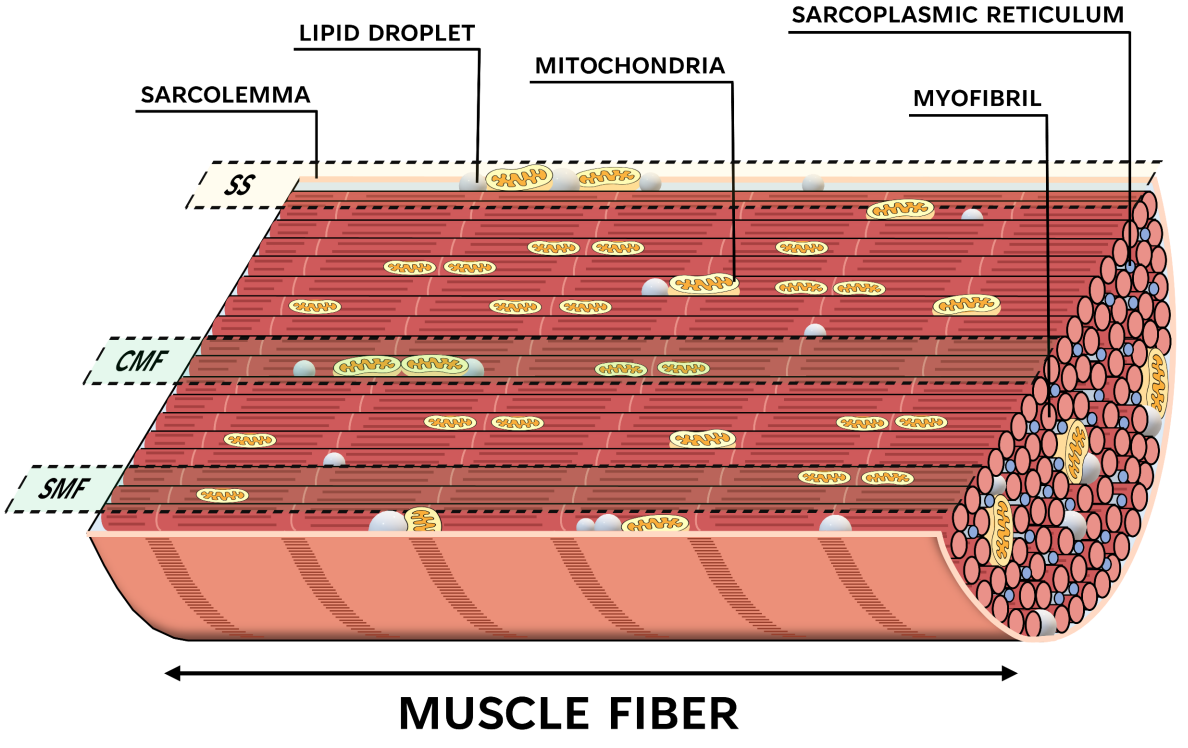

Figure 9A. Three-dimensional (3D) schematics of a single muscle fiber sectioned in the longitudinal orientation. Lipid droplets and mitochondria are located beneath the plasma membrane in the subsarcolemmal (SS) region (yellow marking) or in between the myofibrils in the superficial (SMF) and central (CMF) myofibrillar regions (green markings).

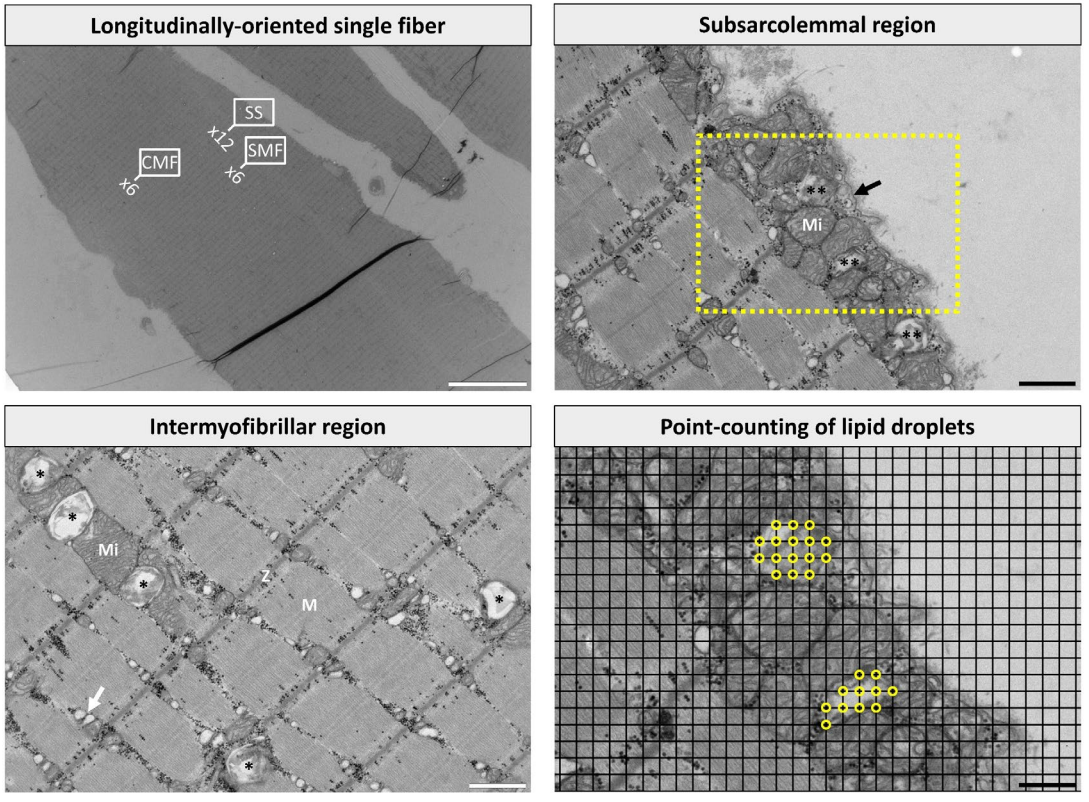

Figure 9B. Acquisition of transmission electron micrographs was systematically randomized to cover the subsarcolemmal (SS) and the superficial (SMF) and central (CMF) myofibrillar regions of single muscle fibers (scale bar = 10 μm). The SMF and CMF regions cover the intermyofibrillar (IMF) region. Lipid droplets in the IMF and SS regions (scale bars = 1 μm). Sarcolemma (black arrow), mitochondria (Mi), triad junction (white arrow), Z-disc (Z), and M-band (M). Point counting of SS lipid droplet volume fractions with a 135 nm horizontal × vertical grid overlay (scale bar = 0.5 μm). The open yellow circles indicate intersections touching lipid droplets.

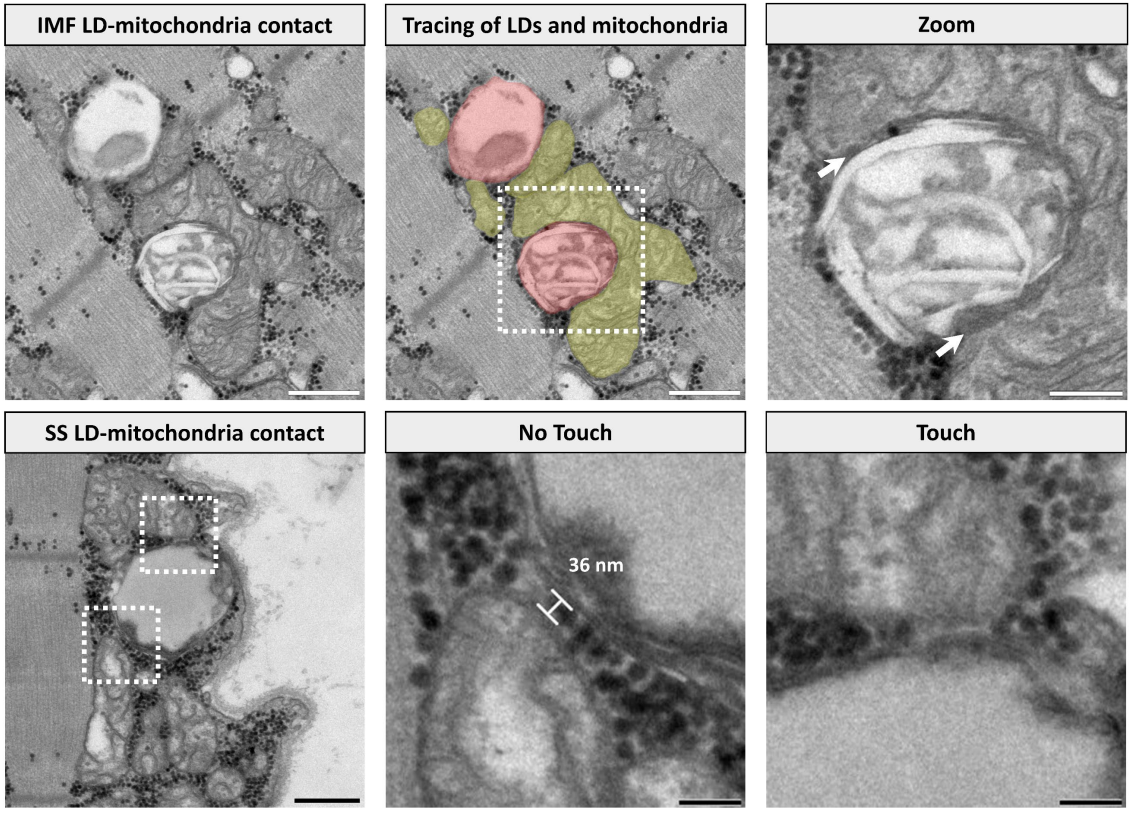

Figure 10. Representative transmission electron micrographs showing inter-organelle contact between lipid droplets (LDs) and neighboring mitochondria in the intermyofibrillar (IMF) and subsarcolemmal (SS) regions (scale bars = 0.5 μm). LD-mitochondria contact was estimated by manually tracing LDs (red pattern) and length of contact sites with mitochondria (yellow pattern) (scale bar = 0.5 μm). Mitochondrial outer membranes interacting with LDs (white arrows) revealed contact sites of increased electron density (zoom, scale bar = 0.2 μm). As electrons rather than light waves are used, the resolution can be used to analyze detailed structures of high quality, making it possible to accurately differentiate between organelles in contact or not (zoom of white dotted squares; scale bars = 0.1 μm).

Table 2. Transmission electron microscopy and analysis of lipid droplets and mitochondria

	Study II	Study III
Fixation and embedding	Muscle biopsy specimens were prepared for TEM as described previously (Jensen *et al.*, 2022). Specimens were fixed in a 2.5% glutaraldehyde solution with a 0.1 M sodium cacodylate buffer (pH 7.3) and stored at 5°C for 24 hours. Specimens were then washed four times in a 0.1 M sodium cacodylate buffer and post-fixed in 1% osmium tetroxide (OsO_4) and 1.5% potassium ferrocyanide ($K_4Fe(CN)_6$) with a 0.1 M sodium cacodylate buffer at 4°C for 120 min. Following the post-fixation, specimens were rinsed twice in double-distilled water, dehydrated by submerging in a graded series of alcohol and infiltrated with graded mixtures of propylene oxide and epoxy resin (Epon) at room temperature. The next day, specimens were embedded in 100% fresh Epon and polymerized at 60°C for 48 hours.	
Sectioning	Ultra-thin (60 nm) sections of the longitudinally oriented fibers were made at three depths separated by 150 µm to sample as many fibers as possible using an ultramicrotome (Leica EM UC7, Leica Camera AG, DE) and collected on hole copper grids.	
Contrasting and microscopy tool	The sections were contrasted with uranyl acetate and lead citrate for 20 min, and then in a lead citrate solution (1% in double-distilled water) for 15 min before examination and capture of electron micrographs in a JEM-1400plus transmission electron microscope (JEOL Ltd., Tokyo, JP) with a CCD camera (Quemesa, Olympus, Tokyo, JP).	
Acquisition of electron micrographs	Micrographs were captured at a ×6,000 magnification in a total of 10 randomly selected muscle fibers per biopsy. For each fiber, 24 micrographs were attained in a randomized, systematic order, i.e., 12 micrographs from the subsarcolemmal space and 6 micrographs from both the superficial and central myofibrillar space (**Fig. 9A and B**). With an area of 61.4 µm^2 per micrograph, the 24 micrographs per fiber are expected to give satisfactorily high precision of the estimated subcellular LD volume fractions (Nielsen *et al.*, 2017).	
Fiber type categorization	Muscle fibers were classified as type 1 or 2 based on their distinct differentiation in Z-disc width, which was shown to associate with myofibrillar ATPase properties (Sjöström *et al.*, 1982a; Sjöström *et al.*, 1982b). The fibers with the thickest and thinnest Z-disc were classified as type 1 and 2 fibers, respectively. All intermediate fibers were discarded, and only distinct type 1 and 2 fibers were included in the analysis (n=3 of each fiber type per biopsy).	
Z-disc width	The median (IQR) Z-disc width for type 1 fibers was 82 (77–89) nm, and for type 2 fibers was 64 (61–69) nm.	The median (IQR) Z-disc width for type 1 fibers was 83 (78–88) nm, and for type 2 fibers was 65 (63–69) nm.

Identification of organelles	The criteria for identifying LDs included a minimum diameter of 200 nm, a near-spherical white-greyish appearance, and the absence of a distinctly visible membrane. We included LDs with membrane-like structures or irregular partitioning of triglycerides and cholesterol esters (high and low electron density, respectively) segregated in the droplet (Fujimoto & Parton, 2011). Identification of mitochondria was based on previously described work in mammalian skeletal muscles (Hoppeler *et al.*, 1973).	
Point-counting techniques	Point-counting techniques (**Fig. 9B**) were performed regarding the principles of stereology (Hoppeler *et al.*, 1973; Weibel, 1979). Point grids with a size of 135 nm (LDs) and 350 nm (mitochondria) were overlaid onto each micrograph, generating a total of 2,992 and 442 points per micrograph, respectively, for point counting. All point-counting was conducted with a commercial imaging software, iTEM (EMSIS, Münster, DE).	Not performed in this study.
Estimation of volume fractions	Two subcellular localizations of LDs and mitochondria were defined: 1) the intermyofibrillar space and 2) the subsarcolemmal space. Intermyofibrillar LDs and mitochondria were expressed as volume per myofibrillar space and calculated by estimates in the superficial and central regions. Muscle fibers are assumed to have a cylindrical shape. As the superficial region occupies three times more volume than the central region, volume estimates from the superficial myofibrillar space were weighted three times more than those from the central myofibrillar space. Subsarcolemmal LDs and mitochondria were expressed as volume per fiber surface area and calculated by estimates in this region. We measured the length of visible myofibrils parallel to the sarcolemma and used it as a direct measure of fiber length. Fiber surface area was then calculated as the length of the subsarcolemmal space multiplied by the thickness of the ultra-thin sections (60 nm). Volume fractions of total LDs and mitochondria were obtained by adding the intermyofibrillar and subsarcolemmal volume fractions per myofibrillar space. The subsarcolemmal volume fractions (per fiber surface area) were divided by 20, based on the assumption that muscle fibers are cylindrical and that the volume beneath a surface area of 1 μm^2 is 20 μm^3 according to the formula: $V_b = r \cdot 0.5 \cdot A$ where *r* is the fiber radius (40 µm), and *A* is the fiber surface area. Finally, the relative distributions of subcellular LDs and mitochondria to total volume fractions were determined.	
	In this study, we estimated the volume fractions of LDs and mitochondria. Estimations were based on point-counting values.	In this study, we estimated the volume fractions of LDs. Estimations were based on values of LD area (size: μm^2) (see "Estimation of LD morphology"). Both fully observable LDs and those partly outside micrographs were included in the estimates.

Analysis of LD size and shape (morphology) characteristics	LD size and shape characteristics were analyzed using RADIUS (EMSIS GmbH, Münster, DE) by manually tracing an interpolated polygon to outline all fully detectable LDs. LDs partly outside micrographs or coexisting subcellular regions were excluded from these analyses. Area (LD size) is reported in squared micrometers (μm^2). Diameter and perimeter are reported in micrometers; Feret's diameter describes the longest distance (µm) between parallel tangents at opposing boundaries of the LD; aspect ratio [(major axis)/(minor axis)] is computed as the maximal ratio between the length and width of a bounding box; perimeter-to-area (P:A) ratio [divided by a factor of 10] determines the exposed perimeter to a given area of the LD; shape factor [area/area of a circle with an equal perimeter] and convexity [area/area of the measured droplets convex hull] are dimensionless quantities describing the complexity and curvature of the LD; sphericity $[(\text{width}/\text{length})^2]$ reflects the circularity of the LD with values of '1' indicating a perfect sphere.	
Calculation of LD numbers	The number of LDs was calculated by dividing the volume fractions of subcellular LDs by the mean volume of individual LDs in their respective subcellular localization. Assuming that LDs are geometrically shaped like spheres, the mean volume of individual droplets was calculated using the formula: $$V = \frac{4}{3} \cdot \pi \cdot r^3$$ where r is the radius, which was based on the mean LD diameter of the morphological measures.	
Analysis of LD-mitochondria contact	For each fully observable LD in physical contact with adjacent mitochondrial outer membranes (**Fig. 10**), the length of contact sites was determined by manually tracing a polyline in a sequence of connected points. All fully observable LDs without any mitochondrial contact were reported as '0'. Contact between LDs and mitochondria was represented by 1) the absolute length of contact and 2) the relative contact of the LD perimeter in contact with adjacent mitochondria. From all LDs, we finally estimated the percentage of LDs in "touch" with mitochondria.	
Coefficient of error (CE) in point-counting estimates	The precision of stereological estimates, represented by the coefficient of error (CE_{est}), was approximated for the subcellular volume fractions of LDs and mitochondria as proposed by (Howard & Reed, 2005): $$CE\left(\frac{\sum y}{\sum x}\right) = \sqrt{\frac{n}{n-1}\left(\frac{\sum x^2}{\sum x \cdot \sum x} + \frac{\sum y^2}{\sum y \cdot \sum y} - \frac{2 \cdot \sum(x \cdot y)}{\sum x \cdot \sum y}\right)}$$ For each estimate, *n* is the number of micrographs (72 micrographs), *x* is the total count of points per micrograph (LDs;	Not calculated in this study.

	2,992 points, mitochondria: 442 points), and *y* is the points hitting the object of interest. A total of 11,808 electron micrographs from 492 fibers (Pre: 258; Post: 234) were analyzed in this study. The median (IQR) CE_{est} for the volume fractions of subsarcolemmal LDs was 0.23 (0.20–0.27) at Pre and 0.25 (0.20–0.32) at Post, and for intermyofibrillar LDs it was 0.20 (0.16–0.24) at Pre and 0.16 (0.14–0.21) at Post. The median (IQR) CE_{est} for the volume fractions of subsarcolemmal mitochondria was 0.13 (0.11–0.14) at Pre and 0.11 (0.10–0.12) at Post, and for intermyofibrillar mitochondria it was 0.06 (0.06–0.08) at Pre and 0.06 (0.05–0.06) at Post.	
Inter-individual reliability in point-counting estimates	Point counting of LDs and mitochondria was performed by three blinded investigators, where the electron micrographs from the different groups, time points, and fiber types were distributed equally between the investigators. An assessment of inter-investigator reproducibility indicated a CV of 0.5–10.5% in the point-counting estimates based on a total of 36 electron micrographs from 3 muscle fibers (analyzed for each fiber type per biopsy). Raw data for point counting of mitochondria were adjusted to a bias of 22% in the subsarcolemmal region and 38% in the intermyofibrillar region.	Not calculated in this study.
Coefficient of error (CE) in the morphological estimates	A total of 8,123 LDs (intermyofibrillar: Pre: 2,529, Post: 2,842; subsarcolemmal: Pre: 1,473, Post: 1,279) were analyzed in this study. In all participants, the intra-individual variation in LD morphology (based on LD area) indicated that at least seven LDs were needed to obtain satisfactorily high precision estimates:	A total of 4,654 LDs (Intermyofibrillar Pre: 1,668, Post: 1,506, and Subsarcolemmal Pre: 700, Post: 780) were analyzed in this study. Out of this number, 698 LDs were partly outside micrographs. Based on LD area, intra-individual variation in LD morphology indicated that at least six LDs were needed to achieve satisfactorily high-precision estimates:

	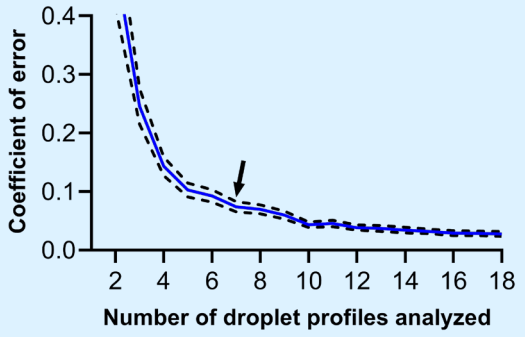 Thus, only participants with a minimum of seven LDs were included in the present study. The median (IQR) number of estimates across groups, subcellular regions, and fiber types involved analysis of 24 (16–46) LDs at Pre and 29 (16–51) LDs at Post.	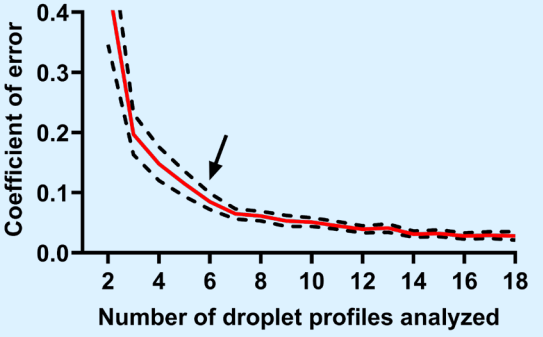 Thus, only participants with a minimum of six LDs were included in these analyses. The median (IQR) number of estimates across groups, fiber types, and subcellular regions involved analysis of 18 (11–31) LDs at pre and 17 (13–26) LDs at post.
Inter-individual reliability in the morphological estimates	Analyses were conducted by three blinded investigators with the electron micrographs equally distributed between the different groups, time points, and fiber types. Some measures for mitochondrial contact were checked by two investigators. Based on seven LDs, inter-investigator analyses for reproducibility indicated a CV of 1.6–9.2% in the estimates of morphological characteristics and a CV of 14.7–17.9% in mitochondrial contact. The inter-investigator analyses also revealed some systematic biases (up to 34%) in the measures of LD morphology and contact sites with mitochondria. The raw data was adjusted for these biases.	All analyses were conducted by one blinded investigator, with the electron micrographs equally distributed between the groups, time points, and fiber types in 12 separate folders. Measures from folders 1–4, 5–8, and 9–12 were checked by a principal investigator to detect and adjust any possible drift over time. Based on six LDs, inter-investigator analyses for reproducibility revealed a CV of 1–5% in the measures of LD morphology and 9–18% in the measures of mitochondrial contact. The raw data was adjusted for some systematic biases in the measures of mitochondrial contact (5–29%).

04 Results

04.01 Study I

04.01.01 Baseline characteristics

At baseline, patients with type 2 diabetes had higher HbA1c and fasting plasma glucose, triglycerides, serum insulin, and C-peptide than obese and lean controls (**Table 3**). As expected, the two obese groups had higher body weight, BMI, waist-to-hip ratio (WHR), total fat mass, and lean body mass than the lean controls. Although the self-reported physical activity levels did not differ between the three groups (**Supplemental Table 1**), $\dot{V}O_2$max (ml O_2/kg/min) differed between all three groups, with the highest and lowest values observed in the lean controls and patients with type 2 diabetes, respectively (**Table 3**).

Under insulin stimulation, patients with type 2 diabetes had lower GDR and NOX by ~40% and ~49%, respectively, and higher FATox (LOX in **Table 4**) by ~75–90% than obese and lean controls (**Table 4**). These findings corresponded with a lower insulin-stimulated RER in patients with type 2 diabetes than in lean controls, concomitant with a decreased ability to increase RER (Δ) than both lean and obese controls. CHOox (GOX in **Table 4**) and HGP did not differ between the three groups.

04.01.02 Compliance to the HIIT protocol

The attendance rate was above 95% and comparable between all three groups (**Supplemental Table 1**). All participants completed at least 21 of the total 23 sessions, and ~50% did not miss a single session. There were no injuries reported during the eight weeks of HIIT. Although the training volume increased from two to five HIIT blocks during the eight weeks intervention (**Fig. 5**), corresponding to an increase of 10 to 25 × 1-min intervals per session, the participants managed to increase the workload during cycling (~2–3%) and rowing (~7–10%) from weeks 1–4 to 5–8 (**Supplemental Table 2**).

Table 3. Clinical and biochemical characteristics, Pre and Post HIIT

Characteristics	Lean		Obese		T2D	
Clinical characteristics	**Pre**	**Post**	**Pre**	**Post**	**Pre**	**Post**
N	18	16	15	15	15	13
Age (years)	56.2 ± 1.5		53.8 ± 1.8		55.2 ± 1.7	
Weight (kg)	78.9 ± 2.0	77.3 ± 2.2*	100.0 ± 2.9††	98.5 ± 2.6*††	103.1 ± 3.7††	102.5 ± 4.1*††
BMI (kg/m^2)	24.0 ± 0.4	23.7 ± 0.4*	30.8 ± 0.7††	30.3 ± 0.6*††	31.2 ± 0.8††	30.8 ± 0.9*††
Waist (cm)	90 ± 1	87 ± 2**	106 ± 2††	102 ± 2**††	109 ± 2††	106 ± 2**††
WHR	0.94 ± 0.01	0.93 ± 0.01*	1.00 ± 0.01††	0.98 ± 0.01*†	1.05 ± 0.01††‡	1.01 ± 0.01**††‡
Total Fat Mass (kg)	20.1 ± 1.0	18.2 ± 1.2**	32.0 ± 1.9††	29.7 ± 1.8**††	34.8 ± 2.3††	33.0 ± 2.5**††
Total Lean Body Mass (kg)	56.9 ± 1.3	57.1 ± 1.4*	65.3 ± 1.3††	66.2 ± 1.2*††	64.8 ± 1.7††	66.8 ± 2.0*††
VO_2max (l O_2/min)	2.98 ± 0.11	3.27 ± 0.10*	3.31 ± 0.15†	3.58 ± 0.10*	2.65 ± 0.11†‡	3.09 ± 0.10**‡
VO_2max (ml O_2/kg/min)	38.0 ± 1.5	42.8 ± 1.7**	33.4 ± 1.8†	36.6 ± 1.2*†	25.8 ± 0.9††‡	30.5 ± 1.0**††‡
Biochemical characteristics						
HbA1c (mmol/mol)	35 ± 1	34 ± 1*	35 ± 1	34 ± 1*	54 ± 4††‡‡	51 ± 4*††‡‡
HbA1c (%)	5.4 ± 0.1	5.2 ± 0.1*	5.3 ± 0.1	5.2 ± 0.1*	7.1 ± 0.3††‡‡	6.8 ± 0.3*††‡‡
Plasma glucose (mmol/l)	5.2 ± 0.1	5.4 ± 0.1	5.6 ± 0.1	5.4 ± 0.1*	9.6 ± 0.7††‡‡	8.8 ± 0.7**††‡‡
Serum insulin (pmol/l)	61 ± 9	62 ± 12	71 ± 8	65 ± 7	117 ± 19†‡	98 ± 15*†
Serum C-peptide (pmol/l)	727 ± 63	697 ± 68	825 ± 60	765 ± 52	1120 ± 77††‡	1040 ± 75††‡
C-peptid/insulin ratio	13.9 ± 1.1	14.3 ± 1.4	12.9 ± 0.9	13.0 ± 1.0	11.6 ± 1.1	12.8 ± 1.6
Plasma triglycerides (mmol/l)	1.52 ± 0.23	1.43 ± 0.31	1.59 ± 0.19	1.35 ± 0.13	2.47 ± 0.40†‡	2.08 ± 0.37†‡
Plasma LDL (mmol/l)	3.2 ± 0.2	3.0 ± 0.2	3.5 ± 0.2	3.3 ± 0.2*	3.0 ± 0.2‡	2.8 ± 0.2
Plasma HDL (mmol/l)	1.2 ± 0.1	1.3 ± 0.1*	1.2 ± 0.1	1.3 ± 0.1	1.0 ± 0.1	1.1 ± 0.1†‡
Plasma total-cholesterol (mmol/l)	4.9 ± 0.2	4.8 ± 0.2	5.4 ± 0.1	5.1 ± 0.2	4.9 ± 0.3	4.7 ± 0.2

Data are means ± SEM. *P<0.05 and **P<0.001 vs. pre-training, †P<0.05 and ††P<0.001 vs. lean, ‡P<0.05 and ‡‡P<0.001 vs. obese. T2D, type 2 diabetes; WHR, waist-to-hip ratio; Pre, pre-training; Post, post-training.

Table 4. Metabolic characteristics during clamp, Pre and Post HIIT

Characteristics	Lean		Obese		T2D	
	Pre	Post	Pre	Post	Pre	Post
N	18	16	15	15	15	13
Plasma glucose basal (mmol/l)	5.1 ± 0.1	5.2 ± 0.1	5.4 ± 0.1	5.2 ± 0.1	9.0 ± 0.8††‡‡	8.1 ± 0.7*††‡‡
Plasma glucose clamp (mmol/l)	5.4 ± 0.1	5.2 ± 0.1	5.2 ± 0.1	5.5 ± 0.2	5.4 ± 0.1	5.2 ± 0.1
Serum insulin basal (pmol/l)	50 ± 8	40 ± 6	52 ± 9	42 ± 4	103 ± 18††‡	77 ± 13†‡
Serum insulin clamp (pmol/l)	691 ± 37	666 ± 40	669 ± 29	703 ± 42	723 ± 60	700 ± 59
GDR basal (mg/min/m^2)	75 ± 2	78 ± 2	78 ± 2	81 ± 5	82 ± 2	82 ± 5
GDR clamp (mg/min/m^2)	356 ± 30	463 ± 36**	351 ± 26	447 ± 29*	210 ± 24†‡	317 ± 36**†‡
GDR basal (mg/min/kg LBM)	2.7 ± 0.0	2.7 ± 0.1	2.6 ± 0.1	2.6 ± 0.2	2.7 ± 0.1	2.6 ± 0.1
GDR clamp (mg/min/kg LBM)	12.3 ± 1.0	16.0 ± 1.1**	11.5 ± 0.8	15.0 ± 1.0**	7.3 ± 0.8††‡	10.4 ± 1.1*††‡
GIR clamp (mg/min/m^2)	325 ± 6	442 ± 33**	325 ± 22	439 ± 33**	189 ± 28†‡	300 ± 36**††‡
HGP basal (mg/min/m^2)	76 ± 1	78 ± 2	78 ± 2	80 ± 5	77 ± 3	77 ± 4
HGP clamp (mg/min/m^2)	28 ± 11	25 ± 12	19 ± 14	17 ± 11	22 ± 5	13 ± 7
ΔHGP, (mg/min/m^2)	-48 ± 11	-53 ± 13	-59 ± 14	-63 ± 12	-55 ± 5	-64 ± 8
NOX basal (mg/min/m^2)	37 ± 5	42 ± 6	51 ± 5	60 ± 7	42 ± 9	57 ± 9*
NOX clamp (mg/min/m^2)	265 ± 27	367 ± 35**	266 ± 26	368 ± 27**	136 ± 20†‡	240 ± 34**†‡
GOX basal (mg/min/m^2)	38 ± 5	36 ± 6	28 ± 5	21 ± 7	40 ± 10	25 ± 12*
GOX clamp (mg/min/m^2)	90 ± 5	96 ± 8	88 ± 6	79 ± 12	74 ± 9	78 ± 11
LOX basal (mg/min/m^2)	29 ± 2	30 ± 2	31 ± 2	35 ± 3	34 ± 4	41 ± 4*†
LOX clamp (mg/min/m^2)	11 ± 2	10 ± 3	12 ± 2	18 ± 4*	21 ± 2†‡	19 ± 4†
RER basal	0.80 ± 0.01	0.80 ± 0.01	0.78 ± 0.01	0.77 ± 0.01	0.80 ± 0.02	0.77 ± 0.02*
RER clamp	0.91 ± 0.01	0.91 ± 0.02	0.90 ± 0.01	0.87 ± 0.02	0.86 ± 0.01†	0.87 ± 0.02
ΔRER	0.10 ± 0.01	0.11 ± 0.01	0.11 ± 0.01	0.10 ± 0.01	0.06 ± 0.01†‡	0.10 ± 0.02

Data are means ± SEM. *P<0.05 and **P<0.001 vs. pre-training, †P<0.05 and ††P<0.001 vs. lean, ‡P<0.05 and ‡‡P<0.001 vs. obese. Δ-values were calculated as clamp minus basal values for HGP and RER. T2D, type 2 diabetes; Pre, pre-training; Post, post-training; GDR, glucose disposal rate; GIR, glucose infusion rate; HGP, hepatic glucose production; NOX, non-oxidative glucose metabolism; GOX, glucose oxidation rate; LOX, lipid oxidation rate; RER, Respiratory exchange ratio. LBM, lean body mass.

04.01.03 Effects of HIIT on $\dot{V}O_2$max and body composition

HIIT increased $\dot{V}O_2$max (l O_2/min) by 15% in the patients with type 2 diabetes, 8% in the obese controls, and 10% in the lean controls (**Table 3** and **Fig. 11B**). Although there was considerable heterogeneity in the responses of $\dot{V}O_2$max to HIIT (**Fig. 11F**), we did not identify any differences between groups. Across all three groups, HIIT lowered body weight, BMI, and WHR (**Table 3**). The reduction in body weight was explained by a more considerable reduction in total fat mass (~1.6–2.3 kg) than an increase in total lean body mass (~0.6–1.5 kg) (**Table 3** and **Fig. 11C and D**). We did not detect any differences in these HIIT-induced responses between the groups.

04.01.04 Effects of HIIT on Glycemic control and lipid profile

HIIT induced a clinically relevant decline in HbA1c (4±2 mmol/mol) and fasting plasma glucose (1.0±0.4 mmol/l) in patients with type 2 diabetes (**Table 3**). Although the HIIT-induced responses were highest in patients with type 2 diabetes, HbA1c also slightly decreased in obese and lean controls, while fasting plasma glucose decreased in obese controls. In addition, HIIT increased plasma HDL in lean controls and decreased plasma LDL in obese controls, whereas plasma triglycerides and total cholesterol were unaffected in all three groups. We did not detect any differences in these responses between the groups.

04.01.05 Effects of HIIT on insulin sensitivity and indirect calorimetry during the clamp

HIIT increased insulin-stimulated GDR (mg/min/m^2) by 42% in patients with type 2 diabetes, 27% in obese controls, and 29% in lean controls (**Table 4** and **Fig. 11A**). Interestingly, post-training values in the patients with type 2 diabetes reached a comparable level with pre-training levels in both the obese and lean controls. However, we observed large inter-individual variability in the responses of insulin-stimulated GDR to HIIT (**Fig. 11E**), but with no differences between groups. Similar positive results were detected for insulin-stimulated glucose infusion rate (GIR) and GDR relative to lean body mass, accompanied by increases in insulin-stimulated NOX but not CHOox (GOX in **Table 4**). While insulin-suppressed FATox (LOX in **Table 4**) was unaffected in patients with type 2 diabetes and lean controls, it increased in obese controls. Nevertheless, post-training FATox was higher in patients with type 2 diabetes than in lean controls. In patients with type 2 diabetes, HIIT decreased basal CHOox and increased basal FATox, which caused a reduction in basal RER. As a result, the attenuated ΔRER, observed in patients with type 2 diabetes at baseline, was absent after HIIT. HIIT did not induce changes in HGP or the ability of insulin to suppress HGP (ΔHGP) in any of the groups. We did not detect any differences in these responses between the groups.

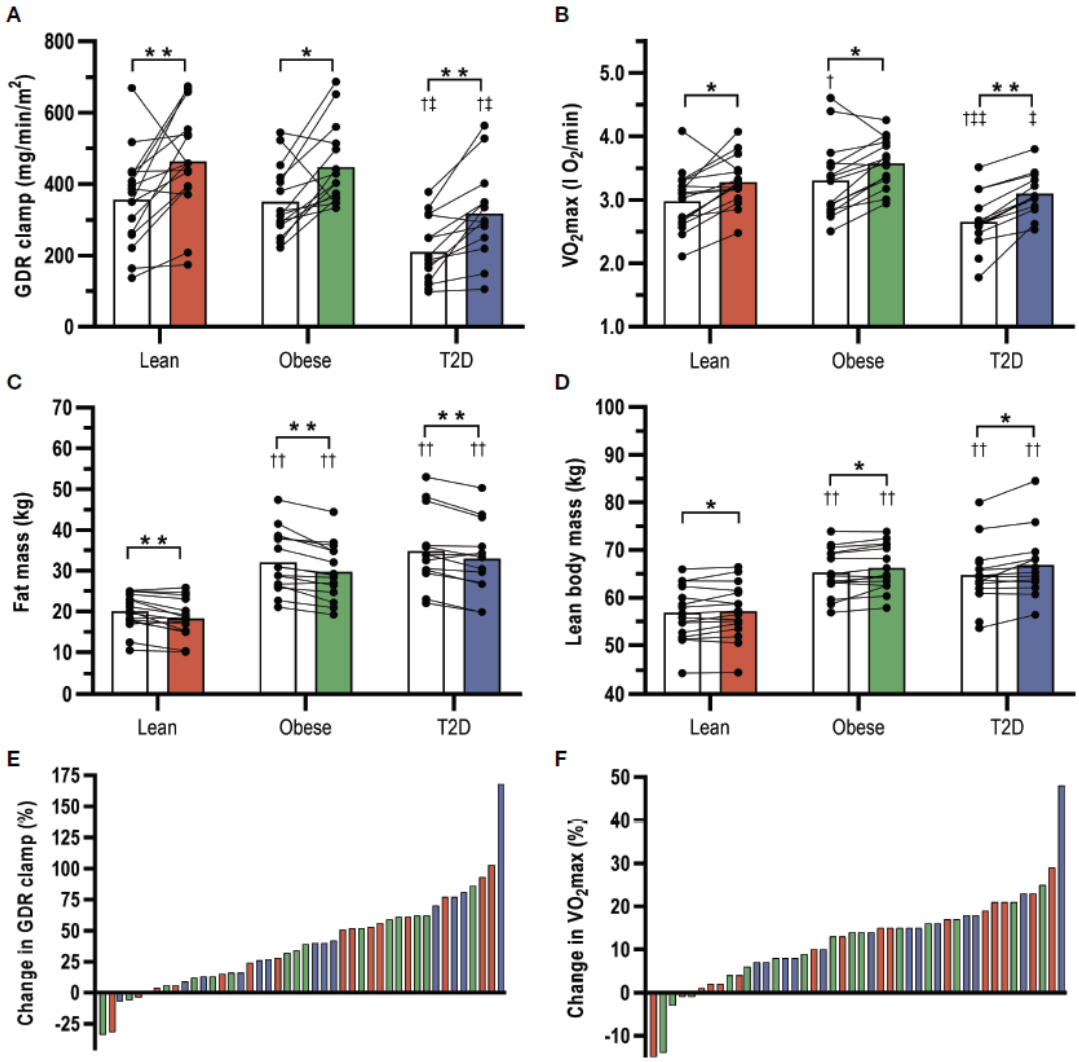

Figure 11. Effects of HIIT on insulin-stimulated glucose disposal rate (GDR; ***A***), $\dot{V}O_2$max (***B***), total fat mass (***C***), and total lean body mass (***D***). Interindividual variability in the HIIT-induced responses of GDR (***E***) and $\dot{V}O_2$max (***F***) in patients with type 2 diabetes (T2D; blue bars), and glucose tolerant obese (green bars) and lean (red bars) controls. Data are presented as means ± standard error of the mean. Lean, Pre: n=18 and Post: n=16. Obese, Pre and Post: n=15. T2D, Pre: n=15 and Post: n=13. **P*<0.05 and ***P*<0.001 vs. Pre; **†***P*<0.05 and **††***P*<0.001 vs. Lean; **‡***P*<0.05 and **‡‡***P*<0.001 vs. Obese.

04.02 Study II

04.02.01 Substrate oxidation rates during graded exercise

Baseline characteristics

Before and after the HIIT intervention and ~2 hours after consuming a standardized mixed meal, we measured indirect calorimetry during a graded exercise test to estimate individual substrate oxidation rates in a second (2^{nd}) polynomial curve analysis (**Fig. 12A and B**). Impaired fat oxidation capacity has been suggested in the etiology of type 2 diabetes (Kelley & Simoneau, 1994; van de Weijer *et al.*, 2013; Gavin *et al.*, 2018), potentially contributing to the accumulation of intramuscular LDs in these patients (Phielix & Mensink, 2008). Although FATox during exercise was numerically lower in patients with type 2 diabetes than in obese and lean controls, we did not detect any differences between groups in MFO or FAT_{max} (**Fig. 12C and D**). Similarly, we did not detect any systematic group differences in FATox at specific relative (20, 40, 60, and 80% $\dot{V}O_2max$) or absolute (40, 60, 80, and 100 watts) intensities (**Fig. 12A and B**). Nevertheless, CHOox was 30–90% higher at 100–220 watts in patients with type 2 diabetes than in lean and obese controls (**Fig. 12B**). In the lean controls, MFO was positively associated with insulin-stimulated GDR, but this was not shown for patients with type 2 diabetes or obese controls (**Supplemental Fig. 1**).

Effects of HIIT

Various HIIT regimes have been reported to increase FATox in different populations (Astorino & Schubert, 2018). However, according to our knowledge, only Stoa *et al.* (2017) have examined the effects of HIIT on FATox in patients with type 2 diabetes, demonstrating no effect after 12 weeks of intervention. Across all three groups, we showed that HIIT increased FATox curves (%$\dot{V}O_2max$), representative of a change in the vertical (y-axis) but not horizontal (x-axis) direction (**Fig. 12A**). In comparison, CHOox curves (%$\dot{V}O_2max$) were almost stable. As a result, MFO increased by ~40–60% in all three groups (**Fig. 12D**), while FAT_{max} was unchanged (**Fig. 12C**). Evaluating the HIIT effects on absolute intensities, FATox increased at 40–100 watts while sparing CHOox at 40–220 watts (**Fig. 12B**). In sum, FATox was not reduced in patients with type 2 diabetes and increased adequately in all three groups after HIIT, suggesting that the FATox capacity is not responsible for insulin resistance in type 2 diabetes.

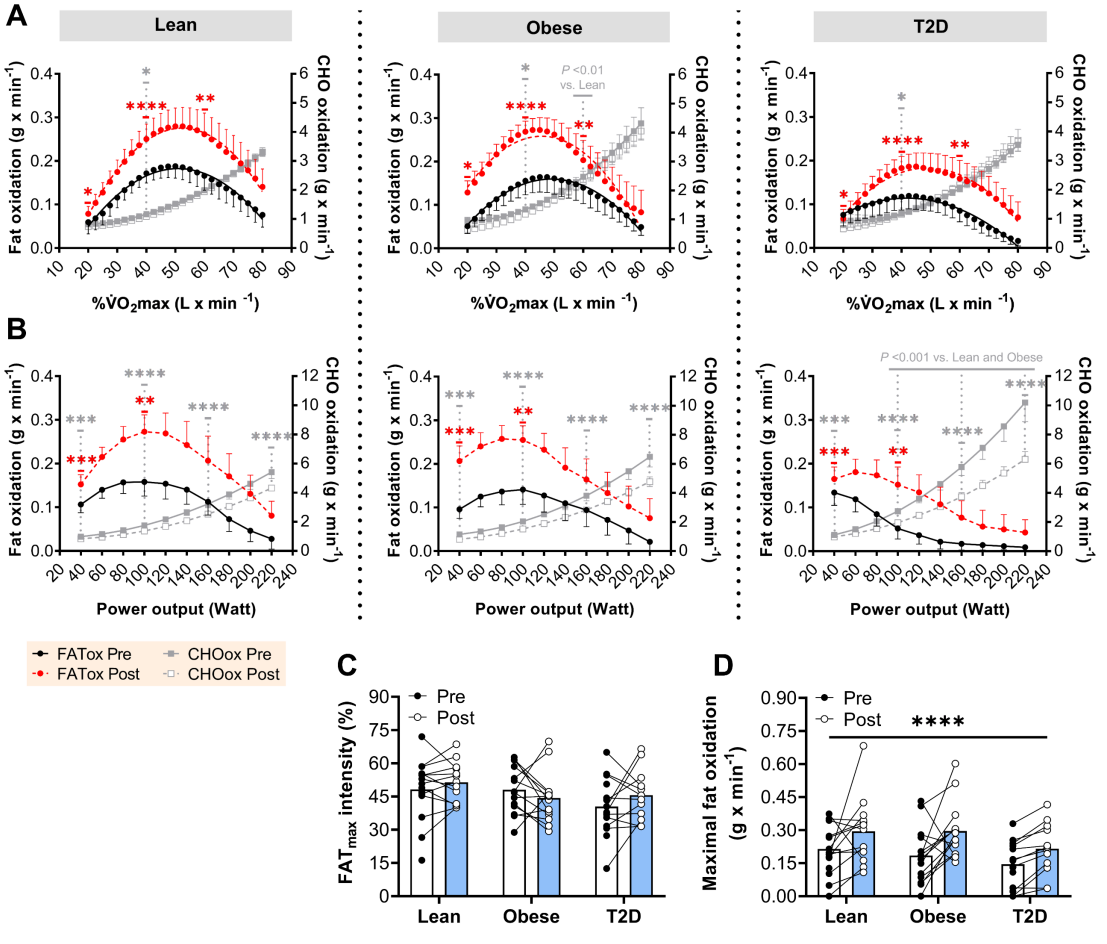

Figure 12. Substrate oxidation rates (g/min) during submaximal graded exercise Pre and Post HIIT. Fat and carbohydrate oxidation (FATox and CHOox, respectively) are expressed relative to maximal oxygen uptake (%$\dot{V}O_2$max; ***A***) and absolute to power output (watt; ***B***). The estimated values were plotted for each participant to construct a second (2^{nd}) polynomial curve ($\boldsymbol{y = ax^2 + bc + c}$). Effects of HIIT on FAT_{max} (***C***), the relative intensity (%$\dot{V}O_2$max) needed to elicit the maximal fat oxidation rate (MFO; ***D***). Data are presented as means ± SD in *A* and *B* and means with adjacent values in *C* and *D*. Lean, Pre: n=15 and Post: n=13. Obese, Pre: n=14 and Post: n=14. T2D, Pre: n=14 and Post: n=12. Simple linear mixed-effects model: **P*<0.05; ***P*<0.01; ****P*<0.001; *****P*<0.0001.

04.02.02 Lipid droplet volume fractions, size, and numbers

Baseline characteristics

Using TEM, we can discriminate between LDs stored beneath the sarcolemma or throughout the myofibrillar interior in the subsarcolemmal and intermyofibrillar regions, respectively (**Fig. 9**). Here, we show that patients with type 2 diabetes store increased volume fractions of LDs (**Fig. 13A**), predominantly as ~70% and ~40% larger individual LDs in the subsarcolemmal region than lean and obese controls, respectively (**Fig. 13C**), with no difference between groups in the numbers of either intermyofibrillar or subsarcolemmal LDs (**Fig. 13B**) or size of intermyofibrillar LDs (**Fig. 13C**).

Interestingly, the size distribution of subsarcolemmal LDs in type 2 fibers (**Fig. 14**) revealed that, while both the obese controls and patients with type 2 diabetes display more moderately enlarged LDs (0.7 to 0.8 μm^2 profile area) than lean controls, only the patients with type 2 diabetes store extremely large LDs (>0.9 μm^2 profile area). Although they only represent ~10% of the subsarcolemmal LD numbers in type 2 diabetes, their extremely large size can describe the ~twofold increase in subsarcolemmal LDs, as observed in patients with type 2 diabetes. Thus, in the subsarcolemmal region, obesity may induce enlarged LDs (~twofold), but type 2 diabetes differentiates from obesity by storing extremely large LDs (~10-fold). Compared with the normal-sized LDs, these extremely large subsarcolemmal LDs did not deviate in shape (**Fig. 15A**) or the absolute length of contact with neighboring mitochondria (**Fig. 15B**). However, due to their larger surface area, only ~5% of their surface is in contact with mitochondria (**Fig. 15C**). Remarkably, when differentiating in single muscle fibers of varying subsarcolemmal mitochondrial content, we observed that these enlarged subsarcolemmal LDs were situated in fibers containing reduced levels of mitochondria (**Fig. 15D**).

Although patients with type 2 diabetes have no or only minor decreases in the volume fractions of intermyofibrillar and subsarcolemmal mitochondria (**Fig. 13D**), they demonstrate a shift in the relative distribution as characterized by reduced amounts of subsarcolemmal mitochondria relative to intermyofibrillar mitochondria than in lean controls (**Fig. 20A**). Consequently, the altered network of LDs and mitochondria leads to a deficiency of mitochondrial content to LD load in patients with type 2 diabetes, which is independent of obesity (**Fig. 13E**).

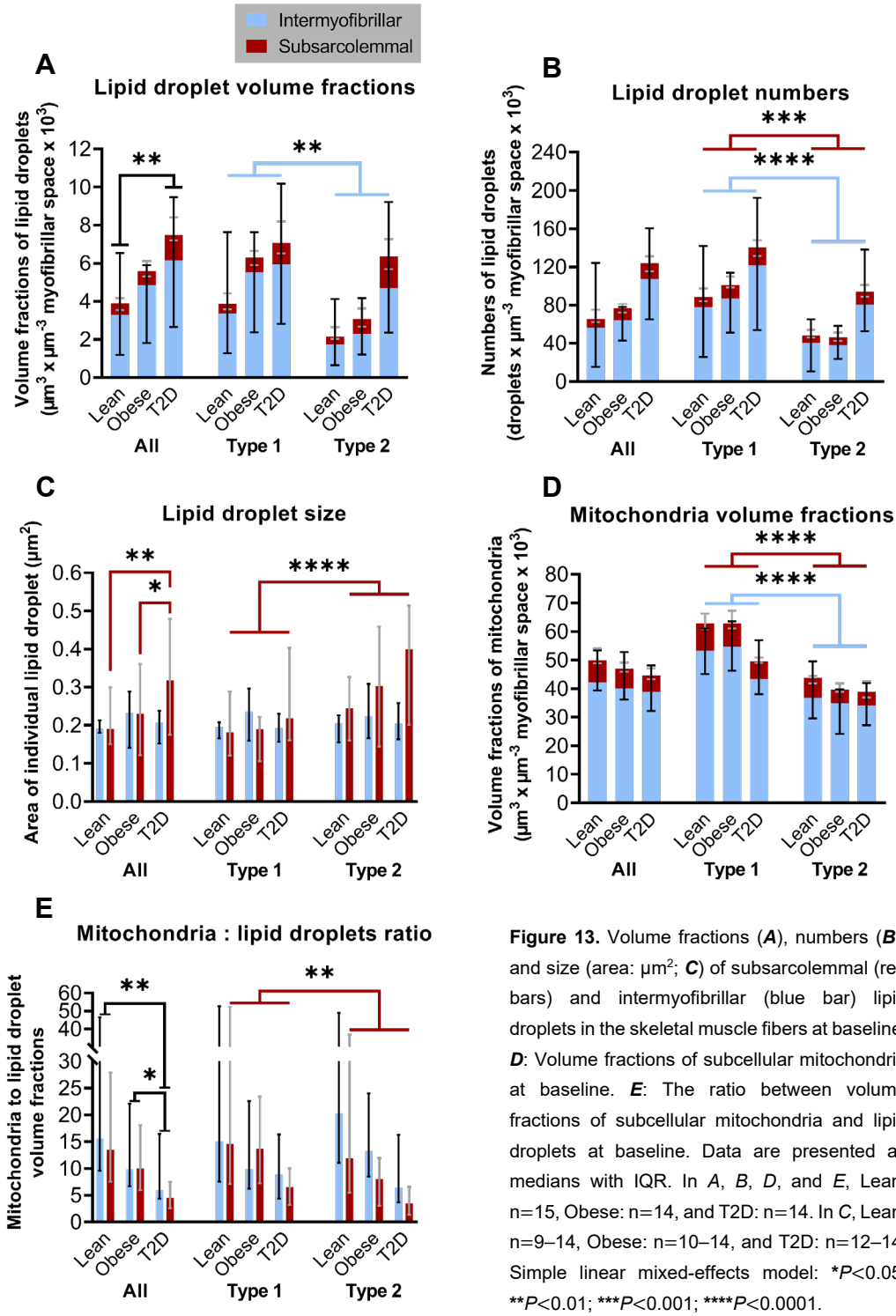

Figure 13. Volume fractions (***A***), numbers (***B***), and size (area: µm^2; ***C***) of subsarcolemmal (red bars) and intermyofibrillar (blue bar) lipid droplets in the skeletal muscle fibers at baseline. ***D***: Volume fractions of subcellular mitochondria at baseline. ***E***: The ratio between volume fractions of subcellular mitochondria and lipid droplets at baseline. Data are presented as medians with IQR. In *A*, *B*, *D*, and *E*, Lean: n=15, Obese: n=14, and T2D: n=14. In *C*, Lean: n=9–14, Obese: n=10–14, and T2D: n=12–14. Simple linear mixed-effects model: **P*<0.05; ***P*<0.01; ****P*<0.001; *****P*<0.0001.

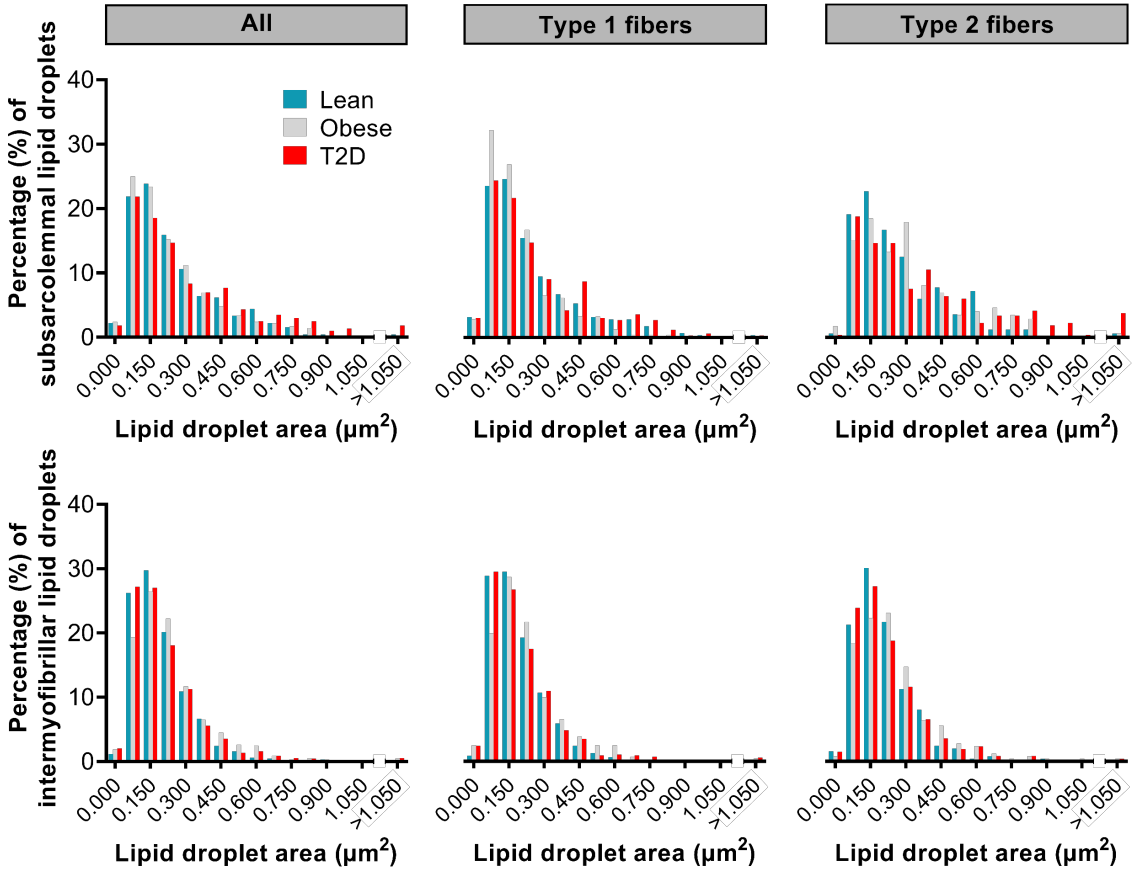

Figure 14. Histograms showing distributions of lipid droplet size (area: μm^2) at baseline. Values were obtained from subsarcolemmal (All: n=1,473; Type 1 fibers: n=864; Type 2 fibers: n=609) and intermyofibrillar (All: n=2,529; Type 1 fibers: n=1,556; Type 2 fibers: n=973) lipid droplets across groups.

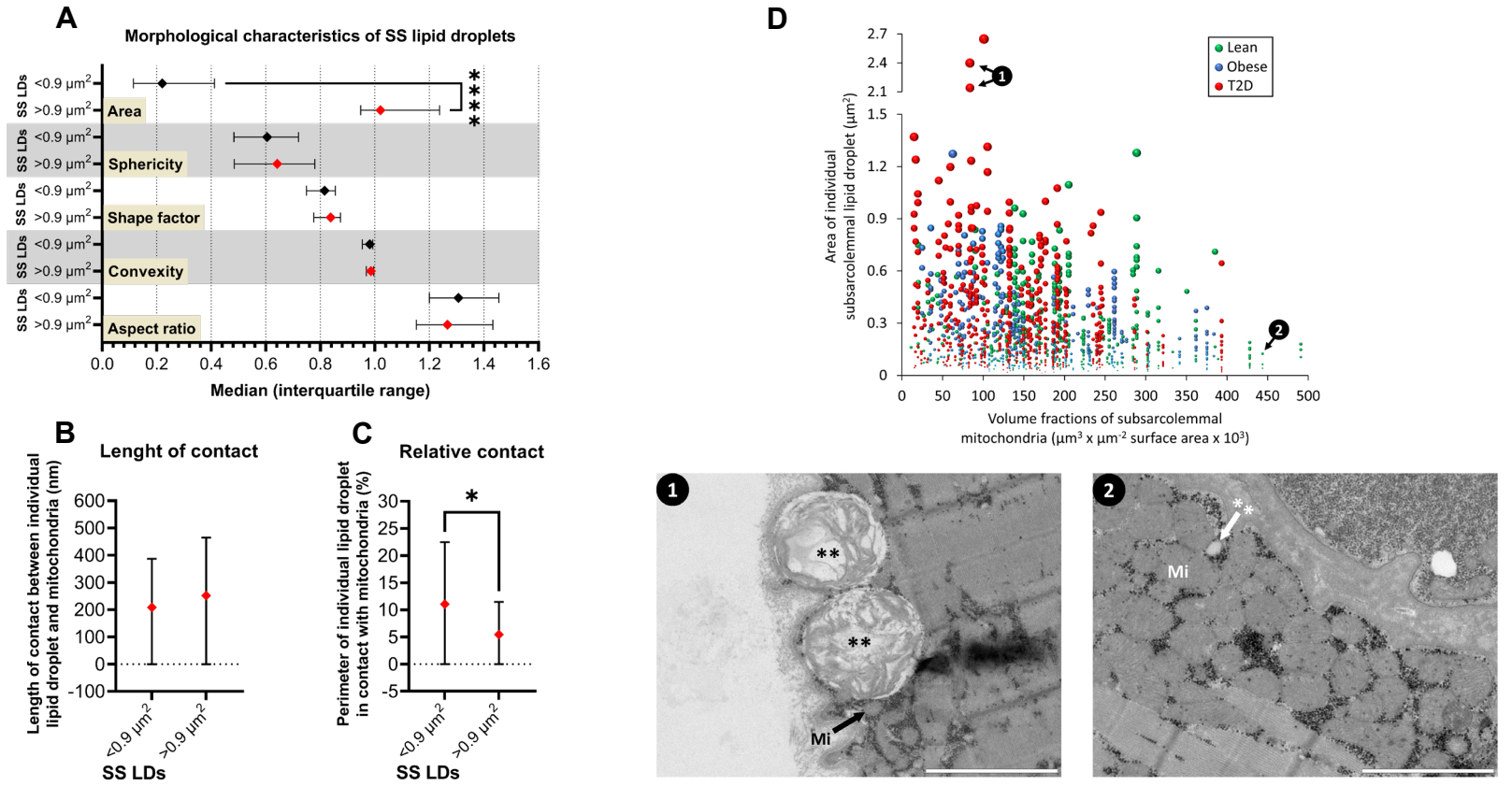

Figure 15. ***A***: Morphological characteristics of subsarcolemmal (SS) lipid droplets (LDs) with differential size (area: < and > 0.9 µm²) in patients with type 2 diabetes at baseline. ***B*** and ***C***: Length of contact (nm; *B*) and relative contact (%; *C*) between SS LDs (area: < and > 0.9 µm²) and mitochondria in patients with type 2 diabetes at baseline. ***D***: Size (µm²) of individual SS LDs in corresponding single muscle fibers with varying mitochondrial content at baseline (n=1,473). Electron micrographs numbered 1 and 2 correspond to SS LDs (**) as plotted above (scale bars = 2 µm). In *A*–*C*, data are presented as medians with IQR and n=600. Linear regression analysis: **P*<0.05 and *****P*<0.0001.

Effects of HIIT

The eight weeks of HIIT changed the volumetric composition of LDs and mitochondria in skeletal muscle fibers of all three groups (**Fig. 16–20**). In patients with type 2 diabetes, the pre-training excessive load of subsarcolemmal LDs in type 2 fibers was reduced to a lower and comparable level with the obese and lean controls (**Fig. 16A**). Contrary, across all three groups, the volume fractions of intermyofibrillar LDs increased slightly (~20%) in type 2 fibers (**Fig. 16A**), accompanied by marked increments in the volume fractions of both subsarcolemmal (~30–50%) and intermyofibrillar (~20–40%) mitochondria (**Fig. 18A**). These changes in composition reduced the relative contribution of subsarcolemmal LDs to total volume fractions of LDs by ~5–15% points (**Fig. 19**) and increased the relative contribution of subsarcolemmal mitochondria to the total volume fractions of mitochondria by ~2–4% points (**Fig. 20**). As a result, HIIT increased the mitochondrial content relative to the LD load in the subsarcolemmal region of all three groups (**Fig. 18B**).

To understand this HIIT-induced redistribution of LDs, we discriminated between the numbers and size of individual droplets (**Fig. 16B** and **17A**). In the subsarcolemmal region, the decrease in the volume fractions of LDs could exclusively be explained by a decline in the size of LDs (**Fig. 17A**). Furthermore, in patients with type 2 diabetes, the extremely large subsarcolemmal LDs disappeared after HIIT (**Fig. 17B**). In the intermyofibrillar region, the increase in the volume fractions of LDs was ascribed by an increase in the numbers of LDs (**Fig. 16B**). Thus, adaptations to HIIT remodel intramuscular TAGs to be stored preferentially in a higher number of smaller LDs, located in the intermyofibrillar region.

In lean controls after HIIT, volume fractions of subsarcolemmal LDs were negatively associated with insulin-stimulated GDR (R^2=0.41, P=0.02), but this was not observed in obese controls or patients with type 2 diabetes (**Supplemental Fig. 2**). We did not detect any other associations between GDR and volume fractions, numbers, or size of intermyofibrillar or subsarcolemmal LDs Pre or Post HIIT.

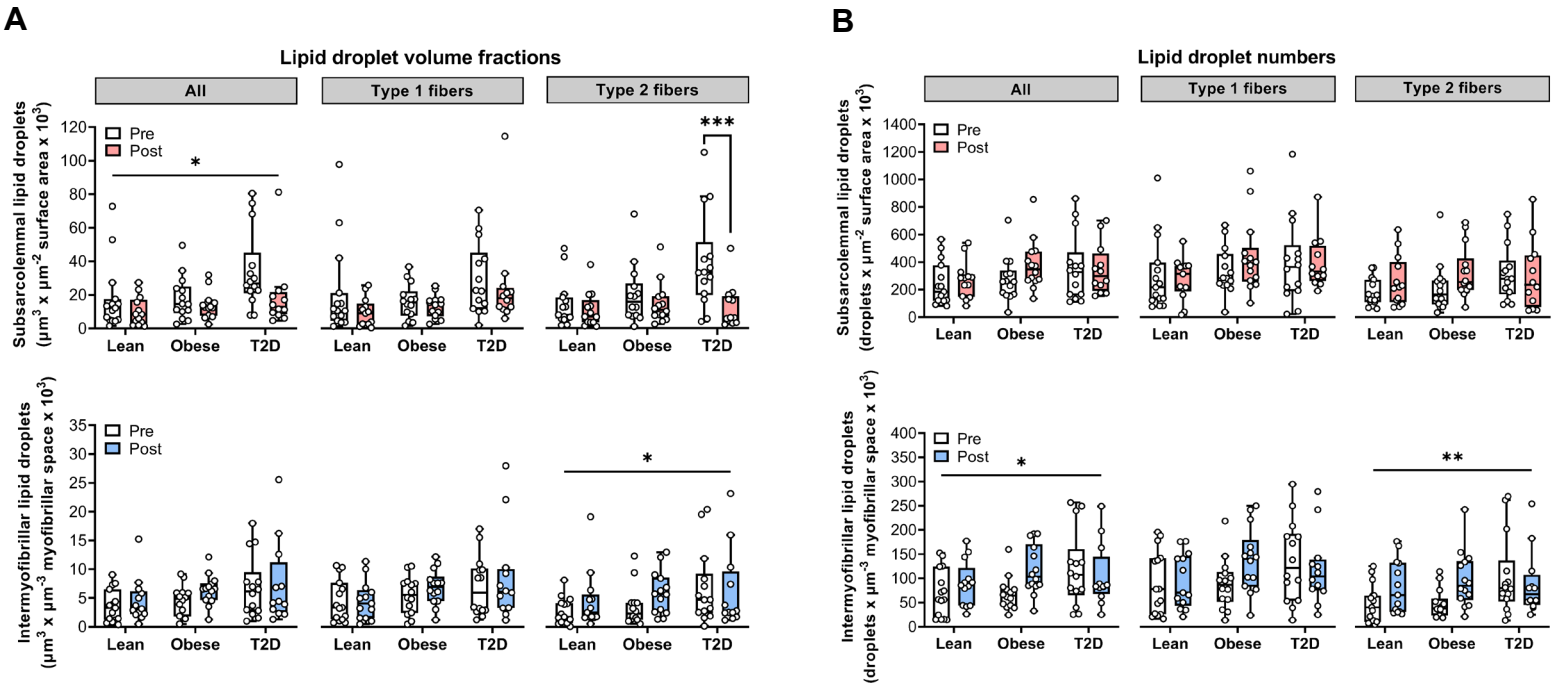

Figure 16. Effects of HIIT on lipid droplet volume fractions (A) and numbers (B) in the subsarcolemmal (red boxes) and intermyofibrillar (blue boxes) regions of skeletal muscle fibers. Box and whiskers represent medians, IQR, and adjacent values. Lean, Pre: n=15 and Post: n=13. Obese, Pre: n=14 and Post: n=14. T2D, Pre: n=14 and Post: n=12. Simple linear mixed-effects model: **P*<0.05; ***P*<0.01; ****P*<0.001.

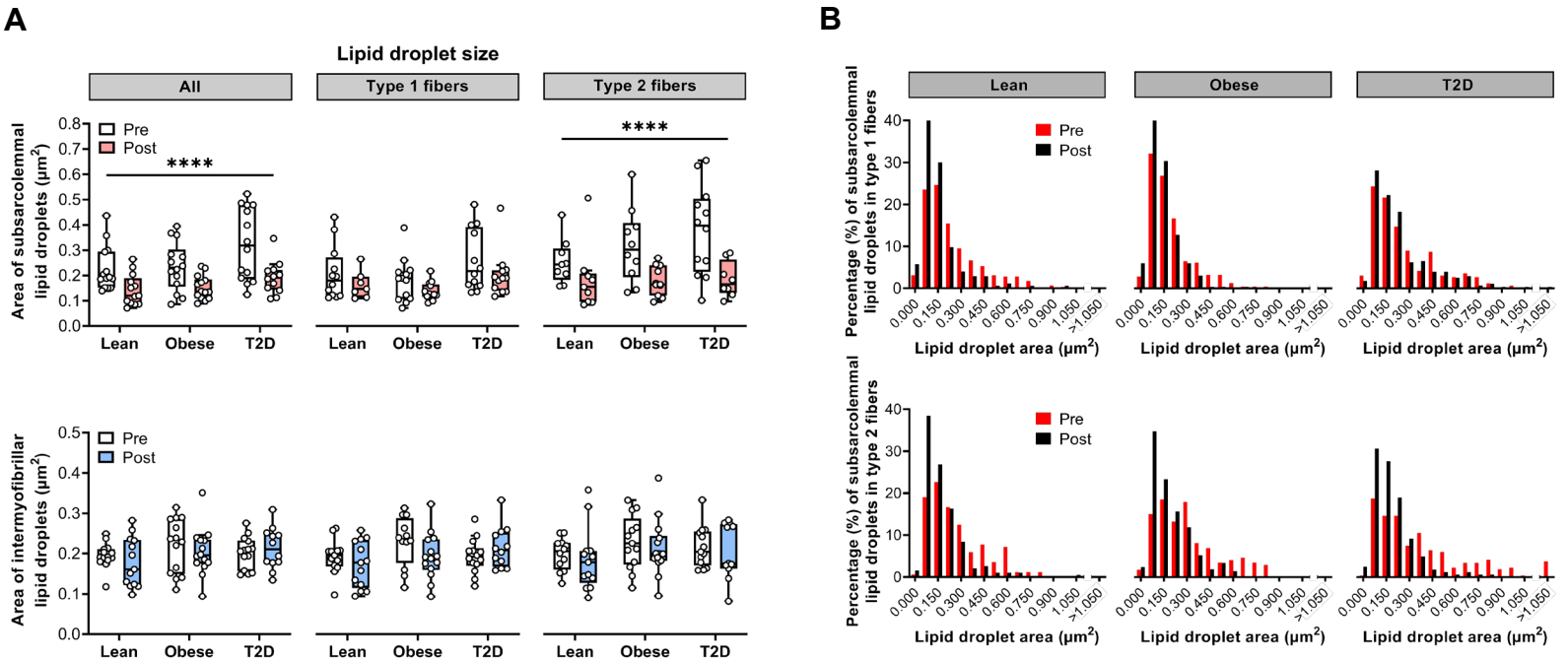

Figure 17. ***A***: Effects of HIIT on lipid droplet size (area: μm^2) in the subsarcolemmal (red boxes) and intermyofibrillar (blue boxes) regions of skeletal muscle fibers. ***B***: Histograms displaying distributions (%) of subsarcolemmal lipid droplet size (area: μm^2) Pre and Post HIIT. Values were estimated from lipid droplets in type 1 (Lean: n=458; Obese: n=513; T2D: n=608) and type 2 (Lean: n=359; Obese: n=384; T2D: n=430) fibers. In *A*, box and whiskers represent medians, IQR, and adjacent values. In *A*, Lean: n=7–14; Obese: n=10–14; T2D: n=8–14. Simple linear mixed-effects model: ****P<0.0001.

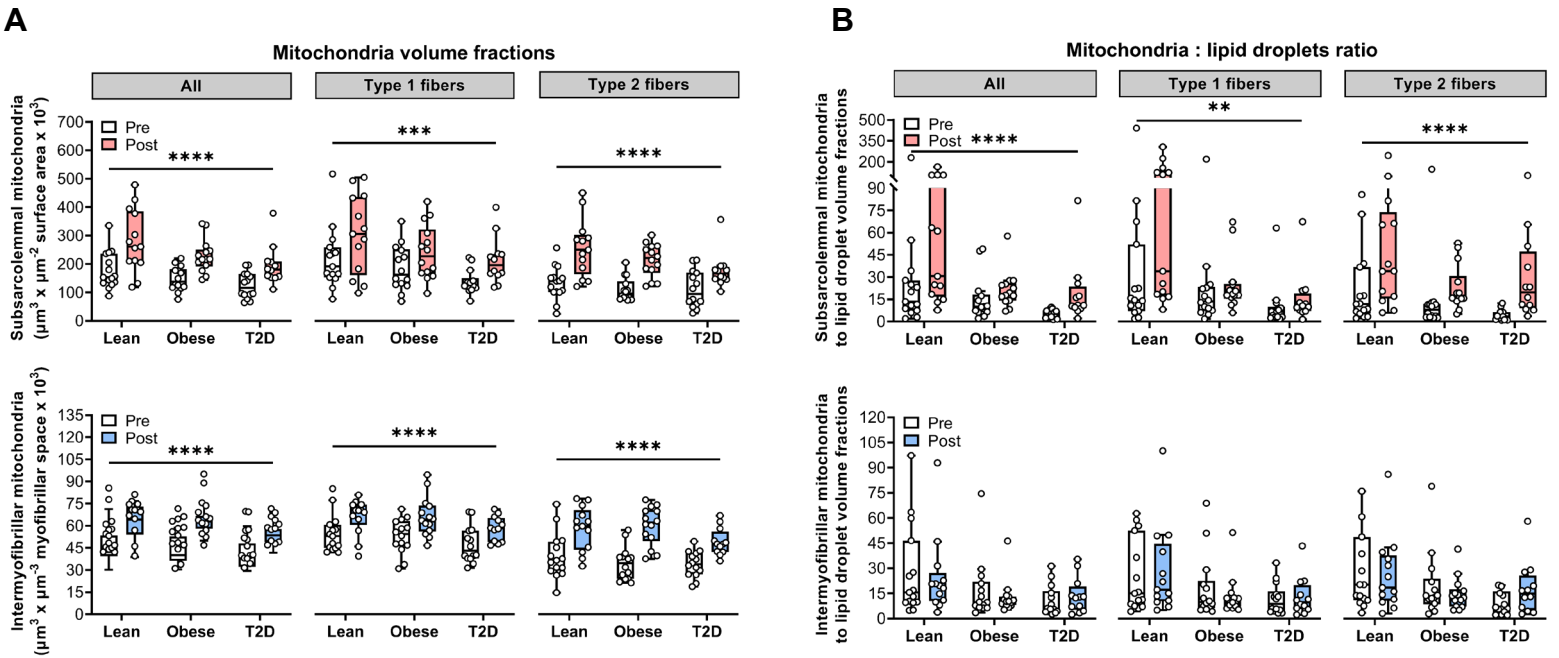

Figure 18. Effects of HIIT on mitochondria volume fractions (***A***) and the ratio between volume fractions of mitochondria and lipid droplets (***B***) in the subsarcolemmal (red boxes) and intermyofibrillar (blue boxes) regions of skeletal muscle fibers. Box and whiskers represent medians, IQR, and adjacent values. Lean, Pre: n=15 and Post: n=13. Obese, Pre: n=14 and Post: n=14. T2D, Pre: n=14 and Post: n=12. Simple linear mixed-effects model: *****P*<0.01; ******P*<0.001; *******P*<0.0001.

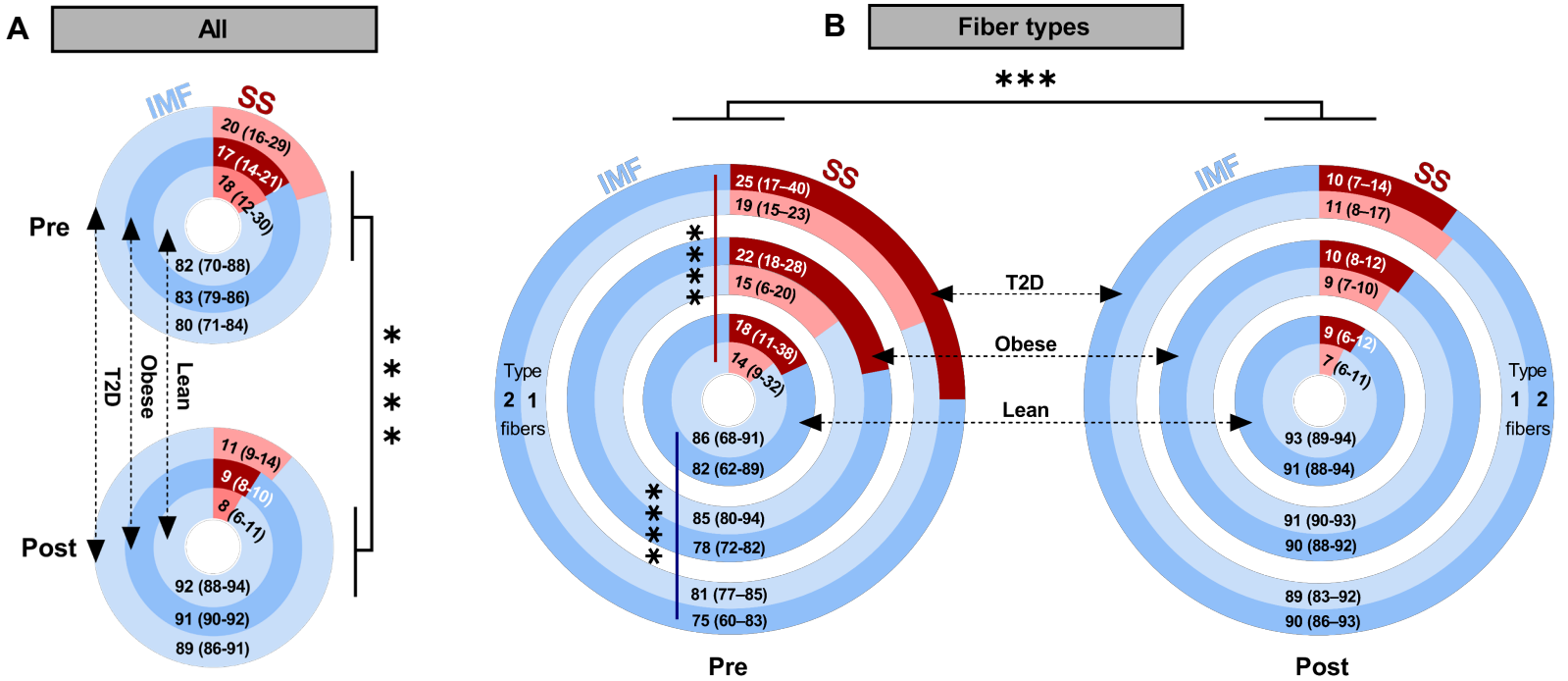

Figure 19. Donut charts describing the relative distributions (%) of intermyofibrillar (IMF; blue colors) and subsarcolemmal (SS; red colors) lipid droplets to total volume fractions for all fibers (***A***) and discriminated between type 1 and 2 fibers (***B***) Pre and Post HIIT. Data are presented as medians with IQR in parenthesis. Lean, Pre: n=15 and Post: n=13. Obese, Pre: n=14 and Post: n=14. T2D, Pre: n=14 and Post: n=12. Simple linear mixed-effects model: ***$P<0.001$; ****$P<0.0001$.

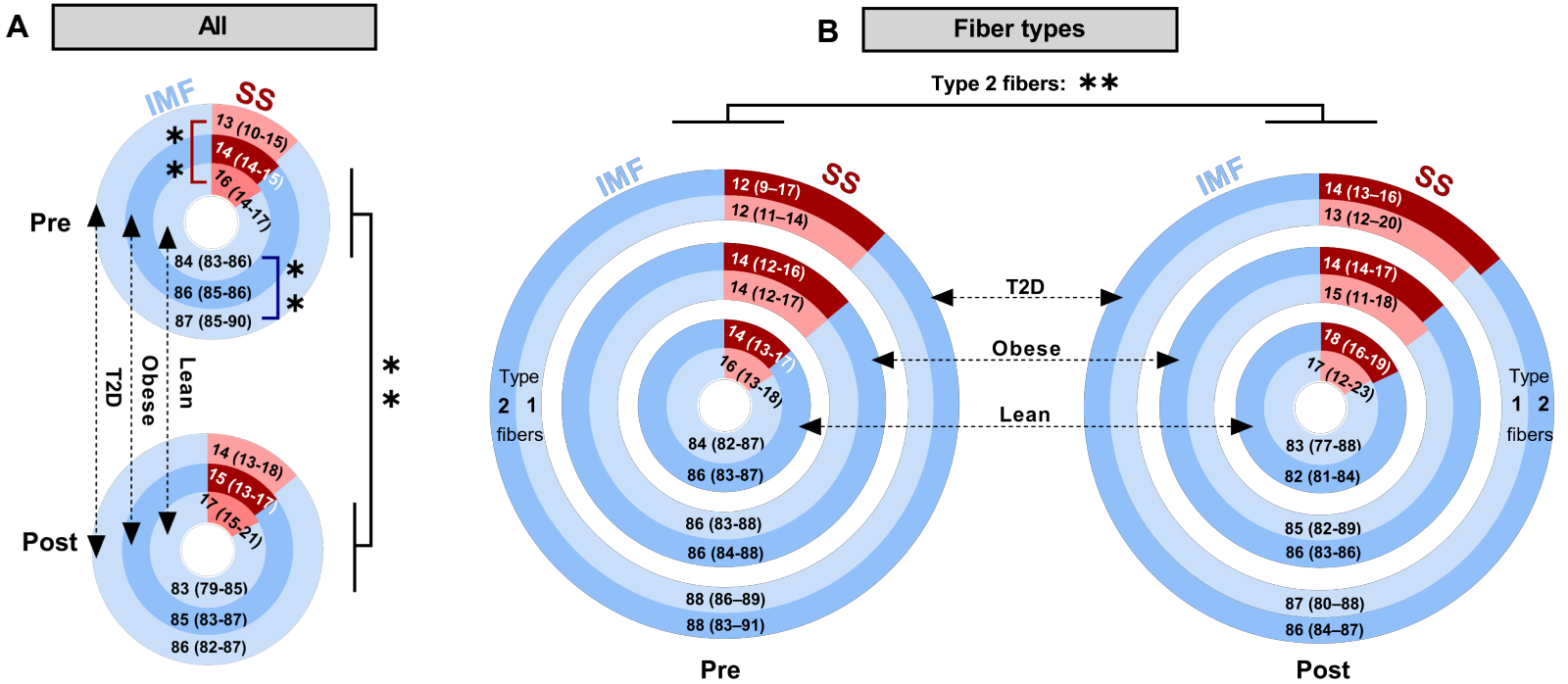

Figure 20. Donut charts describing the relative distributions (%) of intermyofibrillar (IMF; blue colors) and subsarcolemmal (SS; red colors) mitochondria to total volume fractions for all fibers (***A***) and discriminated between type 1 and 2 fibers (***B***) Pre and Post HIIT. Data are presented as medians with IQR in parenthesis. Lean, Pre: n=15 and Post: n=13. Obese, Pre: n=14 and Post: n=14. T2D, Pre: n=14 and Post: n=12. Simple linear mixed-effects model: ***P*<0.01.

04.02.03 Lipid droplet morphology

Baseline characteristics

To understand the architecture and complexity of LD morphology in general and in patients with type 2 diabetes and glucose-tolerant controls, we quantified LD size and shape descriptors by tracing the surface of individual droplet organelles in electron micrographs. When plotting individual estimates for sphericity and shape factor, we observed that LD organelles come in a broad range of shapes (**Fig. 21**). Analysis of shape descriptors at baseline further revealed that individual LD organelles deviate noticeably from spheres in all three groups (**Fig. 22** and **Supplemental Table 3**). Across fiber types, estimates of median shape factor were ~0.78–0.81, while estimates of median sphericity were ~0.57–0.69 (1.0 is a perfect sphere). In addition, although not detecting any meaningful differences between the groups, shape descriptors for convexity and shape factor were slightly lower in type 1 fibers than in type 2 fibers (**Supplemental Table 3**). Together, these findings indicate that LDs stored in skeletal muscle cells are better described as ellipsoids than spheres.

Interestingly, we demonstrated that the ellipsoid-shaped LD, combined with a reduced convexity, increases its P:A ratio by ~10–20% compared to a spherically-shaped LD of equal size, suggesting that size and shape descriptors, together, may contribute to changes in the P:A ratio of individual LDs. Furthermore, when elaborating size descriptors for perimeter, diameter, and Feret, subsarcolemmal LDs were bigger across fiber types in patients with type 2 diabetes than in obese and lean controls (**Supplemental Table 3**). These observations corresponded with a decreased P:A ratio of subsarcolemmal LDs in the patients with type 2 diabetes than in obese but not lean controls.

Effects of HIIT

Across fiber types, HIIT did not change LD shape descriptors for either convexity, shape factor, or sphericity in any of the three groups (**Fig. 22**). However, in the subsarcolemmal region of all three groups, LDs displayed declines in size descriptors for perimeter, diameter, and Feret. Comparable to the changes found in the subsarcolemmal LD area (**Fig. 17A**), these specific declines were related to the changes in type 2 fibers (**Supplemental Fig. 3**). As a result, the P:A ratio of individual LDs increased in the subsarcolemmal region across fiber types (**Fig. 22**) and in type 2 fibers (**Supplemental Fig. 3**) of all three groups. These findings suggest LDs as dynamic organelles that form various structures, considerably controlled by the properties of the muscle fiber to perform one or more specialized jobs.

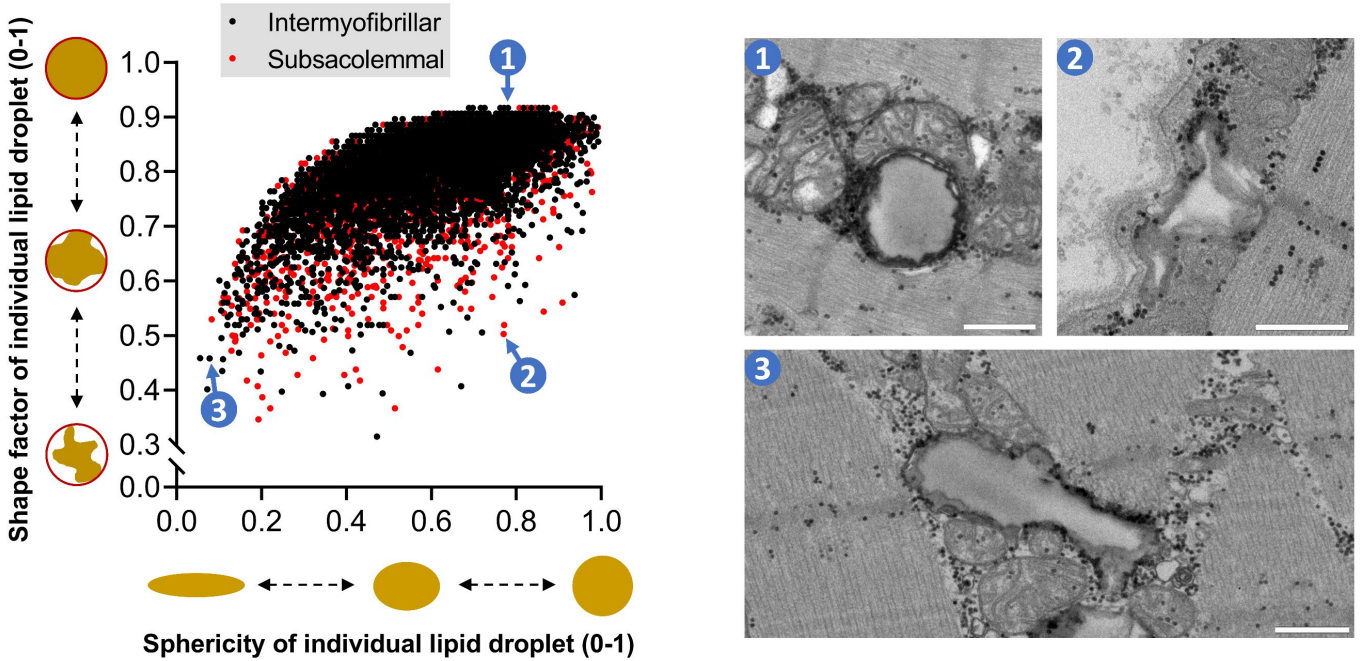

Figure 21. Quantification of lipid droplet shape factor and sphericity in the intermyofibrillar (black circles) and subsarcolemmal (red circles) regions. A total of 8,123 (Pre: n=5,321; Post: n=2,751) droplet organelles were analyzed across groups by manually tracing their surface membrane. Electron micrographs numbered 1–3 correspond to the plotted lipid droplets beside (scale bars = 0.5 μm).

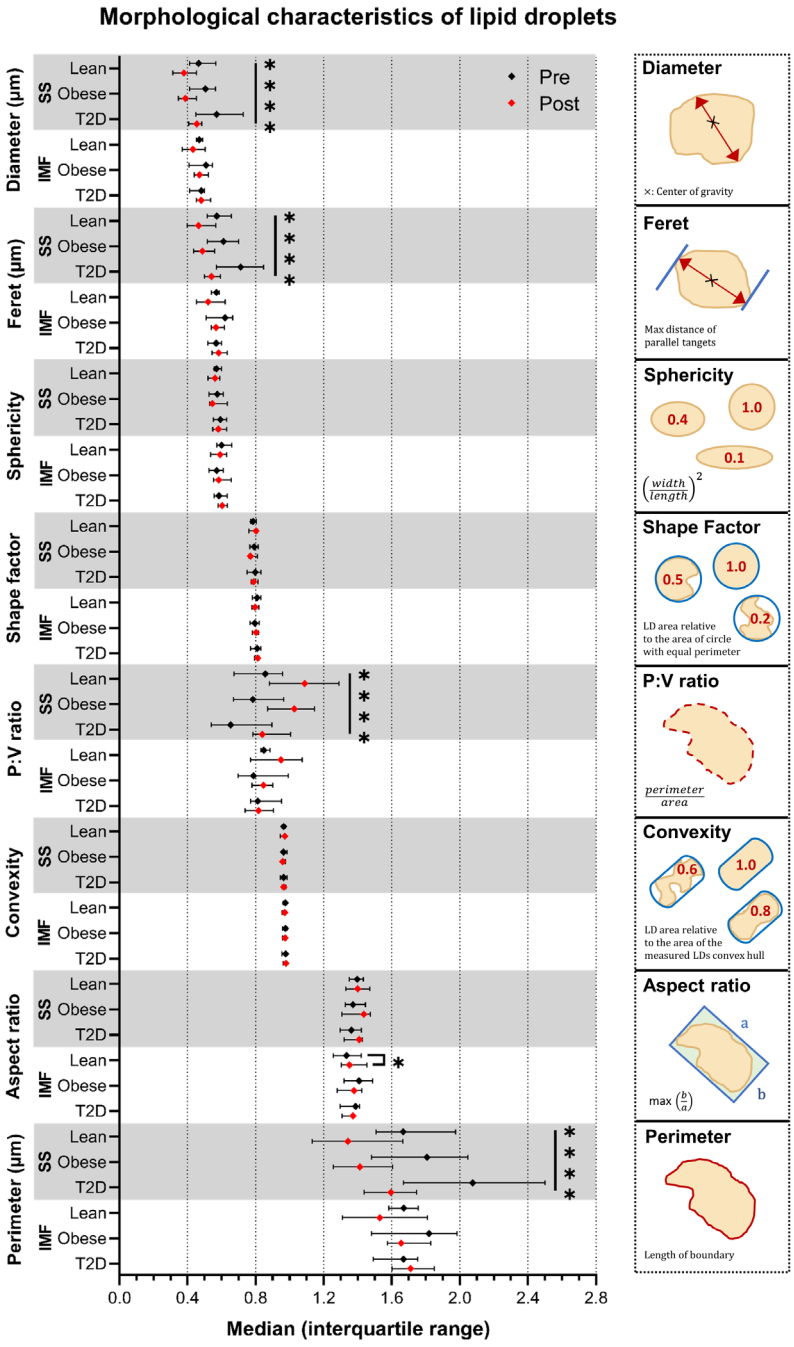

Figure 22. Effects of HIIT on lipid droplet morphology across fiber types. Multiple size and shape descriptors were assessed by manually tracing the surface of individual subsarcolemmal (SS) and intermyofibrillar (IMF) lipid droplets in an interpolated polygon. Graphical explanations are displayed for each variable. P:V ratio, perimeter-to-volume ratio (same as P:A ratio). Data are presented as medians with IQR. Lean: n=13–14; Obese: n=14–14; T2D: n=12–14. Simple linear mixed-effects model: *P<0.05; ****P<0.0001.

04.02.04 Lipid droplet-mitochondrial contact

Baseline characteristics

We determined various indicators for LD-mitochondrial contact in electron micrographs by manually outlining individual droplets and tracing the length of inter-organelle contact with neighboring mitochondria (Fig. 10). When quantifying the percentage (%) of LDs in contact with mitochondria, the obese controls and patients with type 2 diabetes have ~10% and ~20% fewer touches, respectively, in the subsarcolemmal region of type 2 fibers than lean controls (Fig. 23C). However, this contrasted with the findings in type 1 fibers, displaying ~10% additional touches for subsarcolemmal LDs in the patients with type 2 diabetes than in obese controls. Although not detecting any other differences between groups at baseline, contact between LDs and mitochondria was generally higher in type 1 fibers than in type 2 fibers of all three groups (Fig. 23A–C).

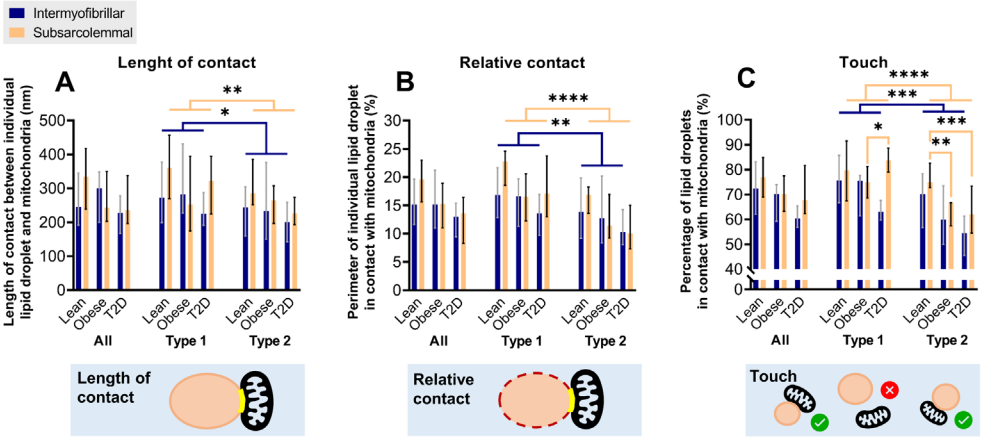

Figure 23. Lipid droplet-mitochondria contact at baseline. Length of contact (nm, ***A***) and relative contact (%, ***B***) between individual lipid droplets and mitochondria in the intermyofibrillar (blue bars) and subsarcolemmal (yellow bars) regions of skeletal muscle fibers at baseline. ***C***: Percentage (%) of lipid droplets in contact (touch) with mitochondria. Graphical explanations for lipid droplet-mitochondria contact. Data are presented as medians with IQR. Lean: n=9–14; Obese: n=10–14; T2D: n=12–14. Simple linear mixes-effects model: **P*<0.05; ***P*<0.01; ****P*<0.001; *****P*<0.0001.

Effects of HIIT

In the intermyofibrillar region, HIIT increased the percentage of LDs in contact with mitochondria across fiber types in patients with type 2 diabetes but also decreased contact in type 2 fibers of the lean controls (**Fig. 25B**). This apparent contradictory finding emphasizes the complexity within LD-mitochondria contact, which seems to be affected by the content of both LDs and mitochondria as well as molecular factors facilitating inter-organelle contact. In the subsarcolemmal region, HIIT decreased the absolute contact length and the touches by ~10–20% in type 2 fibers of all three groups (**Fig. 24** and **25C**). These findings might relate to the observed declines in the size of subsarcolemmal LDs (**Fig. 17A**), thus having a lower physical probability of getting in contact with neighboring mitochondria. However, as patients with type 2 diabetes stored bigger LDs in the subsarcolemmal region (**Fig. 13C**) while having fewer mitochondrial touches (**Fig. 23C**) at baseline, this is conflicting and suggests a dysfunctional interplay between organelles in insulin-resistant conditions.

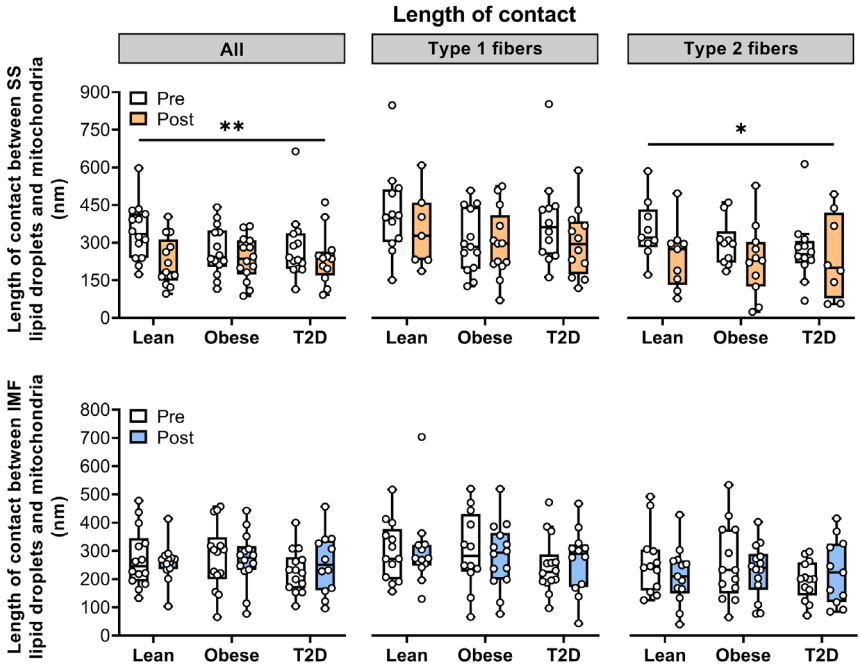

Figure 24. Effects of HIIT on absolute length of contact (nm) between individual lipid droplets and mitochondria length in the subsarcolemmal (SS, yellow boxes) and intermyofibrillar (IMF, blue boxes) regions of skeletal muscle fibers. Box and whiskers represent medians, IQR, and adjacent values. Lean: n=7–14; Obese: n=10–14; T2D: n=8–14. Simple linear mixed-effects model: **P*<0.05; ***P*<0.01.

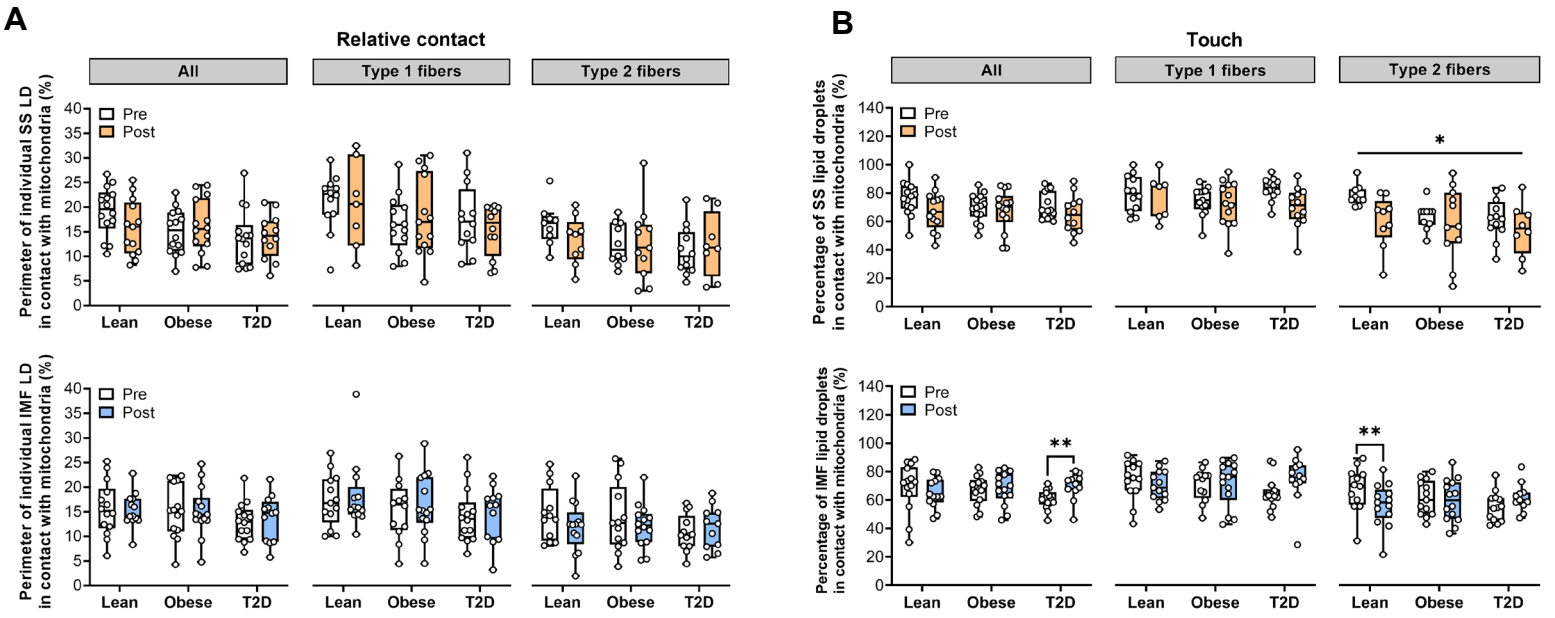

Figure 25. Effects of HIIT on lipid droplet-mitochondria relative contact (%; ***B***) and touch (%; ***C***) in the subsarcolemmal (SS, yellow boxes) and intermyofibrillar (IMF, blue boxes) regions of skeletal muscle fibers. Box and whiskers represent medians, IQR, and adjacent values. Lean: n=7–14; Obese: n=10–14; T2D: n=8–14. Simple linear mixed-effects model: **P*<0.05; ***P*<0.01.

04.03 Study III

04.03.01 Blood sampling and substrate oxidation during the acute exercise test

The participants performed a 60 min acute exercise test with the collection of blood samples, muscle biopsies, and measures of indirect calorimetry (**Fig. 4**). Individual data on average intensity (%$\dot{V}O_2$max) during the exercise were reported at the group level and connected between matched participants from each group (**Fig. 26A**). Although blood lactate increased in all three groups during exercise (**Fig. 26B**), these levels were generally higher in the obese groups than in the lean group, which is consistent with previous studies showing that obesity and insulin resistance is associated with elevated lactate levels (Reaven *et al.*, 1988; Lovejoy *et al.*, 1992). In addition, plasma glucose levels were higher in patients with type 2 diabetes than in lean and obese controls (**Fig. 26C**).

The RER declined throughout the 60 min exercise, from ~0.95 to ~0.90, with no differences between the groups, neither on average for the whole exercise bout nor at time points during the exercise bout (**Fig. 26D and E**). Accordingly, fat oxidation increased gradually (**Fig. 26G**), and average values did not differ between the groups (**Fig. 26F**). However, at the initial step (6–10 min), exercise-induced fat oxidation was markedly lower (~80%) in patients with type 2 diabetes compared to lean controls (**Fig. 26G**), suggesting a diminished acute metabolic response upon exercise stimuli in type 2 diabetes. Carbohydrate oxidation did not change over time and was not different between the groups (**Fig. 26H and I**). In total, energy expenditure increased during the exercise in all three groups, but it was generally lower in patients with type 2 diabetes (**Fig. 26J and K**). This discrepancy can be explained by group-specific differences in physical fitness (**Table 3**), resulting in different median (IQR) workloads (T2D: 80 (70–86) watts; Lean: 115 (87–135) watts; Obese: 103 (69–110) watts) during the exercise at matched relative intensities (%$\dot{V}O_2$max).

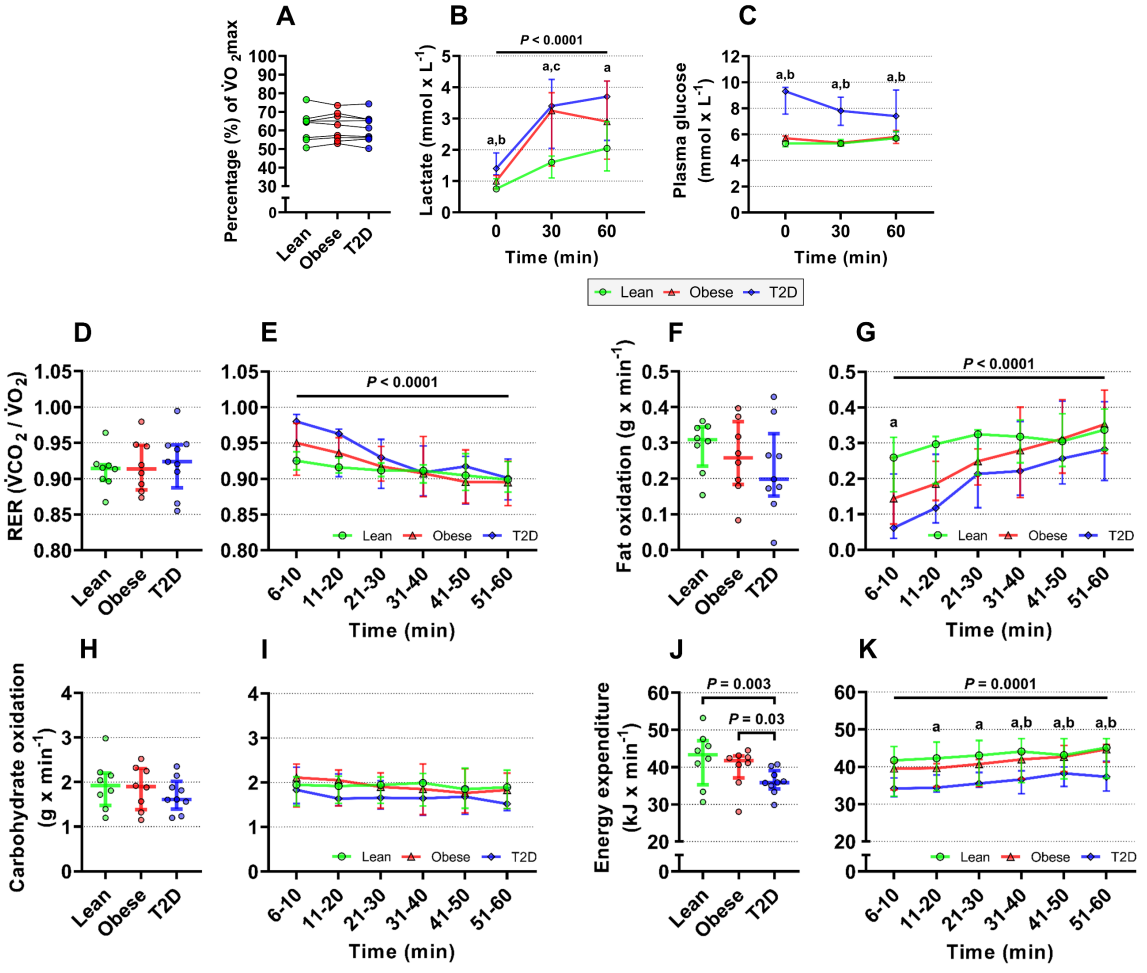

Figure 26. ***A***: Participants were matched in triplets and twins (7 and 2, respectively) due to their respective relative intensity (%$\dot{V}O_2$max) during the acute exercise. Lactate (mmol/L; ***B***) and plasma glucose (mmol/L; ***C***) levels were measured at baseline (min 0), midway (min 30), and immediately after (min 60) the acute exercise. Average and continuous values for respiratory exchange ratio (RER, $\dot{V}CO_2/\dot{V}O_2$; ***D*** and ***E***), fat oxidation (g/min; ***F*** and ***G***), carbohydrate oxidation (g/min; ***H*** and ***I***), and energy expenditure (kJ/min; ***J*** and ***K***) during the acute exercise. Data are presented as medians with IQR. Lean: n=8; Obese: n=8; T2D: n=9. Simple linear mixed-effects model: **a***P*<0.05 in T2D vs. Lean; ***bP***<0.05 in T2D vs. Obese; ***cP***<0.05 in Obese vs. Lean.

04.03.02 Effects of acute exercise on lipid droplet volume fractions, numbers, and size

The 60 min exercise did not change the volume fractions, numbers, or size of LDs at any distinct subcellular regions or fiber types (**Fig. 27** and **28**). Neither did we observe any changes in the relative distributions of LDs (**Supplemental Fig. 4**). However, in lean controls, correlation analysis showed that the individuals with the highest fat oxidation rate during the exercise demonstrated a greater net reduction in the number of intermyofibrillar LDs (**Fig. 29B**). This was not observed for the subsarcolemmal LDs, or in obese controls or patients with type 2 diabetes (**Fig. 29A**).

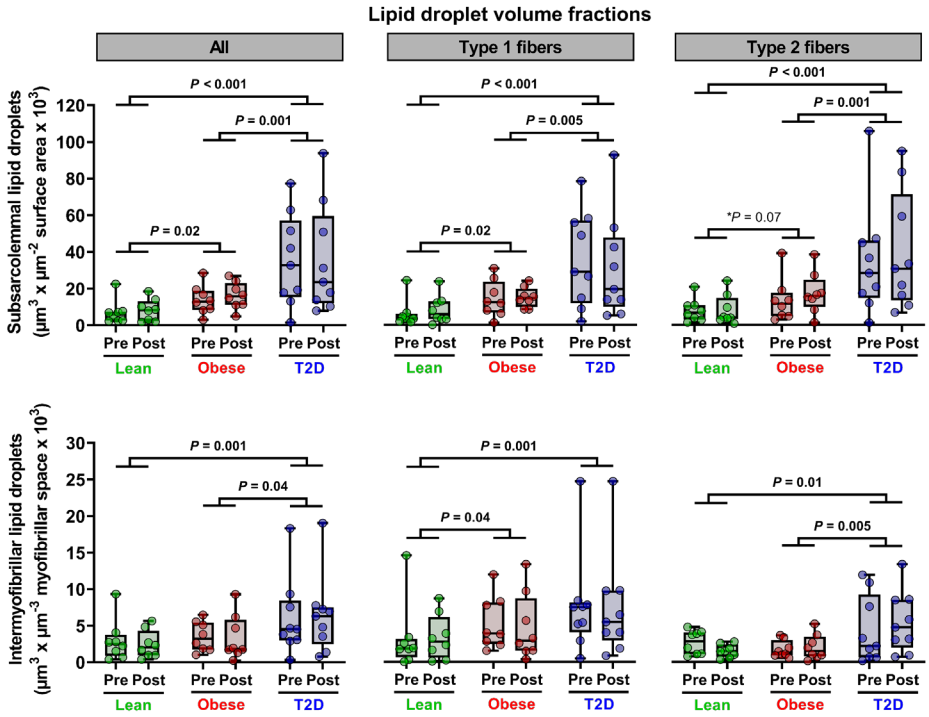

Figure 27. Effects of acute exercise on lipid droplet volume fractions in the intermyofibrillar and subsarcolemmal regions of skeletal muscle fibers. Box and whiskers represent medians, IQR, and adjacent values. Lean: n=8; Obese: n=8; T2D: n=9. Simple linear mixed-effects model.

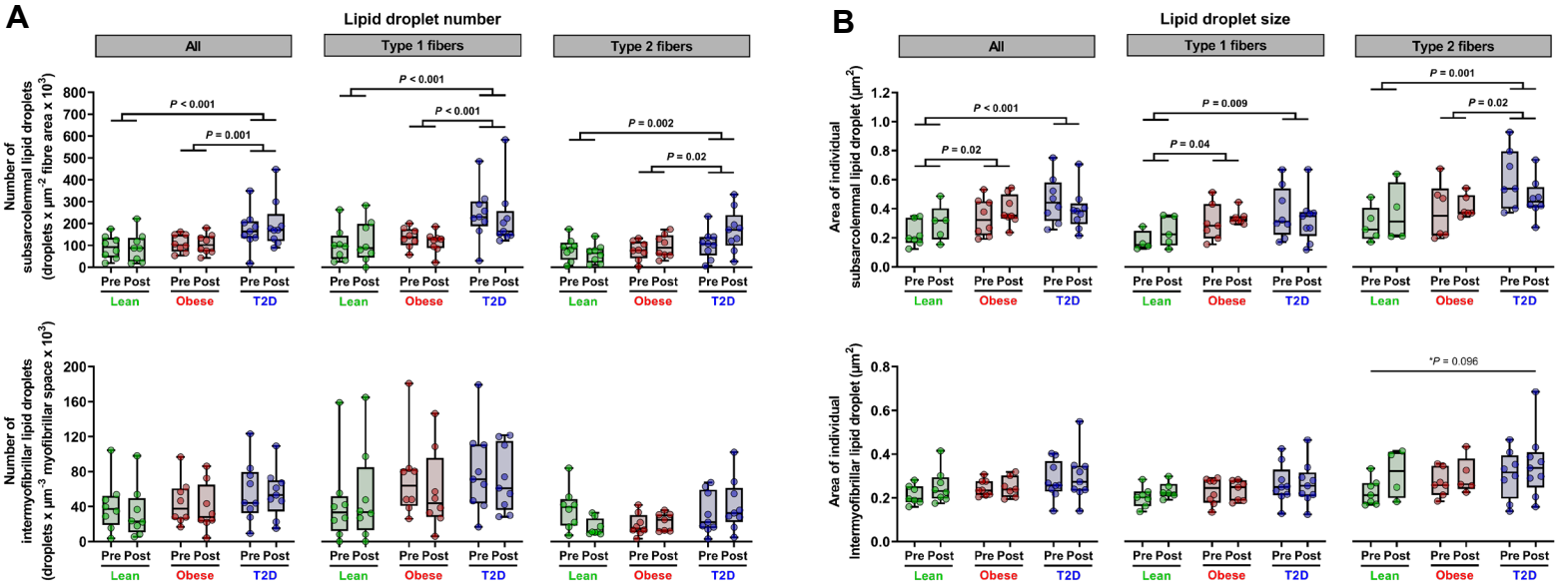

Figure 28. Effects of acute exercise on lipid droplet numbers (***A***) and size (***B***) in the intermyofibrillar and subsarcolemmal regions of skeletal muscle fibers. Box and whiskers represent medians, IQR, and adjacent values. In *A*, Lean: n=8; Obese: n=8; T2D: n=9. In *B*, Lean: n=4–8; Obese: n=5–8; T2D: n=7–9. Simple linear mixed-effects model.

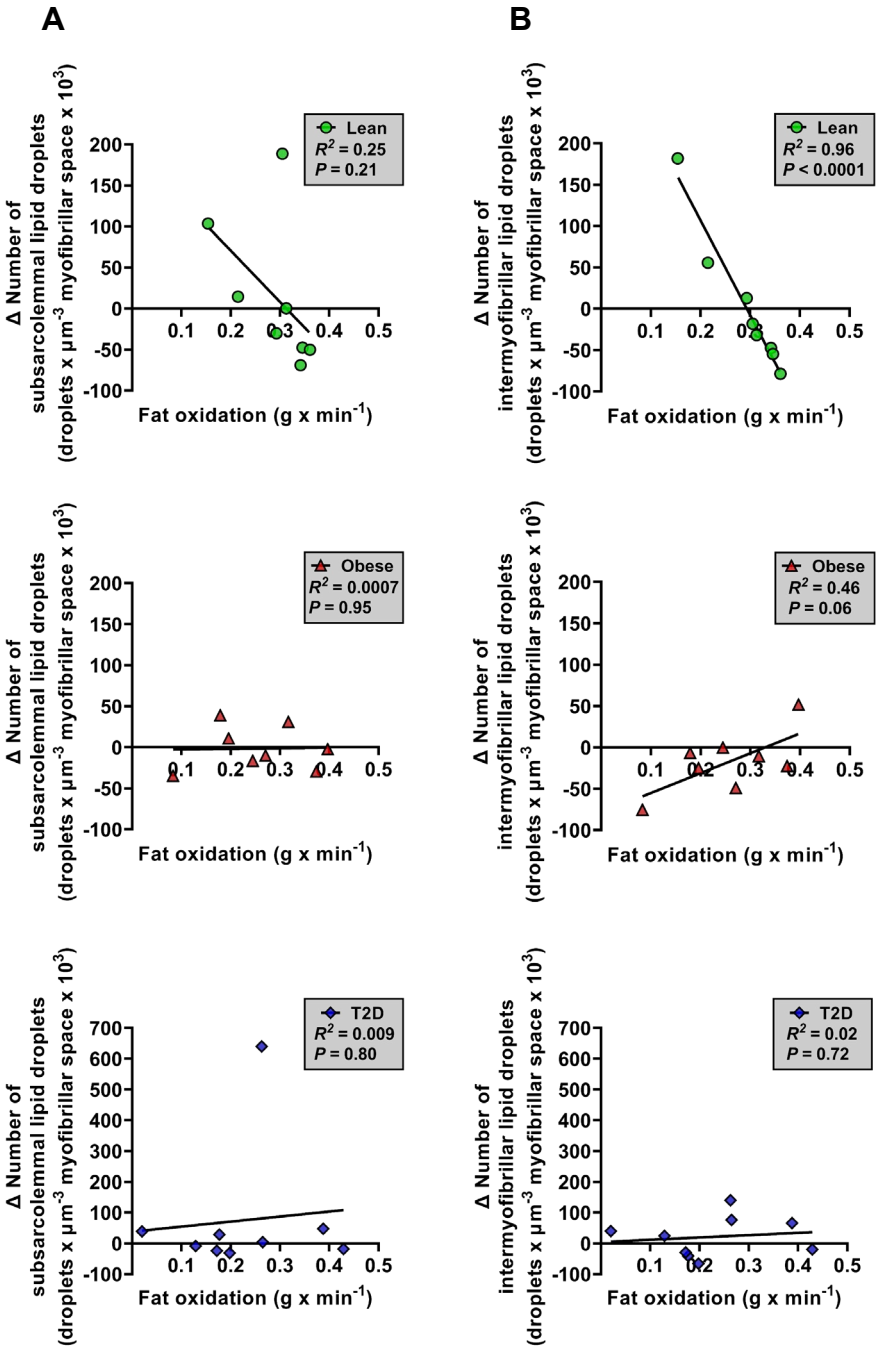

Figure 29. Correlation analysis between exercise-mediated changes (Δ) in subsarcolemmal (***A***) and intermyofibrillar (***B***) lipid droplet numbers and fat oxidation (g/min) in the Lean (green circles), Obese (red triangles) and T2D (blue diamonds). See **Supplemental Fig. 5** for correlation analysis between changes (Δ) in subcellular LD volume fractions and fat oxidation (g/min). Lean: n=8; Obese: n=8; T2D: n=9.

04.03.03 Effects of acute exercise on lipid droplet morphology

Across fiber types, acute exercise did not change LD size descriptors for either perimeter, diameter, Feret, or P:A ratio (**Fig. 30**). However, the higher sphericity (~4%) and lower aspect ratio (~3%) for subsarcolemmal LDs after exercise, indicate that these specific droplets get more spherical in shape after exercise. This effect was most profound in type 1 fibers (**Supplemental Fig. 6**). We did not detect changes in shape descriptors for shape factor or convexity following exercise (**Fig. 30**).

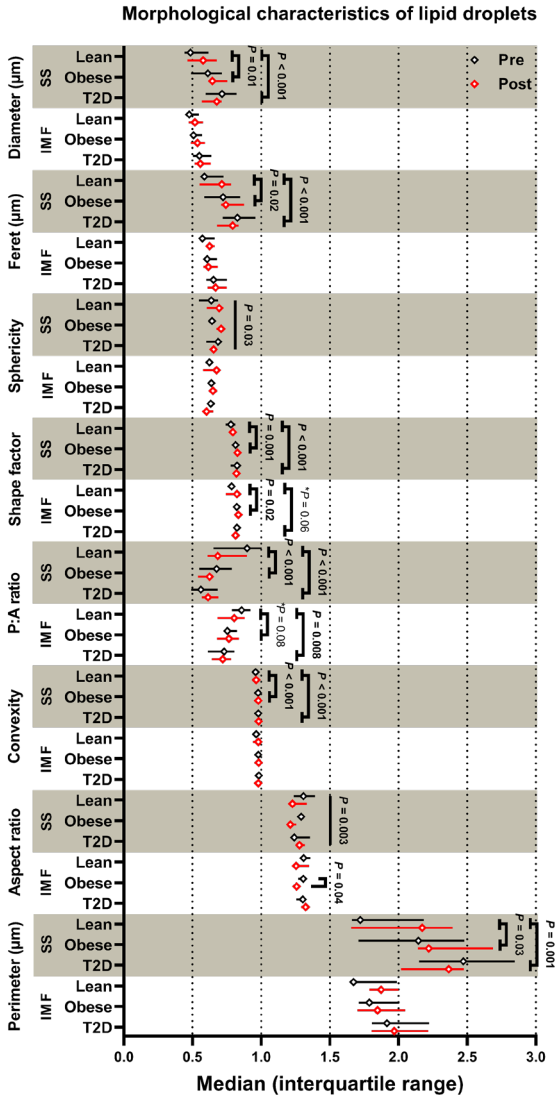

Figure 30. Effects of acute exercise on lipid droplet morphology across fiber types. Multiple size and shape descriptors were examined by manually tracing the surface of individual subsarcolemmal (SS) and intermyofibrillar (IMF) lipid droplets in an interpolated polygon. P:A ratio: perimeter-to-area ratio. Data are presented as medians with IQR. Lean: n=5–8; Obese: n=7–8; T2D: n=8–9. Simple linear mixed-effects model: ***$P<0.001$; ****$P<0.0001$.

04.03.04 Effects of acute exercise on lipid droplet-mitochondrial contact

Acute exercise enhanced the connective interplay between LDs and mitochondria across all three groups (**Fig. 31** and **32**). This effect was most profound in the subsarcolemmal space of type 1 fibers, and here the absolute contact length increased on average from ~275 to ~420 nm (**Fig. 31**) while the relative measured LD-mitochondria contact increased on average from ~10 to ~20% (**Fig. 32A**). Furthermore, these type-specific changes in oxidative muscle fibers also tended to increase the percentage of subsarcolemmal LDs touching mitochondria (**Fig. 32B**). We observed more insecure results in the intermyofibrillar space but with similar trends for increased contact between LDs and mitochondria after exercise (**Fig. 31** and **32**). Here, the effect was most pronounced in the obese controls (**Fig. 31A and B**). Histograms of the length of LD-mitochondrial contact reveal decreases of up to ~15%-point in LDs without any mitochondrial contact and a resultant right shift in the distribution of absolute contact length between organelles; but with no differences between the groups (**Fig. 33A**). Interestingly, length of contact between LDs and mitochondria before exercise (ranging from ~140 to ~430 nm) was associated with the fat oxidation rate during exercise across groups and in patients with type 2 diabetes but, to a lesser extent, in obese and lean controls (**Fig. 33B**). This association was less evident when separating in subcellular regions (**Fig. 33C and D**).

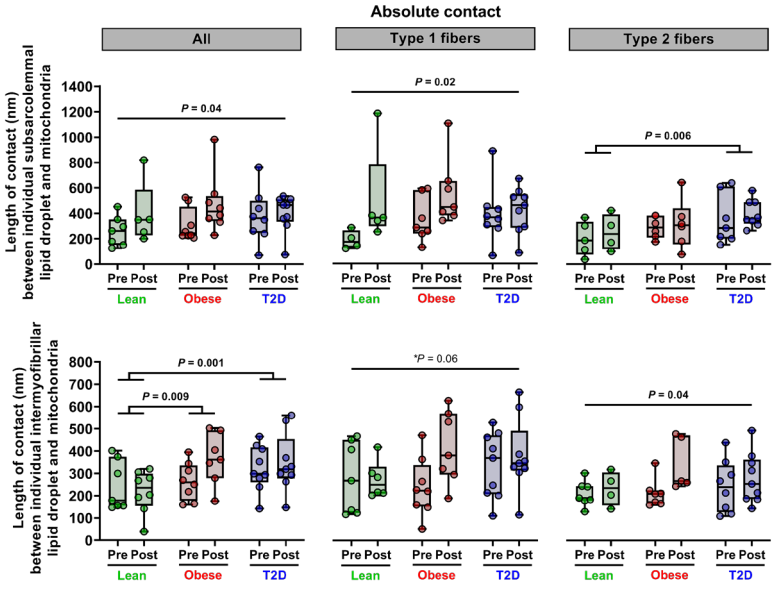

Figure 31. Effects of acute exercise on lipid droplet-mitochondria length of contact (nm) in the subsarcolemmal and intermyofibrillar regions of muscle fibers. Box and whiskers represent medians, IQR, and adjacent values. Lean: n=4–8; Obese: n=5–8; T2D: n=7–9. Simple linear mixed-effects model.

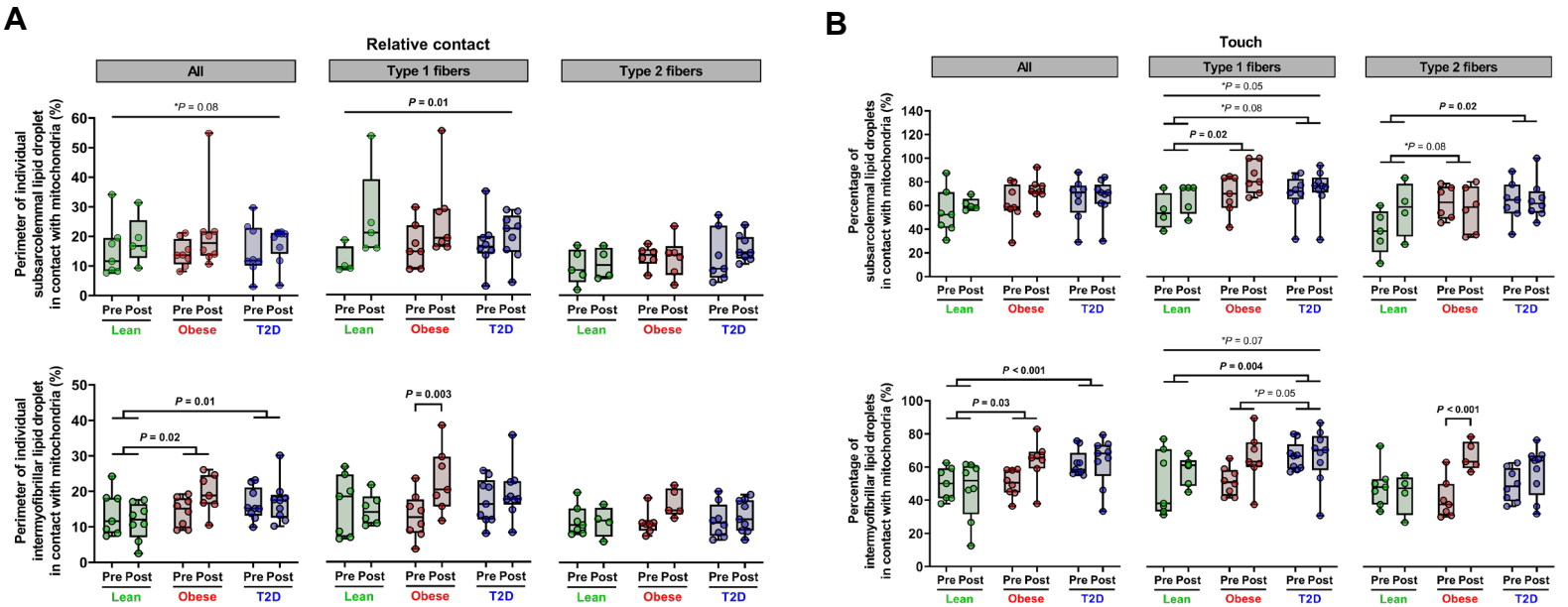

Figure 32. Effects of acute exercise on lipid droplet-mitochondria relative contact (%; ***A***) and touch (%; ***B***) in the subsarcolemmal and intermyofibrillar region of skeletal muscle fibers. Box and whiskers represent medians, IQR, and adjacent values. Lean: n=4–8; Obese: n=5–8; T2D: n=7–9. Simple linear mixed-effects model.

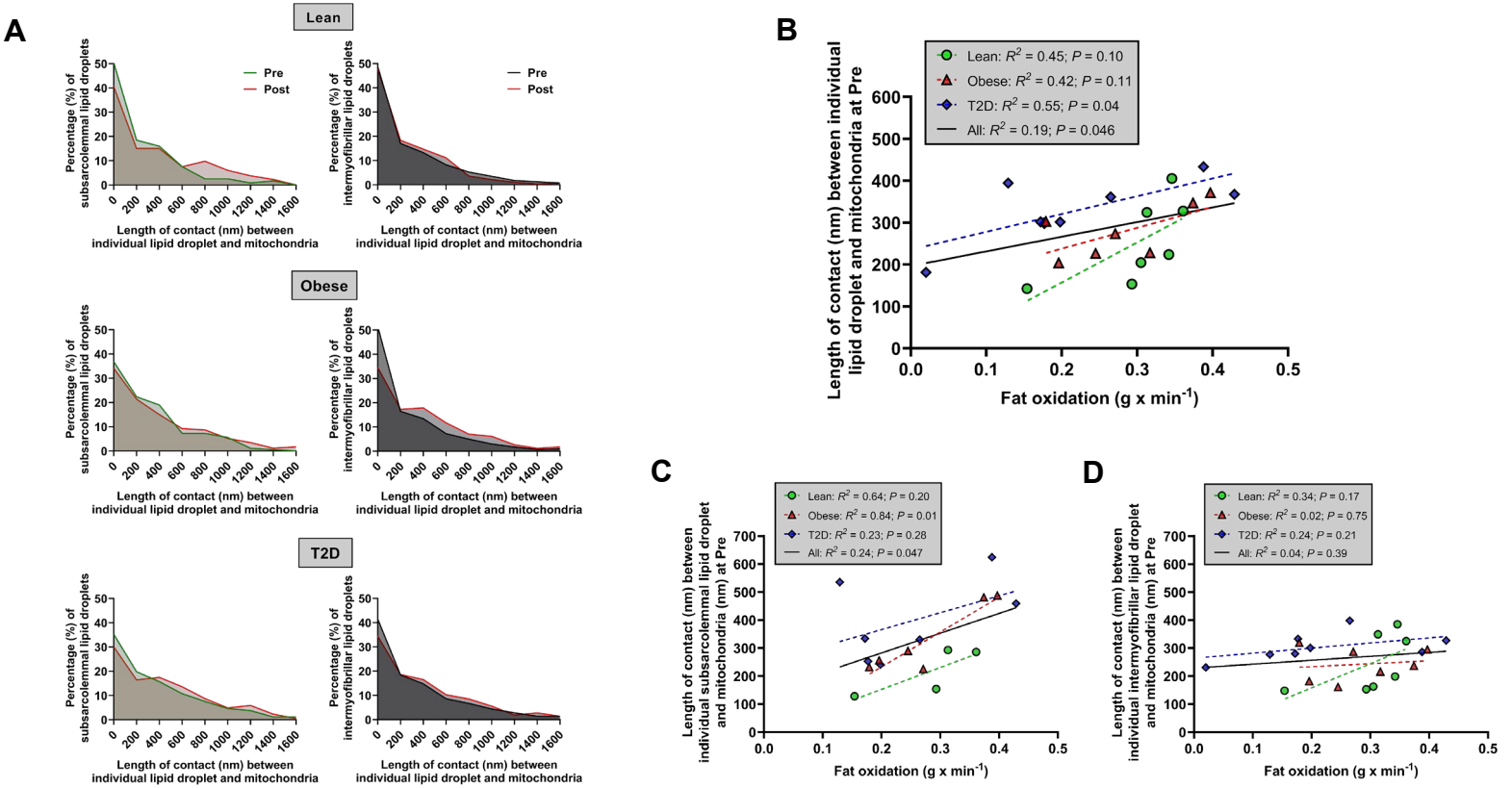

Figure 33. ***A***: Histograms displaying distributions (%) of lipid droplet-mitochondrial length of contact (nm) Pre and Post the acute exercise. Values were estimated from subsarcolemmal (Lean: n=255; Obese: n=363; T2D: n=744) and intermyofibrillar (Lean: n=684; Obese: n=752; T2D: n=1,158) lipid droplets across fiber types. ***B***–***D***: Correlation analysis between LD-mitochondrial length of contact (nm) at baseline (Pre) and fat oxidation (g/min) during exercise across subcellular compartments (***B***) and separated for the subsarcolemmal (***C***) and intermyofibrillar (***D***) regions in the Lean (green circles), Obese (red triangles) and T2D (blue diamonds). In *B*–*D*, Lean: n=4–7; Obese: n=6–7; T2D: n=7–8.

05 Discussion

05.01 Key findings

The present study showed that type 2 diabetes differentiates from obesity by having altered networks of LDs and mitochondria across skeletal muscle fibers. We conducted a comprehensive single-cell morphological analysis and demonstrated that the excessive storage of intramuscular lipids in patients with type 2 diabetes was present as extremely large LDs situated in muscle fibers with a location-specific deficiency in subsarcolemmal mitochondria. HIIT combining rowing and cycling changed this intramuscular deficiency toward non-diabetic characteristics by remodeling the size and subcellular distribution of LDs and the content of mitochondria, accompanied by marked increases in insulin sensitivity, with intact responses in all three groups, and a clinically relevant reduction in HbA1c and fasting plasma glucose levels in patients with type 2 diabetes. These results indicate that supervised HIIT recruiting several muscle groups is a promising exercise mode in inactive individuals with type 2 diabetes or obesity. We also examined the acute effects of exercise on these muscle properties. Although exercise did not change the LD content nor mediated changes in the LD volumetric composition (size or number), the contact between LDs and mitochondria increased irrespective of obesity or type 2 diabetes. This effect was most profound in the subsarcolemmal region of type 1 fibers, and here both touches and the absolute contact length increased in all three groups. Correlation analyses further revealed that 1) in the lean controls, but not in the two obese groups, a high fat oxidation rate was positively associated with a net reduction in intermyofibrillar LD numbers, and 2) across all groups, the magnitude of pre-exercise contact between LDs and mitochondria was a strong predictor for the individual fat oxidation rate during exercise.

05.02 HIIT of rowing and cycling efficiently improves insulin sensitivity in obesity and type 2 diabetes (Study I)

We and others have previously demonstrated that 8–10 weeks of supervised endurance training on cycle ergometers or treadmill increase insulin-stimulated GDR by ~10–20% in patients with type 2 diabetes and glucose-tolerant individuals with obesity (De Filippis *et al.*, 2008; Vind *et al.*, 2011). However, this effect was more profound (~30%) in untrained young, lean individuals following a similar ten-week endurance training intervention (Christensen *et al.*, 2013), suggesting a lower exercise-induced response in obesity and type 2 diabetes, as

previously described (Burns *et al.*, 2007). The present study demonstrates that eight weeks of supervised HIIT combining rowing and cycling improves insulin-stimulated GDR by ~30–40%, irrespective of obesity or type 2 diabetes. Although methodological differences might explain some of these variations in training responses, this HIIT protocol seems to increase insulin sensitivity ~two-fold higher than previous endurance training studies in individuals with obesity or type 2 diabetes (De Filippis *et al.*, 2008; Vind *et al.*, 2011), and importantly, there was no indication of exercise resistance. Interestingly, in response to HIIT, patients with type 2 diabetes achieved a comparable level of insulin sensitivity and metabolic flexibility (ΔRER) as the obese and lean controls at baseline.

Using surrogate markers for insulin sensitivity such as HOMA-IR, previous studies have compared the effects of 11–12 weeks of supervised HIIT and endurance training upon insulin sensitivity in patients with type 2 diabetes (Mitranun *et al.*, 2014; Winding *et al.*, 2018). While HIIT consistently improves HOMA-IR by ~20–25%, similar and no effects are reported after endurance training. Thus, it seems that HIIT has at least the same or even better effects on HOMA-IR compared to endurance training in patients with type 2 diabetes. Intriguingly, only a few studies have examined the effects of HIIT using the HE clamp. In young lean and elderly obese individuals, 6–12 weeks of supervised HIIT increased insulin-stimulated glucose uptake by ~10–20% (Robinson *et al.*, 2017; Søgaard *et al.*, 2018), and in young individuals with overweight, two weeks of the more intense sprint-interval training (SIT) form increased insulin-stimulated GIR by ~25% (Richards *et al.*, 2010). Considering previous HIIT and SIT studies, our results of ~30–40% increases in insulin sensitivity may not solely ascribe to the choice of HIIT vs. endurance training. Based on previous studies demonstrating that insulin sensitivity may only increase in exercised muscle groups (Wojtaszewski *et al.*, 2000; Frosig *et al.*, 2007) and, opposite, decrease in non-exercised muscle groups (Steenberg *et al.*, 2020) upon acute stimuli, we designed this HIIT protocol to take full advantage of insulin-sensitizing effects by recruiting both upper and lower body muscle groups. Although we cannot exclude a role for other differences in the design, e.g., longer training durations of the HIIT sessions during the last weeks as compared with other HIIT protocols (Robinson *et al.*, 2017; Søgaard *et al.*, 2018), the activation of a large quantity of muscle tissue may, to a large extent, explain the marked effects on insulin sensitivity.

05.03 Single-fiber dependent storage of extremely large lipid droplets in patients with type 2 diabetes (Study II)

Our findings align with others, showing that patients with type 2 diabetes have impaired mitochondrial function (Ruegsegger *et al.*, 2018) and that a fragmented mitochondrial network (Jheng *et al.*, 2012; Sergi *et al.*, 2019; Houzelle *et al.*, 2021) might be implicated in the etiology of skeletal muscle insulin resistance. Mechanistically, an imbalance between fission and

fusion proteins leads to more divided and smaller mitochondria (Fealy *et al.*, 2018), which, in turn, have a decreased capacity to oxidize fatty acids (Rambold *et al.*, 2015). The present study demonstrated that single muscle fibers from patients with type 2 diabetes, containing a low density of subsarcolemmal mitochondria, display an excessive accumulation of extremely large LDs. In comparison, single fibers containing a high density of subsarcolemmal mitochondria were not different in LD storage between the three groups. In that respect, long-chain acyl-CoA synthetases (ACSLs) facilitate a critical switch from glucose to fatty acid oxidation (Li *et al.*, 2010). Indeed, compromised ACSL1 function causes a drop in muscle fat oxidation, excessive glucose utilization, and impaired systemic glucose homeostasis (Li *et al.*, 2015). Together with intrinsic declines in electron transport chain activity, as demonstrated in subsarcolemmal mitochondria of patients with type 2 diabetes (Ritov *et al.*, 2005), compromised ACSL1 could mediate the accumulation of enlarged LDs. Single-cell investigations have further revealed that glycogen-related proteins are dysregulated, specifically in type 2 fibers of patients with type 2 diabetes (Frankenberg *et al.*, 2022), but also that reduced insulin signaling in type 2 diabetes is fiber type independent (Albers *et al.*, 2015). Thus, it needs to be investigated how insulin signaling, GLUT4 trafficking, and finally glucose uptake are affected by the network and function of LDs and mitochondria in human skeletal muscle fibers.

We confirm previous studies (Nielsen *et al.*, 2010; Daemen *et al.*, 2018; Koh *et al.*, 2018; Li *et al.*, 2019) and show that patients with type 2 diabetes store ~1.5-fold larger subsarcolemmal LDs than glucose-tolerant lean and BMI-matched obese controls. In the present study, we extend these observations by revealing extremely large subsarcolemmal LDs (0.9 μm^2 profile area) in type 2 fibers of patients with type 2 diabetes. This study is the first to demonstrate this in the context of type 2 diabetes independently of obesity. Intriguingly, these enlarged LDs could explain the ~twofold increase in subsarcolemmal LDs, as observed in patients with type 2 diabetes. By employing TEM, we recently demonstrated that the size, but not the numbers, of subsarcolemmal LDs, were inversely associated with insulin sensitivity in untrained lean males (Nielsen *et al.*, 2017), suggesting that particularly the size of individual subsarcolemmal LDs may play an underlying role in the pathogenesis of insulin resistance. Despite these findings, little is known concerning the physiological conditions of LD size in different cell types (Welte, 2015), and it remains nearly elusive in the human skeletal muscle (Bosma, 2016). In theory, small LDs, which have a high surface-to-volume ratio, may facilitate efficient lipolysis by providing easy access for the lipases to the lipid core, whereas large LDs might result from net TAG storage (Hesselink *et al.*, 2004; Suzuki *et al.*, 2011). Therefore, an optimal surface-to-volume ratio could be the driving force leading to more ellipsoid-shaped LDs, which might be a cost-effective way to increase this ratio. However, this has yet to be investigated in an experimental setup. Nevertheless, we demonstrated that variations in LD shape, together with variations in size, affect its surface-to-volume ratio. Interestingly, in

epithelial cells (CHO K2 cells), isolating LDs into various size categories revealed differential composition and capability to recruit proteins (Zhang *et al.*, 2016), suggesting heterogeneous functions of LD subpopulations. This observation might be of specific relevance for type 2 fibers, in which expressions of lipolytic proteins are lower than in type 1 fibers (Minnaard *et al.*, 2009; Shepherd *et al.*, 2014). Thus, the liberation of fatty acids could be limited for large LDs, making these specific droplets prone to incomplete lipolysis.

05.04 Subsarcolemmal lipid droplets, HIIT remodeling effect, and role for insulin sensitivity (Study II)

We demonstrated that HIIT was an effective training form to increase the number of intermyofibrillar LDs while reducing the size of individual subsarcolemmal LDs. The latter finding aligns with other exercise training studies, including either endurance training (Nielsen *et al.*, 2010; Devries *et al.*, 2013; Samjoo *et al.*, 2013; Li *et al.*, 2014) or HIIT (Koh *et al.*, 2018), consistently reporting a reduction in the volumetric content of subsarcolemmal LDs (~40–50%) of inactive overweight and patients with type 2 diabetes. In addition, the marked improved insulin sensitivity in the present study suggests a role for the subsarcolemmal LDs in insulin-stimulated glucose uptake. Although we did not demonstrate robust correlations, previous studies have reported correlations between volumetric content and size of subsarcolemmal LDs and insulin sensitivity, as measured by the HE-clamp (Nielsen *et al.*, 2010; Nielsen *et al.*, 2017). In the subsarcolemmal space, LDs are located near the sarcolemma, and here, the transverse tubular system (t-system) is not surrounded (and protected) by the sarcoplasmic reticulum. In comparison, intermyofibrillar LDs are often located close to mitochondria but in remote places from the t-system, enclosed by the sarcoplasmic reticulum. In that respect, specific species and localization of bioactive lipids such as diacylglycerols (DAGs) and sphingolipids are suggested to play delirious roles (Bergman & Goodpaster, 2020). Although much controversy exists herein, it is shown that subsarcolemmal ceramides, specifically the C16 and C18 chain lengths, correlate with markers of insulin resistance (Chung *et al.*, 2017; Perreault *et al.*, 2018).

05.05 Effects of HIIT on contact between lipid droplets and mitochondria (Study II)

Previous studies have demonstrated that 4–12 weeks of endurance and sprint interval training increase the number of LDs in contact with neighboring mitochondria in inactive obese and lean controls (Tarnopolsky *et al.*, 2007; Devries *et al.*, 2013; Shepherd *et al.*, 2017). However, this was not shown in patients with type 2 diabetes following 11 weeks of HIIT (Koh *et al.*, 2018). Since a large portion of extracellular fatty acids flux through intramuscular LDs before being oxidized in mitochondria (Meex *et al.*, 2015), this might be a likely adaptation,

suggesting that the tight inter-organelle connection promotes a direct pathway for fatty acid delivery to the mitochondria reticulum for oxidative phosphorylation (Rambold *et al.*, 2015). Thus, the more significant contact between LDs and mitochondria might help the efficient trafficking of LD-derived fatty acids to the mitochondria and cause rises in fat oxidation capacities. However, these observations contrasted with our results showing that HIIT led to decreases in touches and length of contact between subsarcolemmal LDs and mitochondria in type 2 fibers, unraveling the complexity within LD-mitochondria contact. Interestingly, recent insights into brown adipose tissue challenge the proposed directionality of energy transfer between organelles and show that mitochondria interacting with LDs [peridroplet mitochondria (PDM)] have unique functional properties compared with cytoplasmic mitochondria (Benador *et al.*, 2018). With an isolation approach to separate PDM and cytoplasmic "free" mitochondria, PDM exhibited higher pyruvate oxidation but lower beta-oxidation capabilities. Although this remains to be investigated in the skeletal muscle, these findings suggest a putative role for PDM in LD expansion by supplying ATP for TAG synthesis rather than breakdown.

Since previous studies investigating the exercise-mediated changes in LD-mitochondria contact did not report any reductions in LD size (Tarnopolsky *et al.*, 2007; Devries *et al.*, 2013; Shepherd *et al.*, 2017), declines in subsarcolemmal LD size, as demonstrated in the present study, could potentially explain the observed decreases in inter-organelle contact after HIIT. As such, the physical interaction with neighboring partner organelles may also decrease as individual LDs get smaller. However, this assumption conflicts with our results of bigger LDs and reduced mitochondrial contact in the subsarcolemmal region of patients with type 2 diabetes at baseline, indicative of altered LD-mitochondria contact in insulin-resistant conditions. The regulation of energy transfer between contact sites of the two organelles is suggested to be orchestrated by the LD-associated perilipins (PLINs), in which PLIN2 and PLIN5 are the most studied PLINs in the skeletal muscle of type 2 diabetes (Najt *et al.*, 2022). The abundance of PLIN2 at the LD surface seems to be higher in patients with type 2 diabetes than in endurance-trained athletes, whereas PLIN5 abundance might be lower or comparable in inactive individuals versus trained athletes (Daemen *et al.*, 2018; Gemmink *et al.*, 2018a; Gemmink *et al.*, 2021). PLIN2 may not be directly implicated in LD-mitochondria interactions but is proposed to compromise the accessibility of ATGL to the droplet surface (Listenberger *et al.*, 2007; Kaushik & Cuervo, 2015; Gemmink *et al.*, 2021). Overexpression of PLIN2 has resulted in enlarged LDs, ascribed to a drop in lipolysis and upregulation of TAG incorporation into LDs (Bosma *et al.*, 2012). On the other hand, PLIN5 may act as an LD-mitochondria tether facilitating the breakdown of lipids (Wang *et al.*, 2011; Laurens *et al.*, 2016; Gemmink *et al.*, 2018b; Pribasnig *et al.*, 2018). While much controversy exists in the context of PLINs, future studies should focus on how these are implicated in LD-mitochondria networks and LD size and shape dynamics.

05.06 Unaltered volumetric content of lipid droplets after acute exercise (Study III)

Healthy young lean untrained (Decombaz *et al.*, 2001; Shepherd *et al.*, 2012, 2013; Daemen *et al.*, 2021), moderately active (White *et al.*, 2003; Devries *et al.*, 2007; Egger *et al.*, 2013; Bucher *et al.*, 2014; Chee *et al.*, 2016), and endurance-trained athletes (Staron *et al.*, 1989; Romijn *et al.*, 1993; Krssak *et al.*, 2000; Romijn *et al.*, 2000; Brechtel *et al.*, 2001; Decombaz *et al.*, 2001; Schrauwen-Hinderling *et al.*, 2003; van Loon *et al.*, 2003; Zehnder *et al.*, 2005; Stellingwerff *et al.*, 2007; Vermathen *et al.*, 2012; Koh *et al.*, 2017; Bergman *et al.*, 2018; Jevons *et al.*, 2020) but not metabolically compromised (Chee *et al.*, 2016; Bergman *et al.*, 2018) or elderly lean individuals (Chee *et al.*, 2016) reduce intramuscular LDs during acute exercise. Given the differences in methodology and exercise prescriptions in the previous studies, we confirm these results by demonstrating no net reduction in intramuscular LDs in middle-aged patients with type 2 diabetes nor glucose-tolerant lean and obese controls. In individuals with obesity and type 2 diabetes, the compromised usage may originate from dysfunctional adipose tissue (i.e., disinhibition of adipose tissue lipolysis) accompanied by elevated levels of plasma non-esterified fatty acids (NEFAs) (Boon *et al.*, 2007). This notion aligns with a previous study showing that, upon acute administration of a plasma lipid-lowering agent (Acipimox), the contribution of intramuscular lipids to total fat oxidation increases in patients with type 2 diabetes (van Loon *et al.*, 2005). However, under matched plasma NEFA levels, the utilization of intramuscular lipids was higher in trained individuals than in patients with type 2 diabetes (Bergman *et al.*, 2018), indicating that training-related metabolic adaptions may also play a role herein.

As previously described by others and reported in this study, intramuscular LDs are not uniform; they are located in distinct compartments (intermyofibrillar vs. subsarcolemmal), exist in different sizes and shapes, and differ in their contact with other organelles (as mitochondria) and LD-associated PLINs. Contrary to athletes, patients with type 2 diabetes store an increased number of enlarged LDs, which seems most pronounced in the subsarcolemmal space of glycolytic type 2 fibers (Nielsen *et al.*, 2010; Daemen *et al.*, 2018; Koh *et al.*, 2018). Although we did not detect any group-specific changes in LD content in response to exercise, the changes in intermyofibrillar LD content, primarily due to alterations in LD numbers, correlated with fat oxidation in the lean controls only. Furthermore, individuals with the highest fat oxidation rates showed the most significant reduction in intermyofibrillar LDs. This association is in line with a previous study demonstrating that 1 hour of moderate intensity cycling decreased LD content in the intermyofibrillar, but not the subsarcolemmal space, of recreational active young, lean individuals (Chee *et al.*, 2016). Also, in endurance-trained triathletes (Jevons *et al.*, 2020) and elite cross-country skiers (Koh *et al.*, 2017), exercise decreased the LD content and numbers in the intermyofibrillar space of type 1 fibers, with no

change in the size of individual droplets. These observations not only underline the importance of microscopy-based techniques to detect changes in the subcellular compartments but also provide evidence for the distinct roles of the localized LD pools. As previously proposed by Chee *et al.* (2016), the reduction in intermyofibrillar LD numbers during exercise may suggest a preferential utilization of fatty acids from this pool, conceivably in an “all or nothing” fashion. In support of this notion, studies indicate that healthy lean individuals preferentially use fatty acids stored in LDs associated with PLIN2 (Shepherd *et al.*, 2012, 2013) and PLIN5 (Shepherd *et al.*, 2013) during exercise. While data imply that PLIN5 may facilitate TAG breakdown by interacting with ATGL and its co-activator, CGI-58, PLIN2 does not appear to have this effect (Wang *et al.*, 2011; Gemmink *et al.*, 2018b).

Nevertheless, in a recent study (Daemen *et al.*, 2021), two hours of moderate-intensity cycling reduced subsarcolemmal, but not intermyofibrillar LDs, in overnight-fasted healthy untrained young men. Contrary to athletes, LD storage may be more abundant in those untrained individuals, thus favoring a utilization of subsarcolemmal LDs during exercise. However, considering the present results reporting no effect after one hour of exercise, utilization of subsarcolemmal LDs may require exercise stimuli of longer durations. Another plausible explanation for this apparent discrepant finding may be methodological differences in assessing subcellular compartments.

05.07 Enhanced contact between lipid droplets and mitochondria after acute exercise (Study III)

The effects of acute exercise on the contact between LDs and mitochondria have only been reported in active individuals. In recreationally active to endurance-trained women, but not in men, 90-min of moderate-intensity cycling increased the percentage of LDs touching mitochondria (Devries *et al.*, 2007). Although intramuscular LDs declined similarly in both sexes, fat oxidation was higher in women than in men, speculatively facilitated by the enhanced LD-mitochondrial contact. This observation aligns with our data showing that LD-mitochondrial contact length predicts fat oxidation rate across groups. The role of LD-mitochondrial contact on LD metabolism has also been investigated in male elite cross-country skiers (Koh *et al.*, 2017). In these volunteers, ~1 h of exhaustive exercise increased LD-mitochondrial contact in the intermyofibrillar space of type 1 fibers in the legs despite unaltered LD content. The present data confirm this by demonstrating increased exercise-mediated LD-mitochondrial contact without net reduction in intramuscular LD volume fractions. While the methodology used in the present study does not allow statements on fatty acids flux through LDs, the use of muscular LDs during exercise might match the incorporation of fatty acids into LDs, thus preventing a significant net drop in LD content despite increased mitochondrial contact. Indeed, plasma NEFA uptake and oxidation rate increase in the

contracting skeletal muscle, which may preserve intramuscular LD stores (Sacchetti *et al.*, 2002). Although this may not translate to skeletal muscles, recent insights into brown adipose tissue suggest a role for PDM in promoting LD expansion by facilitating TAG synthesis (Benador *et al.*, 2018), as previously described. Another explanation is that the increased contact between LDs and mitochondria upon one hour of exercise precedes a net reduction in the LD stores observed with exercise at longer durations.

As relatively few studies have investigated LD-mitochondrial contact in skeletal muscle, it is unclear whether the dynamics of this inter-organelle interaction in response to exercise are disturbed in individuals with type 2 diabetes. Here, we show that acute exercise increases the LD-mitochondrial contact in patients with type 2 diabetes, similar to the findings in lean and obese untrained controls, suggesting that the exercise-mediated changes in LD-mitochondrial contact are not disturbed in type 2 diabetes. Furthermore, the increased contact with acute exercise is in line with other studies (Devries *et al.*, 2013; Koh *et al.*, 2017) but contrasts with our results from HIIT and also the mixed results found after exercise training (Tarnopolsky *et al.*, 2007; Shepherd *et al.*, 2017; Koh *et al.*, 2018). Our detailed analyses suggest that the increased contact ascribes to a higher number of LDs touching mitochondria and that the absolute length of contact increases upon exercise. In contrast to the findings in elite cross-country skiers showing increased contact in the intermyofibrillar space (Koh *et al.*, 2017), the increased LD-mitochondrial contact in the present study was primarily evident in the subsarcolemmal space of type 1 fibers. The untrained individuals in the current study may have higher storage of subsarcolemmal LDs than endurance-trained, who primarily store LDs in the intermyofibrillar space (Nielsen *et al.*, 2010; Daemen *et al.*, 2018; Koh *et al.*, 2018), likely explaining this discrepancy. Another potential explanation for this subsarcolemmal-derived LD-mitochondrial contact may be fatty acid trafficking from this region towards centrally located intermyofibrillar LDs. As mitochondria directly interact with other mitochondria around myofibrils, forming a specialized network proposed to distribute energy throughout the entire cell, the funneling of fatty acids between subcellular compartments could rely on region-specific functions (Parry & Glancy, 2021; Willingham *et al.*, 2021). Intriguingly, as exercise training more profoundly affects mitochondrial density (Nielsen *et al.*, 2010; Koh *et al.*, 2018) and oxidative capacity (Bizeau *et al.*, 1998; Koves *et al.*, 2005) in the subsarcolemmal space than in the intermyofibrillar space, the profound changes in LD-mitochondrial contact in the subsarcolemmal space may also represent higher plasticity of this specific compartment.

The physical contact between LDs and mitochondria is generally considered a direct pathway for fatty acid delivery to the mitochondrion (Parry & Glancy, 2021), thereby supporting ATP maintenance during exercise. This notion is in line with recent data indicating that mitochondria bound to LDs may also have differential cellular functions than their non-

interacting counterparts (Bleck *et al.*, 2018). The literature indicates that PLIN5 may act as an LD-mitochondrial tether (Wang *et al.*, 2011; Gemmink *et al.*, 2018b; Pribasnig *et al.*, 2018). However, the exact underlying mechanisms for LD-mitochondrial contact in humans and whether PLIN5 is essential for these functional processes during exercise are yet unknown.

05.08 Limitations of the study

First, since we did not register actual food intake before any testing day, we cannot exclude that any differences in substrate availability may have influenced the results. Second, the study design does not allow us to conclude whether the adaptions to training were due to the HIIT protocol, the recruitment of upper and lower muscle groups, or a combination. Third, we did not measure fiber type distributions, which might have influenced our correlation analysis between intramuscular LDs and whole-body insulin sensitivity. Fourth, our study only included males, which limits the generalization and extrapolation of the results to females. Finally, in study III, the participants performed the acute exercise at differential intensities (ranging from 51 to 75 %$\dot{V}O_2$max), which precludes any conclusion on the specific intensity and limits the interpretation of the results.

05.09 Conclusions and future directions

In conclusion, our results show that a deficient mitochondrial network and excessive LD load are evident in the skeletal muscle of patients with type 2 diabetes independent of obesity. The excessive LD load was explained by individual droplets of considerable large size located in specific fibers poor of subsarcolemmal mitochondria. HIIT combining rowing and cycling redistributed these LDs to be stored in a higher number of smaller organelles, preferentially in the intermyofibrillar region of type 2 fibers. At the same time, HIIT efficiently increases insulin sensitivity, $\dot{V}O_2$max, and body composition, with concomitant responses in obesity and type 2 diabetes. Patients with type 2 diabetes also experienced a clinically relevant decline in HbA1c and fasting plasma glucose levels. These results indicate that supervised HIIT engaging large quantities of muscle mass is a promising and well-tolerated exercise mode in sedentary individuals with type 2 diabetes and obesity. However, long-term studies in both males and females are required to evaluate the metabolic benefits of this HIIT protocol entirely. Furthermore, when evaluating the acute effects of exercise on these muscle properties, our results show that the contact between LDs and mitochondria increases irrespective of obesity and type 2 diabetes and despite no changes in LD volumetric density, numerical density, profile size, or subcellular distribution. Primarily ascribed to increases in the fraction of LDs touching mitochondria and the magnitude of contact, this effect seems most profound in the subsarcolemmal region of type 1 fibers. Future studies should investigate

how the contact between LDs and mitochondria influences fatty acid metabolism and mitochondrial function.

While most studies have examined mitochondria and LDs independently, there is an unmet need for more detailed investigations into the functional relationship between LDs and mitochondria and how this might be disturbed in insulin-resistant conditions. Besides more detailed investigations into the heterogenous aspects of LD morphology and subcellular distribution, future studies should develop a quantitative three-dimensional (3D) and super-resolution microscopy approach to map mitochondrial network organization and functional protein mediators (PLINs) to evaluate the relationship between LDs and mitochondria in the skeletal muscle. Moreover, although imaging modalities can provide valuable spatial information about organelles and structures, these findings are static and unable to capture the dynamic aspects of fatty acid trafficking through the muscle cell. Ideally, future studies should explore the combined use of stable isotope tracing and subcellular fractioning to detect the flux of lipid metabolites and their relation to insulin resistance.

06 References

Achten J, Gleeson M & Jeukendrup AE. (2002). Determination of the exercise intensity that elicits maximal fat oxidation. *Med Sci Sports Exerc* **34,** 92-97.

Albers PH, Pedersen AJ, Birk JB, Kristensen DE, Vind BF, Baba O, Nohr J, Hojlund K & Wojtaszewski JF. (2015). Human muscle fiber type-specific insulin signaling: impact of obesity and type 2 diabetes. *Diabetes* **64,** 485-497.

Alessi DR, James SR, Downes CP, Holmes AB, Gaffney PR, Reese CB & Cohen P. (1997). Characterization of a 3-phosphoinositide-dependent protein kinase which phosphorylates and activates protein kinase Balpha. *Curr Biol* **7,** 261-269.

Astorino TA & Schubert MM. (2018). Changes in fat oxidation in response to various regimes of high intensity interval training (HIIT). *Eur J Appl Physiol* **118,** 51-63.

Benador IY, Veliova M, Mahdaviani K, Petcherski A, Wikstrom JD, Assali EA, Acín-Pérez R, Shum M, Oliveira MF, Cinti S, Sztalryd C, Barshop WD, Wohlschlegel JA, Corkey BE, Liesa M & Shirihai OS. (2018). Mitochondria Bound to Lipid Droplets Have Unique Bioenergetics, Composition, and Dynamics that Support Lipid Droplet Expansion. *Cell Metab* **27,** 869-885 e866.

Bergman BC & Goodpaster BH. (2020). Exercise and Muscle Lipid Content, Composition, and Localization: Influence on Muscle Insulin Sensitivity. *Diabetes* **69,** 848-858.

Bergman BC, Perreault L, Strauss A, Bacon S, Kerege A, Harrison K, Brozinick JT, Hunerdosse DM, Playdon MC, Holmes W, Bui HH, Sanders P, Siddall P, Wei T, Thomas MK, Kuo MS & Eckel RH. (2018). Intramuscular triglyceride synthesis: importance in muscle lipid partitioning in humans. *Am J Physiol Endocrinol Metab* **314,** E152-E164.

Bizeau ME, Willis WT & Hazel JR. (1998). Differential responses to endurance training in subsarcolemmal and intermyofibrillar mitochondria. *J Appl Physiol (1985)* **85,** 1279-1284.

Bleck CKE, Kim Y, Willingham TB & Glancy B. (2018). Subcellular connectomic analyses of energy networks in striated muscle. *Nat Commun* **9,** 5111.

Boon H, Blaak EE, Saris WH, Keizer HA, Wagenmakers AJ & van Loon LJ. (2007). Substrate source utilisation in long-term diagnosed type 2 diabetes patients at rest, and during exercise and subsequent recovery. *Diabetologia* **50,** 103-112.

Bosma M. (2016). Lipid droplet dynamics in skeletal muscle. *Exp Cell Res* **340,** 180-186.

Bosma M, Hesselink MK, Sparks LM, Timmers S, Ferraz MJ, Mattijssen F, van Beurden D, Schaart G, de Baets MH, Verheyen FK, Kersten S & Schrauwen P. (2012). Perilipin 2 improves insulin sensitivity in skeletal muscle despite elevated intramuscular lipid levels. *Diabetes* **61,** 2679-2690.

Brechtel K, Niess AM, Machann J, Rett K, Schick F, Claussen CD, Dickhuth HH, Haering HU & Jacob S. (2001). Utilisation of intramyocellular lipids (IMCLs) during exercise as assessed by proton magnetic resonance spectroscopy (1H-MRS). *Horm Metab Res* **33,** 63-66.

Bucher J, Krusi M, Zueger T, Ith M, Stettler C, Diem P, Boesch C, Kreis R & Christ E. (2014). The effect of a single 2 h bout of aerobic exercise on ectopic lipids in skeletal muscle, liver and the myocardium. *Diabetologia* **57,** 1001-1005.

Buhman KK, Chen HC & Farese RV, Jr. (2001). The enzymes of neutral lipid synthesis. *J Biol Chem* **276,** 40369-40372.

Burns N, Finucane FM, Hatunic M, Gilman M, Murphy M, Gasparro D, Mari A, Gastaldelli A & Nolan JJ. (2007). Early-onset type 2 diabetes in obese white subjects is characterised by a marked defect in beta cell insulin secretion, severe insulin resistance and a lack of response to aerobic exercise training. *Diabetologia* **50,** 1500-1508.

Chee C, Shannon CE, Burns A, Selby AL, Wilkinson D, Smith K, Greenhaff PL & Stephens FB. (2016). Relative Contribution of Intramyocellular Lipid to Whole-Body Fat Oxidation Is Reduced With Age but Subsarcolemmal Lipid Accumulation and Insulin Resistance Are Only Associated With Overweight Individuals. *Diabetes* **65,** 840-850.

Christensen B, Nellemann B, Larsen MS, Thams L, Sieljacks P, Vestergaard PF, Bibby BM, Vissing K, Stodkilde-Jorgensen H, Pedersen SB, Moller N, Nielsen S, Jessen N & Jorgensen JO. (2013). Whole body metabolic effects of prolonged endurance training in combination with erythropoietin treatment in humans: a randomized placebo controlled trial. *Am J Physiol Endocrinol Metab* **305,** E879-889.

Chung JO, Koutsari C, Blachnio-Zabielska AU, Hames KC & Jensen MD. (2017). Intramyocellular Ceramides: Subcellular Concentrations and Fractional De Novo Synthesis in Postabsorptive Humans. *Diabetes* **66,** 2082-2091.

Colberg SR, Sigal RJ, Yardley JE, Riddell MC, Dunstan DW, Dempsey PC, Horton ES, Castorino K & Tate DF. (2016). Physical Activity/Exercise and Diabetes: A Position Statement of the American Diabetes Association. *Diabetes Care* **39,** 2065-2079.

Cross DA, Alessi DR, Cohen P, Andjelkovich M & Hemmings BA. (1995). Inhibition of glycogen synthase kinase-3 by insulin mediated by protein kinase B. *Nature* **378,** 785-789.

Daemen S, Gemmink A, Brouwers B, Meex RCR, Huntjens PR, Schaart G, Moonen-Kornips E, Jorgensen J, Hoeks J, Schrauwen P & Hesselink MKC. (2018). Distinct lipid droplet characteristics and distribution unmask the apparent contradiction of the athlete's paradox. *Mol Metab* **17,** 71-81.

Daemen S, van Polanen N, Bilet L, Phielix E, Moonen-Kornips E, Schrauwen-Hinderling VB, Schrauwen P & Hesselink MKC. (2021). Postexercise changes in myocellular lipid droplet characteristics of young lean individuals are affected by circulatory nonesterified fatty acids. *Am J Physiol Endocrinol Metab* **321,** E453-E463.

De Bock K, Dresselaers T, Kiens B, Richter EA, Van Hecke P & Hespel P. (2007). Evaluation of intramyocellular lipid breakdown during exercise by biochemical assay, NMR spectroscopy, and Oil Red O staining. *Am J Physiol Endocrinol Metab* **293,** E428-434.

De Filippis E, Alvarez G, Berria R, Cusi K, Everman S, Meyer C & Mandarino LJ. (2008). Insulin-resistant muscle is exercise resistant: evidence for reduced response of nuclear-encoded mitochondrial genes to exercise. *Am J Physiol Endocrinol Metab* **294,** E607-614.

De Nardi AT, Tolves T, Lenzi TL, Signori LU & Silva A. (2018). High-intensity interval training versus continuous training on physiological and metabolic variables in prediabetes and type 2 diabetes: A meta-analysis. *Diabetes Res Clin Pract* **137,** 149-159.

Decombaz J, Schmitt B, Ith M, Decarli B, Diem P, Kreis R, Hoppeler H & Boesch C. (2001). Postexercise fat intake repletes intramyocellular lipids but no faster in trained than in sedentary subjects. *Am J Physiol Regul Integr Comp Physiol* **281,** R760-769.

DeFronzo RA. (1988). Lilly lecture 1987. The triumvirate: beta-cell, muscle, liver. A collusion responsible for NIDDM. *Diabetes* **37,** 667-687.

DeFronzo RA, Jacot E, Jequier E, Maeder E, Wahren J & Felber JP. (1981). The effect of insulin on the disposal of intravenous glucose. Results from indirect calorimetry and hepatic and femoral venous catheterization. *Diabetes* **30,** 1000-1007.

Delesse MA. (1847). Procédé mécanique pour déterminer la composition des roches. *C R Acad Sci Paris* **25,** 544–545.

Devries MC, Lowther SA, Glover AW, Hamadeh MJ & Tarnopolsky MA. (2007). IMCL area density, but not IMCL utilization, is higher in women during moderate-intensity endurance exercise, compared with men. *Am J Physiol Regul Integr Comp Physiol* **293,** R2336-2342.

Devries MC, Samjoo IA, Hamadeh MJ, McCready C, Raha S, Watt MJ, Steinberg GR & Tarnopolsky MA. (2013). Endurance training modulates intramyocellular lipid compartmentalization and morphology in skeletal muscle of lean and obese women. *J Clin Endocrinol Metab* **98,** 4852-4862.

Ebbesson SO & Tang D. (1965). A method for estimating the number of cells in histological sections. *J R Microsc Soc* **85,** 449-464.

Egger A, Kreis R, Allemann S, Stettler C, Diem P, Buehler T, Boesch C & Christ ER. (2013). The effect of aerobic exercise on intrahepatocellular and intramyocellular lipids in healthy subjects. *PLoS One* **8,** e70865.

Farese RV, Jr. & Walther TC. (2009). Lipid droplets finally get a little R-E-S-P-E-C-T. *Cell* **139,** 855-860.

Fealy CE, Mulya A, Axelrod CL & Kirwan JP. (2018). Mitochondrial dynamics in skeletal muscle insulin resistance and type 2 diabetes. *Transl Res* **202,** 69-82.

Fletcher B, Gulanick M & Lamendola C. (2002). Risk factors for type 2 diabetes mellitus. *J Cardiovasc Nurs* **16,** 17-23.

Frankenberg NT, Mason SA, Wadley GD & Murphy RM. (2022). Skeletal muscle cell-specific differences in type 2 diabetes. *Cell Mol Life Sci* **79,** 256.

Frayn KN. (1983). Calculation of substrate oxidation rates in vivo from gaseous exchange. *J Appl Physiol Respir Environ Exerc Physiol* **55,** 628-634.

Frosig C, Sajan MP, Maarbjerg SJ, Brandt N, Roepstorff C, Wojtaszewski JF, Kiens B, Farese RV & Richter EA. (2007). Exercise improves phosphatidylinositol-3,4,5-trisphosphate responsiveness of atypical protein kinase C and interacts with insulin signalling to peptide elongation in human skeletal muscle. *J Physiol* **582,** 1289-1301.

Fujimoto T & Parton RG. (2011). Not just fat: the structure and function of the lipid droplet. *Cold Spring Harb Perspect Biol* **3,** a004838.

Fukumoto S & Fujimoto T. (2002). Deformation of lipid droplets in fixed samples. *Histochem Cell Biol* **118,** 423-428.

Gavin TP, Ernst JM, Kwak HB, Caudill SE, Reed MA, Garner RT, Nie Y, Weiss JA, Pories WJ, Dar M, Lin CT, Hubal MJ, Neufer PD, Kuang S & Dohm GL. (2018). High Incomplete Skeletal Muscle Fatty Acid Oxidation Explains Low Muscle Insulin Sensitivity in Poorly Controlled T2D. *J Clin Endocrinol Metab* **103,** 882-889.

Gemmink A, Daemen S, Brouwers B, Hoeks J, Schaart G, Knoops K, Schrauwen P & Hesselink MKC. (2021). Decoration of myocellular lipid droplets with perilipins as a marker for in vivo lipid droplet dynamics: A super-resolution microscopy study in trained athletes and insulin resistant individuals. *Biochim Biophys Acta Mol Cell Biol Lipids* **1866,** 158852.

Gemmink A, Daemen S, Brouwers B, Huntjens PR, Schaart G, Moonen-Kornips E, Jorgensen J, Hoeks J, Schrauwen P & Hesselink MKC. (2018a). Dissociation of intramyocellular lipid storage and insulin resistance in trained athletes and type 2 diabetes patients; involvement of perilipin 5? *J Physiol* **596,** 857-868.

Gemmink A, Daemen S, Kuijpers HJH, Schaart G, Duimel H, Lopez-Iglesias C, van Zandvoort M, Knoops K & Hesselink MKC. (2018b). Super-resolution microscopy localizes perilipin 5 at lipid droplet-mitochondria interaction sites and at lipid droplets juxtaposing to perilipin 2. *Biochim Biophys Acta Mol Cell Biol Lipids* **1863,** 1423-1432.

Gemmink A, Schrauwen P & Hesselink MKC. (2020). Exercising your fat (metabolism) into shape: a muscle-centred view. *Diabetologia* **63,** 1453-1463.

Gollnick PD, Armstrong RB, Sembrowich WL, Shepherd RE & Saltin B. (1973). Glycogen depletion pattern in human skeletal muscle fibers after heavy exercise. *J Appl Physiol* **34,** 615-618.

Goodpaster BH, He J, Watkins S & Kelley DE. (2001). Skeletal muscle lipid content and insulin resistance: evidence for a paradox in endurance-trained athletes. *J Clin Endocrinol Metab* **86,** 5755-5761.

Graham L & Orenstein JM. (2007). Processing tissue and cells for transmission electron microscopy in diagnostic pathology and research. *Nat Protoc* **2,** 2439-2450.

Hayat MA. (1986). Glutaraldehyde: Role in electron microscopy. *Micron and Microscopica Acta* **17,** 115-135.

Heckman CJ & Enoka RM. (2012). Motor unit. *Compr Physiol* **2,** 2629-2682.

Hesselink MK, Mensink M & Schrauwen P. (2004). Intramyocellular lipids and insulin sensitivity: does size really matter? *Obes Res* **12,** 741-742.

Higaki Y, Wojtaszewski JF, Hirshman MF, Withers DJ, Towery H, White MF & Goodyear LJ. (1999). Insulin receptor substrate-2 is not necessary for insulin- and exercise-stimulated glucose transport in skeletal muscle. *J Biol Chem* **274,** 20791-20795.

Hoeks J, Hesselink MK, Russell AP, Mensink M, Saris WH, Mensink RP & Schrauwen P. (2006). Peroxisome proliferator-activated receptor-gamma coactivator-1 and insulin resistance: acute effect of fatty acids. *Diabetologia* **49,** 2419-2426.

Hoppeler H. (1999). Skeletal muscle substrate metabolism. *Int J Obes Relat Metab Disord* **23 Suppl 3,** S7-10.

Hoppeler H, Howald H, Conley K, Lindstedt SL, Claassen H, Vock P & Weibel ER. (1985). Endurance training in humans: aerobic capacity and structure of skeletal muscle. *J Appl Physiol (1985)* **59,** 320-327.

Hoppeler H, Lüthi P, Claassen H, Weibel ER & Howald H. (1973). The ultrastructure of the normal human skeletal muscle. A morphometric analysis on untrained men, women and well-trained orienteers. *Pflugers Arch* **344,** 217-232.

Hother-Nielsen O, Henriksen JE, Holst JJ & Beck-Nielsen H. (1996). Effects of insulin on glucose turnover rates in vivo: isotope dilution versus constant specific activity technique. *Metabolism* **45,** 82-91.

Houzelle A, Jörgensen JA, Schaart G, Daemen S, van Polanen N, Fealy CE, Hesselink MKC, Schrauwen P & Hoeks J. (2021). Human skeletal muscle mitochondrial dynamics in relation to oxidative capacity and insulin sensitivity. *Diabetologia* **64,** 424-436.

Howald H, Boesch C, Kreis R, Matter S, Billeter R, Essen-Gustavsson B & Hoppeler H. (2002). Content of intramyocellular lipids derived by electron microscopy, biochemical assays, and (1)H-MR spectroscopy. *J Appl Physiol (1985)* **92,** 2264-2272.

Howald H, Hoppeler H, Claassen H, Mathieu O & Straub R. (1985). Influences of endurance training on the ultrastructural composition of the different muscle fiber types in humans. *Pflugers Arch* **403,** 369-376.

Howard C & Reed M. (2005). Unbiased Stereology: Three-Dimensional Measurement in Microscopy. *Oxford, UK: Bios Scientific*.

Højlund K, Birk JB, Klein DK, Levin K, Rose AJ, Hansen BF, Nielsen JN, Beck-Nielsen H & Wojtaszewski JF. (2009). Dysregulation of glycogen synthase COOH- and NH2-terminal phosphorylation by insulin in obesity and type 2 diabetes mellitus. *J Clin Endocrinol Metab* **94,** 4547-4556.

Højlund K, Frystyk J, Levin K, Flyvbjerg A, Wojtaszewski JF & Beck-Nielsen H. (2006). Reduced plasma adiponectin concentrations may contribute to impaired insulin activation of glycogen synthase in skeletal muscle of patients with type 2 diabetes. *Diabetologia* **49,** 1283-1291.

Jacquier N, Choudhary V, Mari M, Toulmay A, Reggiori F & Schneiter R. (2011). Lipid droplets are functionally connected to the endoplasmic reticulum in Saccharomyces cerevisiae. *J Cell Sci* **124,** 2424-2437.

Jacquier N, Mishra S, Choudhary V & Schneiter R. (2013). Expression of oleosin and perilipins in yeast promotes formation of lipid droplets from the endoplasmic reticulum. *J Cell Sci* **126,** 5198-5209.

Jensen R, Ørtenblad N, di Benedetto C, Qvortrup K & Nielsen J. (2022). Quantification of Subcellular Glycogen Distribution in Skeletal Muscle Fibers using Transmission Electron Microscopy. *J Vis Exp*.

Jevons EFP, Gejl KD, Strauss JA, Ørtenblad N & Shepherd SO. (2020). Skeletal muscle lipid droplets are resynthesized before being coated with perilipin proteins following prolonged exercise in elite male triathletes. *Am J Physiol Endocrinol Metab* **318,** E357-E370.

Jheng HF, Tsai PJ, Guo SM, Kuo LH, Chang CS, Su IJ, Chang CR & Tsai YS. (2012). Mitochondrial fission contributes to mitochondrial dysfunction and insulin resistance in skeletal muscle. *Mol Cell Biol* **32,** 309-319.

Kaushik S & Cuervo AM. (2015). Degradation of lipid droplet-associated proteins by chaperone-mediated autophagy facilitates lipolysis. *Nat Cell Biol* **17,** 759-770.

Kayar SR, Hoppeler H, Howald H, Claassen H & Oberholzer F. (1986). Acute effects of endurance exercise on mitochondrial distribution and skeletal muscle morphology. *Eur J Appl Physiol Occup Physiol* **54,** 578-584.

Kelley DE & Simoneau JA. (1994). Impaired free fatty acid utilization by skeletal muscle in non-insulin-dependent diabetes mellitus. *J Clin Invest* **94,** 2349-2356.

Kiens B. (2006). Skeletal muscle lipid metabolism in exercise and insulin resistance. *Physiol Rev* **86,** 205-243.

Koh HE, Nielsen J, Saltin B, Holmberg HC & Ørtenblad N. (2017). Pronounced limb and fibre type differences in subcellular lipid droplet content and distribution in elite skiers before and after exhaustive exercise. *J Physiol* **595,** 5781-5795.

Koh HE, Ørtenblad N, Winding KM, Hellsten Y, Mortensen SP & Nielsen J. (2018). High-intensity interval, but not endurance, training induces muscle fiber type-specific subsarcolemmal lipid droplet size reduction in type 2 diabetic patients. *Am J Physiol Endocrinol Metab* **315,** E872-E884.

Koves TR, Noland RC, Bates AL, Henes ST, Muoio DM & Cortright RN. (2005). Subsarcolemmal and intermyofibrillar mitochondria play distinct roles in regulating skeletal muscle fatty acid metabolism. *Am J Physiol Cell Physiol* **288,** C1074-1082.

Krssak M, Falk Petersen K, Dresner A, DiPietro L, Vogel SM, Rothman DL, Roden M & Shulman GI. (1999). Intramyocellular lipid concentrations are correlated with insulin sensitivity in humans: a 1H NMR spectroscopy study. *Diabetologia* **42,** 113-116.

Krssak M, Petersen KF, Bergeron R, Price T, Laurent D, Rothman DL, Roden M & Shulman GI. (2000). Intramuscular glycogen and intramyocellular lipid utilization during prolonged exercise and recovery in man: a 13C and 1H nuclear magnetic resonance spectroscopy study. *J Clin Endocrinol Metab* **85,** 748-754.

Laurens C, Bourlier V, Mairal A, Louche K, Badin PM, Mouisel E, Montagner A, Marette A, Tremblay A, Weisnagel JS, Guillou H, Langin D, Joanisse DR & Moro C. (2016). Perilipin 5 fine-tunes lipid oxidation to metabolic demand and protects against lipotoxicity in skeletal muscle. *Sci Rep* **6,** 38310.

Lee J & Pilch PF. (1994). The insulin receptor: structure, function, and signaling. *Am J Physiol* **266,** C319-334.

Leto D & Saltiel AR. (2012). Regulation of glucose transport by insulin: traffic control of GLUT4. *Nat Rev Mol Cell Biol* **13,** 383-396.

Li LO, Grevengoed TJ, Paul DS, Ilkayeva O, Koves TR, Pascual F, Newgard CB, Muoio DM & Coleman RA. (2015). Compartmentalized acyl-CoA metabolism in skeletal muscle regulates systemic glucose homeostasis. *Diabetes* **64,** 23-35.

Li LO, Klett EL & Coleman RA. (2010). Acyl-CoA synthesis, lipid metabolism and lipotoxicity. *Biochim Biophys Acta* **1801,** 246-251.

Li X, Li Z, Zhao M, Nie Y, Liu P, Zhu Y & Zhang X. (2019). Skeletal Muscle Lipid Droplets and the Athlete's Paradox. *Cells* **8,** 249.

Li Y, Lee S, Langleite T, Norheim F, Pourteymour S, Jensen J, Stadheim HK, Storas TH, Davanger S, Gulseth HL, Birkeland KI, Drevon CA & Holen T. (2014). Subsarcolemmal lipid droplet

responses to a combined endurance and strength exercise intervention. *Physiol Rep* **2,** e12187.

Lindenthaler JR, Rice AJ, Versey NG, McKune AJ & Welvaert M. (2018). Differences in Physiological Responses During Rowing and Cycle Ergometry in Elite Male Rowers. *Front Physiol* **9,** 1010.

Listenberger LL, Ostermeyer-Fay AG, Goldberg EB, Brown WJ & Brown DA. (2007). Adipocyte differentiation-related protein reduces the lipid droplet association of adipose triglyceride lipase and slows triacylglycerol turnover. *J Lipid Res* **48,** 2751-2761.

Lovejoy J, Newby FD, Gebhart SS & DiGirolamo M. (1992). Insulin resistance in obesity is associated with elevated basal lactate levels and diminished lactate appearance following intravenous glucose and insulin. *Metabolism* **41,** 22-27.

Meex RC, Hoy AJ, Mason RM, Martin SD, McGee SL, Bruce CR & Watt MJ. (2015). ATGL-mediated triglyceride turnover and the regulation of mitochondrial capacity in skeletal muscle. *Am J Physiol Endocrinol Metab* **308,** E960-970.

Minnaard R, Schrauwen P, Schaart G, Jorgensen JA, Lenaers E, Mensink M & Hesselink MK. (2009). Adipocyte differentiation-related protein and OXPAT in rat and human skeletal muscle: involvement in lipid accumulation and type 2 diabetes mellitus. *J Clin Endocrinol Metab* **94,** 4077-4085.

Mitranun W, Deerochanawong C, Tanaka H & Suksom D. (2014). Continuous vs interval training on glycemic control and macro- and microvascular reactivity in type 2 diabetic patients. *Scand J Med Sci Sports* **24,** e69-76.

Myers MG, Jr., Backer JM, Sun XJ, Shoelson S, Hu P, Schlessinger J, Yoakim M, Schaffhausen B & White MF. (1992). IRS-1 activates phosphatidylinositol 3'-kinase by associating with src homology 2 domains of p85. *Proc Natl Acad Sci U S A* **89,** 10350-10354.

Najt CP, Devarajan M & Mashek DG. (2022). Perilipins at a glance. *J Cell Sci* **135,** jcs259501.

Nielsen J, Christensen AE, Nellemann B & Christensen B. (2017). Lipid droplet size and location in human skeletal muscle fibers are associated with insulin sensitivity. *Am J Physiol Endocrinol Metab* **313,** E721-E730.

Nielsen J, Mogensen M, Vind BF, Sahlin K, Højlund K, Schroder HD & Ørtenblad N. (2010). Increased subsarcolemmal lipids in type 2 diabetes: effect of training on localization of lipids, mitochondria, and glycogen in sedentary human skeletal muscle. *Am J Physiol Endocrinol Metab* **298,** E706-713.

O'Hagan C, De Vito G & Boreham CA. (2013). Exercise prescription in the treatment of type 2 diabetes mellitus : current practices, existing guidelines and future directions. *Sports Med* **43,** 39-49.

Ovadi J & Saks V. (2004). On the origin of intracellular compartmentation and organized metabolic systems. *Mol Cell Biochem* **256-257,** 5-12.

Pan DA, Lillioja S, Kriketos AD, Milner MR, Baur LA, Bogardus C, Jenkins AB & Storlien LH. (1997). Skeletal muscle triglyceride levels are inversely related to insulin action. *Diabetes* **46,** 983-988.

Parry HA & Glancy B. (2021). Energy transfer between the mitochondrial network and lipid droplets in insulin resistant skeletal muscle. *Curr Opin Physiol* **24,** 100487.

Perreault L, Newsom SA, Strauss A, Kerege A, Kahn DE, Harrison KA, Snell-Bergeon JK, Nemkov T, D'Alessandro A, Jackman MR, MacLean PS & Bergman BC. (2018). Intracellular localization of diacylglycerols and sphingolipids influences insulin sensitivity and mitochondrial function in human skeletal muscle. *JCI Insight* **3,** e96805.

Phielix E & Mensink M. (2008). Type 2 diabetes mellitus and skeletal muscle metabolic function. *Physiol Behav* **94,** 252-258.

Pol A, Gross SP & Parton RG. (2014). Review: biogenesis of the multifunctional lipid droplet: lipids, proteins, and sites. *J Cell Biol* **204,** 635-646.

Pribasnig M, Kien B, Pusch L, Haemmerle G, Zimmermann R & Wolinski H. (2018). Extended-resolution imaging of the interaction of lipid droplets and mitochondria. *Biochim Biophys Acta Mol Cell Biol Lipids* **1863,** 1285-1296.

Rambold AS, Cohen S & Lippincott-Schwartz J. (2015). Fatty acid trafficking in starved cells: regulation by lipid droplet lipolysis, autophagy, and mitochondrial fusion dynamics. *Dev Cell* **32,** 678-692.

Reaven GM, Hollenbeck C, Jeng CY, Wu MS & Chen YD. (1988). Measurement of plasma glucose, free fatty acid, lactate, and insulin for 24 h in patients with NIDDM. *Diabetes* **37,** 1020-1024.

Richards JC, Johnson TK, Kuzma JN, Lonac MC, Schweder MM, Voyles WF & Bell C. (2010). Short-term sprint interval training increases insulin sensitivity in healthy adults but does not affect the thermogenic response to beta-adrenergic stimulation. *J Physiol* **588,** 2961-2972.

Riemersma JC. (1968). Osmium tetroxide fixation of lipids for electron microscopy. A possible reaction mechanism. *Biochim Biophys Acta* **152,** 718-727.

Ritov VB, Menshikova EV, He J, Ferrell RE, Goodpaster BH & Kelley DE. (2005). Deficiency of subsarcolemmal mitochondria in obesity and type 2 diabetes. *Diabetes* **54,** 8-14.

Robinson MM, Dasari S, Konopka AR, Johnson ML, Manjunatha S, Esponda RR, Carter RE, Lanza IR & Nair KS. (2017). Enhanced Protein Translation Underlies Improved Metabolic and Physical Adaptations to Different Exercise Training Modes in Young and Old Humans. *Cell Metab* **25,** 581-592.

Romijn JA, Coyle EF, Sidossis LS, Gastaldelli A, Horowitz JF, Endert E & Wolfe RR. (1993). Regulation of endogenous fat and carbohydrate metabolism in relation to exercise intensity and duration. *Am J Physiol* **265,** E380-391.

Romijn JA, Coyle EF, Sidossis LS, Rosenblatt J & Wolfe RR. (2000). Substrate metabolism during different exercise intensities in endurance-trained women. *J Appl Physiol (1985)* **88,** 1707-1714.

Ruegsegger GN, Creo AL, Cortes TM, Dasari S & Nair KS. (2018). Altered mitochondrial function in insulin-deficient and insulin-resistant states. *J Clin Invest* **128,** 3671-3681.

Ryan BJ, Schleh MW, Ahn C, Ludzki AC, Gillen JB, Varshney P, Van Pelt DW, Pitchford LM, Chenevert TL, Gioscia-Ryan RA, Howton SM, Rode T, Hummel SL, Burant CF, Little JP & Horowitz JF. (2020). Moderate-Intensity Exercise and High-Intensity Interval Training Affect Insulin Sensitivity Similarly in Obese Adults. *J Clin Endocrinol Metab* **105,** e2941-e2959.

Sacchetti M, Saltin B, Olsen DB & van Hall G. (2004). High triacylglycerol turnover rate in human skeletal muscle. *J Physiol* **561,** 883-891.

Sacchetti M, Saltin B, Osada T & van Hall G. (2002). Intramuscular fatty acid metabolism in contracting and non-contracting human skeletal muscle. *J Physiol* **540,** 387-395.

Sakamoto K & Holman GD. (2008). Emerging role for AS160/TBC1D4 and TBC1D1 in the regulation of GLUT4 traffic. *Am J Physiol Endocrinol Metab* **295,** E29-37.

Saks V, Beraud N & Wallimann T. (2008). Metabolic compartmentation - a system level property of muscle cells: real problems of diffusion in living cells. *Int J Mol Sci* **9,** 751-767.

Samjoo IA, Safdar A, Hamadeh MJ, Glover AW, Mocellin NJ, Santana J, Little JP, Steinberg GR, Raha S & Tarnopolsky MA. (2013). Markers of skeletal muscle mitochondrial function and lipid accumulation are moderately associated with the homeostasis model assessment index of insulin resistance in obese men. *PLoS One* **8,** e66322.

Sarbassov DD, Guertin DA, Ali SM & Sabatini DM. (2005). Phosphorylation and regulation of Akt/PKB by the rictor-mTOR complex. *Science* **307,** 1098-1101.

Schiaffino S & Reggiani C. (2011). Fiber types in mammalian skeletal muscles. *Physiol Rev* **91,** 1447-1531.

Schrauwen-Hinderling VB, van Loon LJ, Koopman R, Nicolay K, Saris WH & Kooi ME. (2003). Intramyocellular lipid content is increased after exercise in nonexercising human skeletal muscle. *J Appl Physiol (1985)* **95,** 2328-2332.

Sergi D, Naumovski N, Heilbronn LK, Abeywardena M, O'Callaghan N, Lionetti L & Luscombe-Marsh N. (2019). Mitochondrial (Dys)function and Insulin Resistance: From Pathophysiological Molecular Mechanisms to the Impact of Diet. *Front Physiol* **10,** 532.

Shaw CS, Jones DA & Wagenmakers AJ. (2008). Network distribution of mitochondria and lipid droplets in human muscle fibres. *Histochem Cell Biol* **129,** 65-72.

Shepherd SO, Cocks M, Meikle PJ, Mellett NA, Ranasinghe AM, Barker TA, Wagenmakers AJM & Shaw CS. (2017). Lipid droplet remodelling and reduced muscle ceramides following sprint interval and moderate-intensity continuous exercise training in obese males. *Int J Obes (Lond)* **41,** 1745-1754.

Shepherd SO, Cocks M, Tipton KD, Ranasinghe AM, Barker TA, Burniston JG, Wagenmakers AJ & Shaw CS. (2012). Preferential utilization of perilipin 2-associated intramuscular triglycerides during 1 h of moderate-intensity endurance-type exercise. *Exp Physiol* **97,** 970-980.

Shepherd SO, Cocks M, Tipton KD, Ranasinghe AM, Barker TA, Burniston JG, Wagenmakers AJ & Shaw CS. (2013). Sprint interval and traditional endurance training increase net intramuscular triglyceride breakdown and expression of perilipin 2 and 5. *J Physiol* **591,** 657-675.

Shepherd SO, Cocks M, Tipton KD, Witard OC, Ranasinghe AM, Barker TA, Wagenmakers AJ & Shaw CS. (2014). Resistance training increases skeletal muscle oxidative capacity and net intramuscular triglyceride breakdown in type I and II fibres of sedentary males. *Exp Physiol* **99,** 894-908.

Sjöström M, Angquist KA, Bylund AC, Friden J, Gustavsson L & Schersten T. (1982a). Morphometric analyses of human muscle fiber types. *Muscle Nerve* **5,** 538-553.

Sjöström M, Kidman S, Larsen KH & Angquist KA. (1982b). Z- and M-band appearance in different histochemically defined types of human skeletal muscle fibers. *J Histochem Cytochem* **30,** 1-11.

Staron RS, Hikida RS, Murray TF, Hagerman FC & Hagerman MT. (1989). Lipid depletion and repletion in skeletal muscle following a marathon. *J Neurol Sci* **94,** 29-40.

Steenberg DE, Hingst JR, Birk JB, Thorup A, Kristensen JM, Sjoberg KA, Kiens B, Richter EA & Wojtaszewski JFP. (2020). A Single Bout of One-Legged Exercise to Local Exhaustion Decreases Insulin Action in Nonexercised Muscle Leading to Decreased Whole-Body Insulin Action. *Diabetes* **69,** 578-590.

Stellingwerff T, Boon H, Jonkers RA, Senden JM, Spriet LL, Koopman R & van Loon LJ. (2007). Significant intramyocellular lipid use during prolonged cycling in endurance-trained males as assessed by three different methodologies. *Am J Physiol Endocrinol Metab* **292,** E1715-1723.

Stoa EM, Meling S, Nyhus LK, Glenn S, Mangerud KM, Helgerud J, Bratland-Sanda S & Storen O. (2017). High-intensity aerobic interval training improves aerobic fitness and HbA1c among persons diagnosed with type 2 diabetes. *Eur J Appl Physiol* **117,** 455-467.

Suter E, Hoppeler H, Claassen H, Billeter R, Aebi U, Horber F, Jaeger P & Marti B. (1995). Ultrastructural modification of human skeletal muscle tissue with 6-month moderate-intensity exercise training. *Int J Sports Med* **16,** 160-166.

Suzuki M, Shinohara Y, Ohsaki Y & Fujimoto T. (2011). Lipid droplets: size matters. *J Electron Microsc (Tokyo)* **60 Suppl 1,** S101-116.

Sylow L, Jensen TE, Kleinert M, Hojlund K, Kiens B, Wojtaszewski J, Prats C, Schjerling P & Richter EA. (2013). Rac1 signaling is required for insulin-stimulated glucose uptake and is dysregulated in insulin-resistant murine and human skeletal muscle. *Diabetes* **62,** 1865-1875.

Sylow L, Kleinert M, Pehmoller C, Prats C, Chiu TT, Klip A, Richter EA & Jensen TE. (2014). Akt and Rac1 signaling are jointly required for insulin-stimulated glucose uptake in skeletal muscle and downregulated in insulin resistance. *Cell Signal* **26,** 323-331.

Søgaard D, Lund MT, Scheuer CM, Dehlbaek MS, Dideriksen SG, Abildskov CV, Christensen KK, Dohlmann TL, Larsen S, Vigelsø AH, Dela F & Helge JW. (2018). High-intensity interval training improves insulin sensitivity in older individuals. *Acta Physiol (Oxf)* **222,** e13009.

Tappy L, Owen OE & Boden G. (1988). Effect of hyperinsulinemia on urea pool size and substrate oxidation rates. *Diabetes* **37,** 1212-1216.

Tarnopolsky MA, Rennie CD, Robertshaw HA, Fedak-Tarnopolsky SN, Devries MC & Hamadeh MJ. (2007). Influence of endurance exercise training and sex on intramyocellular lipid and mitochondrial ultrastructure, substrate use, and mitochondrial enzyme activity. *Am J Physiol Regul Integr Comp Physiol* **292,** R1271-1278.

Tauchi-Sato K, Ozeki S, Houjou T, Taguchi R & Fujimoto T. (2002). The surface of lipid droplets is a phospholipid monolayer with a unique Fatty Acid composition. *J Biol Chem* **277,** 44507-44512.

Taylor HL, Buskirk E & Henschel A. (1955). Maximal oxygen intake as an objective measure of cardio-respiratory performance. *J Appl Physiol* **8,** 73-80.

Thiam AR & Beller M. (2017). The why, when and how of lipid droplet diversity. *J Cell Sci* **130,** 315-324.

Toledo FG, Menshikova EV, Azuma K, Radikova Z, Kelley CA, Ritov VB & Kelley DE. (2008). Mitochondrial capacity in skeletal muscle is not stimulated by weight loss despite increases in insulin action and decreases in intramyocellular lipid content. *Diabetes* **57,** 987-994.

van de Weijer T, Sparks LM, Phielix E, Meex RC, van Herpen NA, Hesselink MK, Schrauwen P & Schrauwen-Hinderling VB. (2013). Relationships between mitochondrial function and metabolic flexibility in type 2 diabetes mellitus. *PLoS One* **8,** e51648.

van Loon LJ. (2004). Use of intramuscular triacylglycerol as a substrate source during exercise in humans. *J Appl Physiol (1985)* **97,** 1170-1187.

van Loon LJ, Koopman R, Manders R, van der Weegen W, van Kranenburg GP & Keizer HA. (2004). Intramyocellular lipid content in type 2 diabetes patients compared with overweight sedentary men and highly trained endurance athletes. *Am J Physiol Endocrinol Metab* **287,** E558-565.

van Loon LJ, Koopman R, Stegen JH, Wagenmakers AJ, Keizer HA & Saris WH. (2003). Intramyocellular lipids form an important substrate source during moderate intensity exercise in endurance-trained males in a fasted state. *J Physiol* **553,** 611-625.

van Loon LJ, Manders RJ, Koopman R, Kaastra B, Stegen JH, Gijsen AP, Saris WH & Keizer HA. (2005). Inhibition of adipose tissue lipolysis increases intramuscular lipid use in type 2 diabetic patients. *Diabetologia* **48,** 2097-2107.

Venables MC, Achten J & Jeukendrup AE. (2005). Determinants of fat oxidation during exercise in healthy men and women: a cross-sectional study. *J Appl Physiol (1985)* **98,** 160-167.

Vermathen P, Saillen P, Boss A, Zehnder M & Boesch C. (2012). Skeletal muscle (1)H MRSI before and after prolonged exercise. I. muscle specific depletion of intramyocellular lipids. *Magn Reson Med* **68,** 1357-1367.

Vind BF, Pehmoller C, Treebak JT, Birk JB, Hey-Mogensen M, Beck-Nielsen H, Zierath JR, Wojtaszewski JF & Hojlund K. (2011). Impaired insulin-induced site-specific phosphorylation

of TBC1 domain family, member 4 (TBC1D4) in skeletal muscle of type 2 diabetes patients is restored by endurance exercise-training. *Diabetologia* **54,** 157-167.

Walther TC, Chung J & Farese RV, Jr. (2017). Lipid Droplet Biogenesis. *Annu Rev Cell Dev Biol* **33,** 491-510.

Wang H, Bell M, Sreenivasan U, Sreenevasan U, Hu H, Liu J, Dalen K, Londos C, Yamaguchi T, Rizzo MA, Coleman R, Gong D, Brasaemle D & Sztalryd C. (2011). Unique regulation of adipose triglyceride lipase (ATGL) by perilipin 5, a lipid droplet-associated protein. *J Biol Chem* **286,** 15707-15715.

Watt MJ, Heigenhauser GJ & Spriet LL. (2002). Intramuscular triacylglycerol utilization in human skeletal muscle during exercise: is there a controversy? *J Appl Physiol (1985)* **93,** 1185-1195.

Weibel ER. (1979). Stereological Methods Vol. 1 Practical Methods for Biological Morphometry. *Academic Press*.

Weibel ER, Kistler GS & Scherle WF. (1966). Practical stereological methods for morphometric cytology. *J Cell Biol* **30,** 23-38.

Weir JB. (1949). New methods for calculating metabolic rate with special reference to protein metabolism. *J Physiol* **109,** 1-9.

Welte MA. (2015). Expanding roles for lipid droplets. *Curr Biol* **25,** R470-481.

Wendling PS, Peters SJ, Heigenhauser GJ & Spriet LL. (1996). Variability of triacylglycerol content in human skeletal muscle biopsy samples. *J Appl Physiol (1985)* **81,** 1150-1155.

West MJ. (2012). Introduction to stereology. *Cold Spring Harb Protoc* **2012,** pdb.top070623.

White LJ, Ferguson MA, McCoy SC & Kim H. (2003). Intramyocellular lipid changes in men and women during aerobic exercise: a (1)H-magnetic resonance spectroscopy study. *J Clin Endocrinol Metab* **88,** 5638-5643.

Wilfling F, Haas JT, Walther TC & Farese RV, Jr. (2014). Lipid droplet biogenesis. *Curr Opin Cell Biol* **29,** 39-45.

Willingham TB, Ajayi PT & Glancy B. (2021). Subcellular Specialization of Mitochondrial Form and Function in Skeletal Muscle Cells. *Front Cell Dev Biol* **9,** 757305.

Winding KM, Munch GW, Iepsen UW, Van Hall G, Pedersen BK & Mortensen SP. (2018). The effect on glycaemic control of low-volume high-intensity interval training versus endurance training in individuals with type 2 diabetes. *Diabetes Obes Metab* **20,** 1131-1139.

Wojtaszewski JF, Hansen BF, Gade, Kiens B, Markuns JF, Goodyear LJ & Richter EA. (2000). Insulin signaling and insulin sensitivity after exercise in human skeletal muscle. *Diabetes* **49,** 325-331.

Wojtaszewski JF, Higaki Y, Hirshman MF, Michael MD, Dufresne SD, Kahn CR & Goodyear LJ. (1999). Exercise modulates postreceptor insulin signaling and glucose transport in muscle-specific insulin receptor knockout mice. *J Clin Invest* **104,** 1257-1264.

Yamauchi T, Tobe K, Tamemoto H, Ueki K, Kaburagi Y, Yamamoto-Honda R, Takahashi Y, Yoshizawa F, Aizawa S, Akanuma Y, Sonenberg N, Yazaki Y & Kadowaki T. (1996). Insulin signalling and insulin actions in the muscles and livers of insulin-resistant, insulin receptor substrate 1-deficient mice. *Mol Cell Biol* **16,** 3074-3084.

Zehnder M, Ith M, Kreis R, Saris W, Boutellier U & Boesch C. (2005). Gender-specific usage of intramyocellular lipids and glycogen during exercise. *Med Sci Sports Exerc* **37,** 1517-1524.

Zhang S, Wang Y, Cui L, Deng Y, Xu S, Yu J, Cichello S, Serrero G, Ying Y & Liu P. (2016). Morphologically and Functionally Distinct Lipid Droplet Subpopulations. *Sci Rep* **6,** 29539.

Appendix I

Supplemental Figures 1–6

Supplemental Tables 1–3

Supplemental Fig. 1. Correlation analysis between maximal fat oxidation, insulin-stimulated glucose disposal rate, and subsarcolemmal lipid droplet numbers and area

Correlation analyses were performed for Pre and Post values, separated for each group, and merged across groups. Analyses were performed with the assumption of an even (50:50) fiber type distribution in m. vastus lateralis. Lean, Obese, and T2D were represented with black circles, grey triangles, and red diamonds, respectively (corresponding-colored lines).

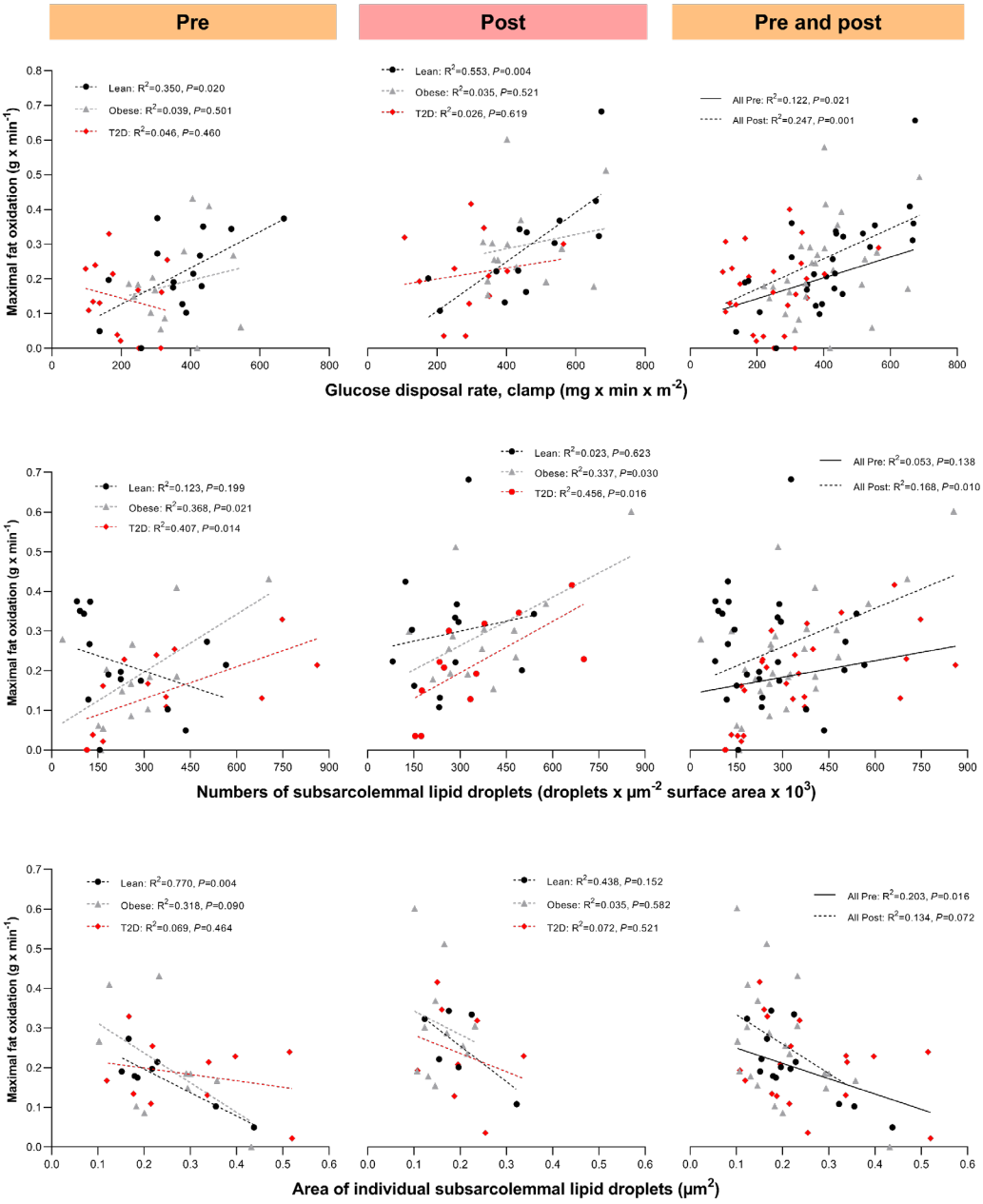

Supplemental Fig. 2. Correlation analysis between insulin-stimulated glucose disposal rate and subsarcolemmal lipid droplet volume fractions, numbers, and area

Correlation analyses were performed for Pre and Post values, separated for each group, and merged across groups. Analyses were performed with the assumption of an even (50:50) fiber type distribution in m. vastus lateralis. Lean, Obese, and T2D were represented with black circles, grey triangles, and red diamonds, respectively (corresponding-colored lines).

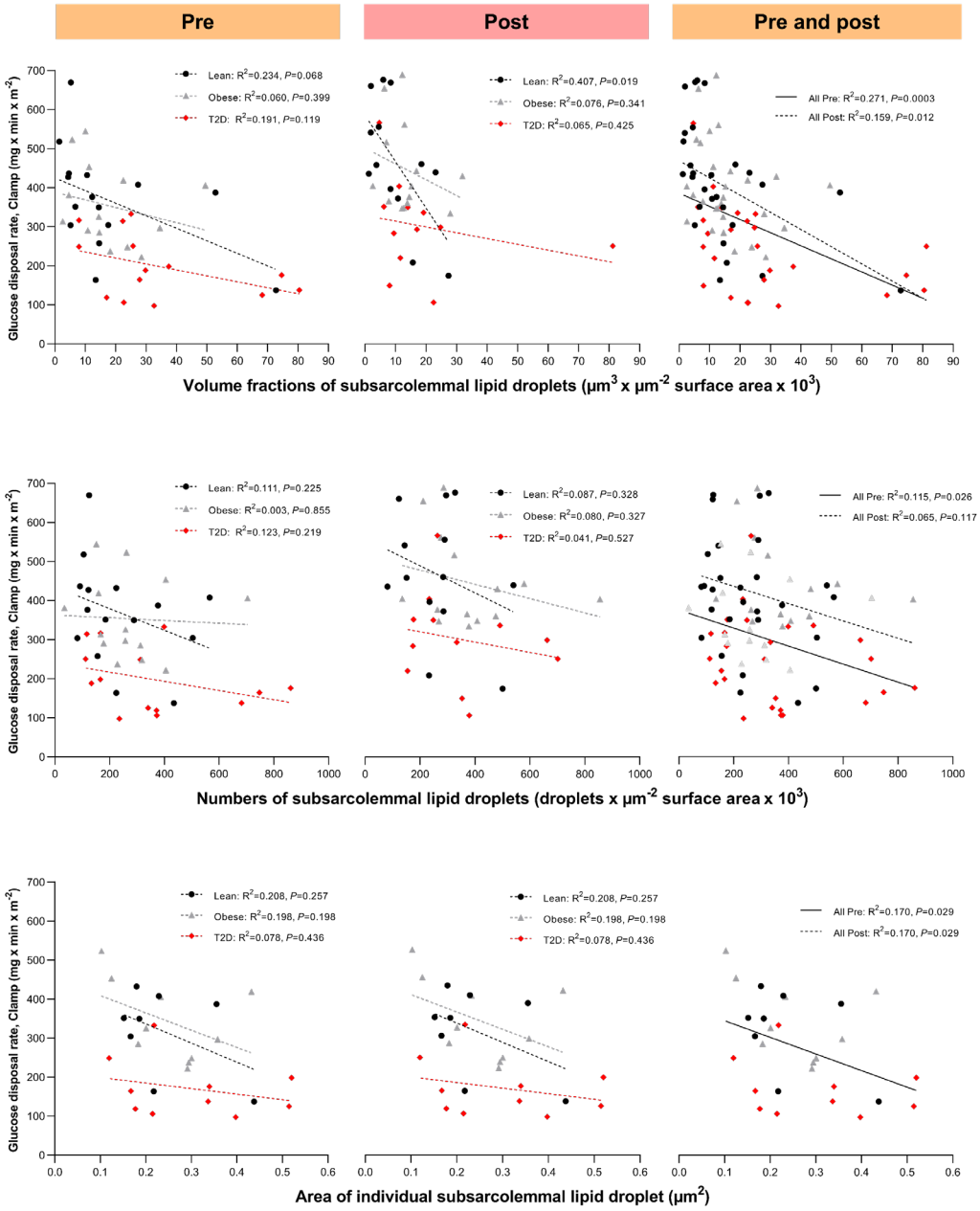

Supplemental Fig. 3. Effects of HIIT on morphological characteristics of lipid droplets discriminated between fiber types

Multiple size and shape descriptors were determined by manually tracing the surface of individual subsarcolemmal (SS) and intermyofibrillar (IMF) lipid droplets in an interpolated polygon. Graphical explanations are displayed for each variable. P:V ratio, perimeter-to-volume ratio (same as P:A ratio). Data are presented as medians with interquartile range. Lean: n=7–14; Obese: n=10–14; T2D: n=8–14. Simple linear mixed-effects model: $P<0.05$; **<0.01; ****<0.0001.

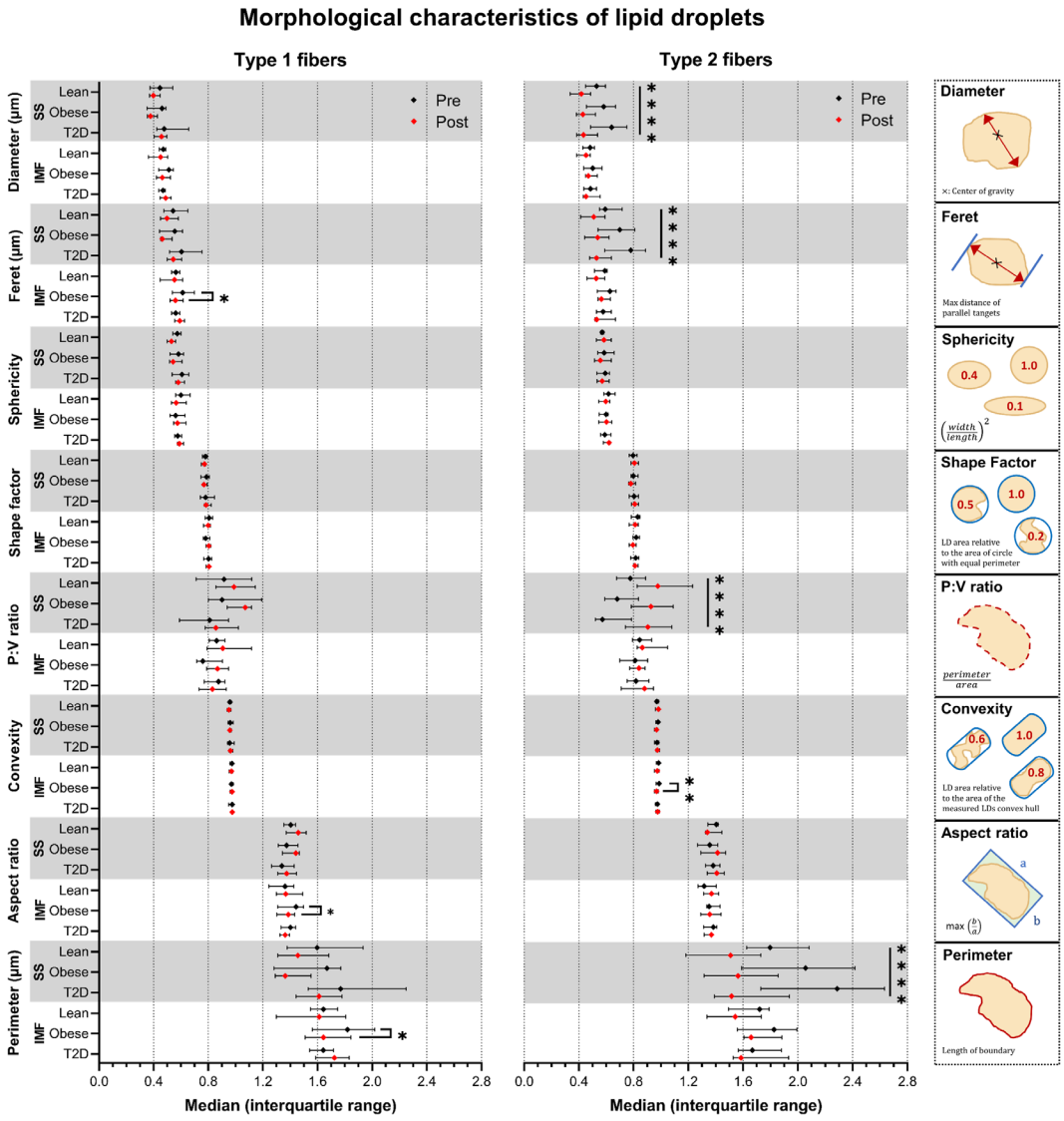

Supplemental Fig. 4. Relative distributions (%) of lipid droplets Pre and Post the acute exercise

Donut charts representing the relative distributions (%) of subsarcolemmal (SS) and intermyofibrillar (IMF) lipid droplets to total volume fractions in skeletal muscle fibers Pre and Post the acute exercise. Lean: n=8; Obese: n=8; T2D: n=9. Simple linear mixed-effects model.

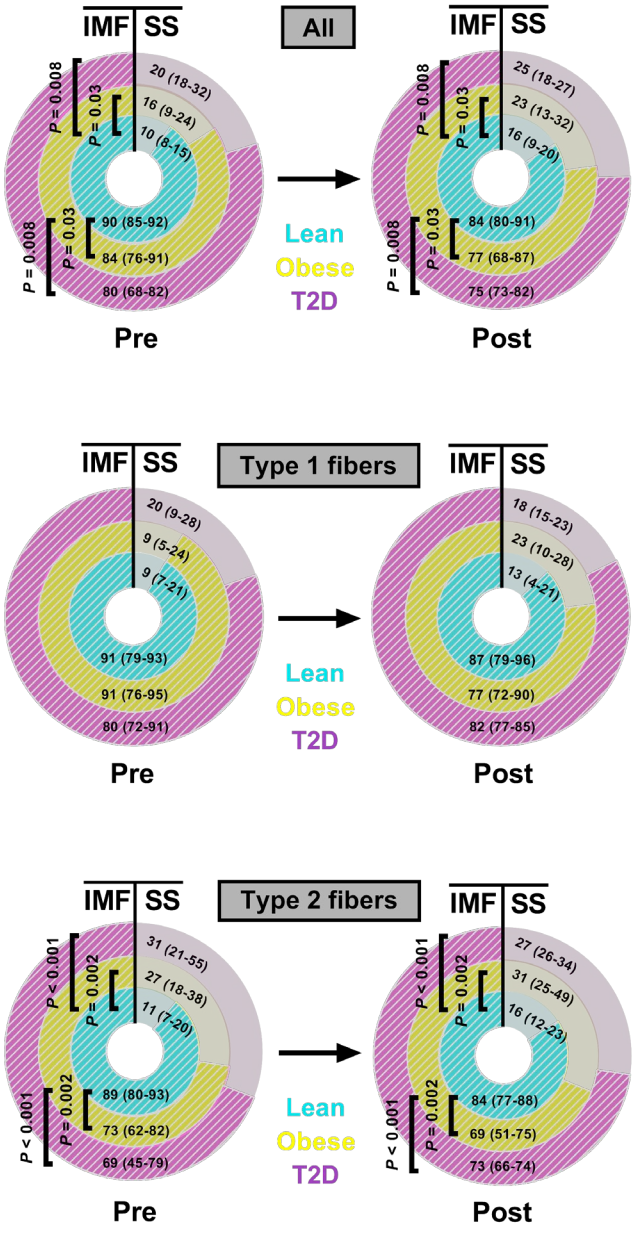

Supplemental Fig. 5. Correlation analysis between exercise-mediated changes (Δ) in subcellular lipid droplet volume fractions and fat oxidation (g/min)

Correlation analyses were performed across the subsarcolemmal (***A***) and intermyofibrillar (***B***) region in the Lean (green circles), Obese (red triangles) and T2D (blue diamonds). Lean: n=8; Obese: n=8; T2D: n=9.

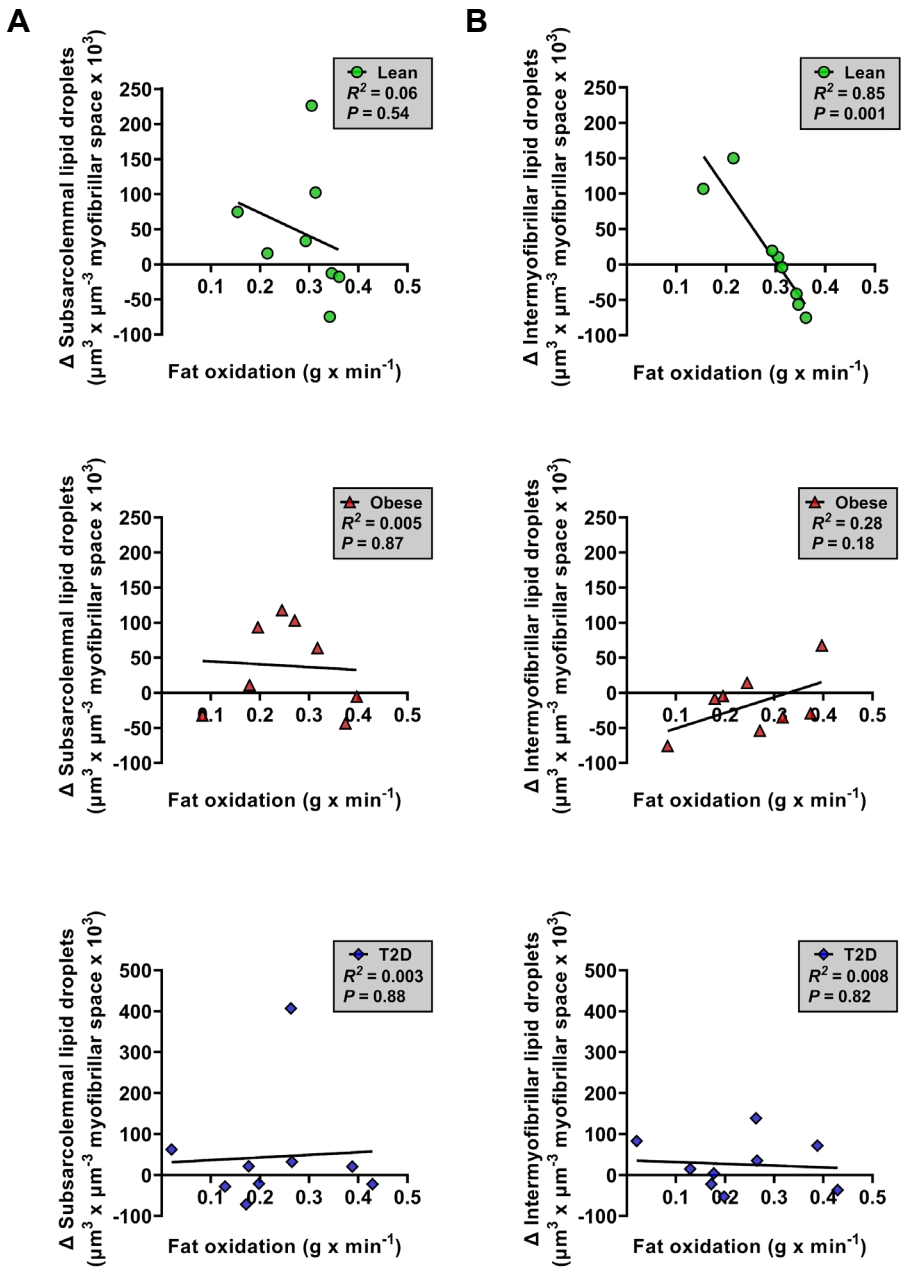

Supplemental Fig. 6. Effects of acute exercise on morphological characteristics of lipid droplets discriminated between fiber types

Multiple size and shape descriptors were examined by manually tracing the surface of individual subsarcolemmal (SS) and intermyofibrillar (IMF) lipid droplets in an interpolated polygon. P:A ratio: perimeter-to-area ratio. Data are presented as medians with IQR. Lean: n=4–8; Obese: n=5–8; T2D: n=7–9. Simple linear mixed-effects model.

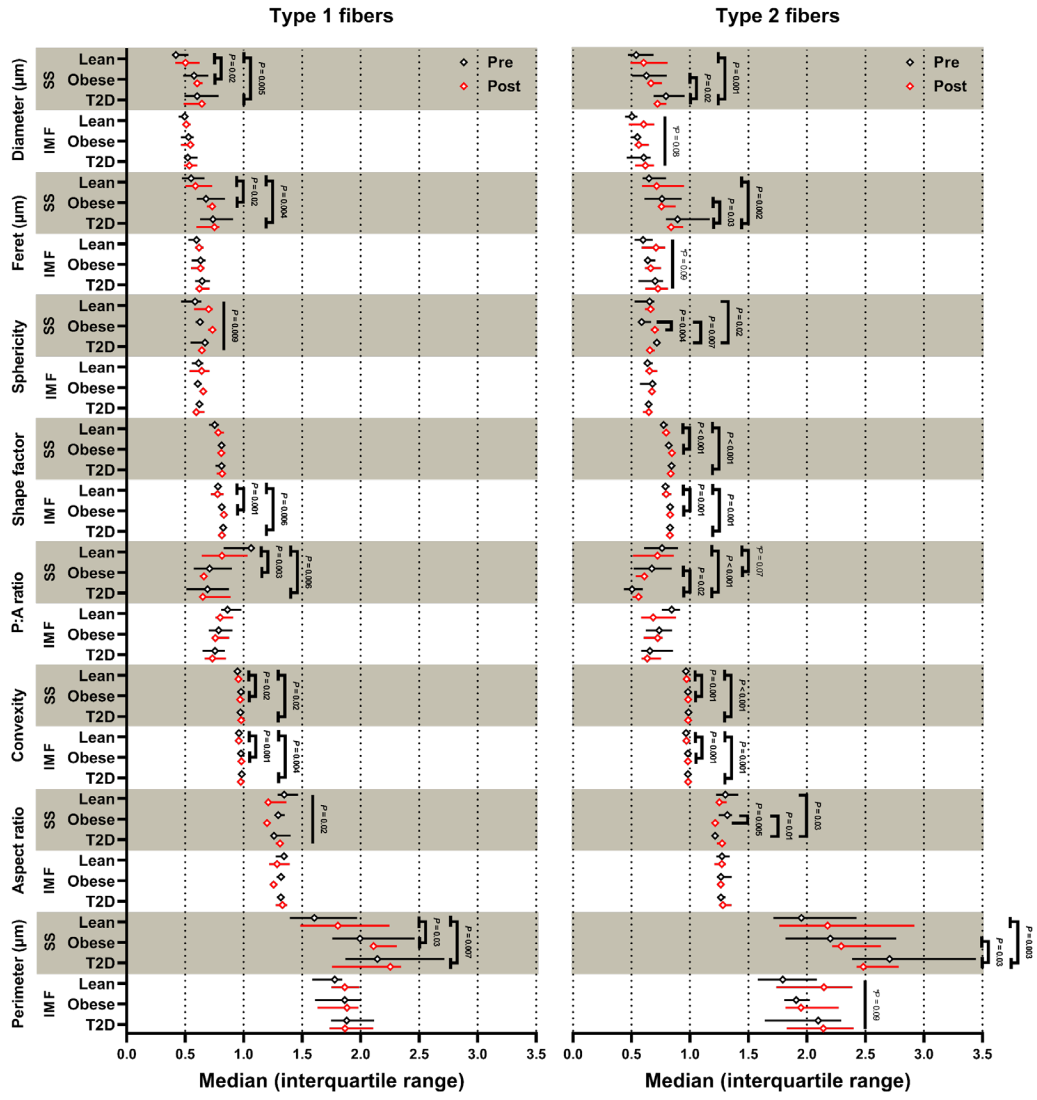

Supplemental Table 1. Physical activity level at baseline and adherence to HIIT

	Lean	Obese	T2D
n	16	15	13
Adherence – week 1-8			
HIIT sessions completed (%)	97±1	98±1	95±1
IPAQ-SF baseline (time spent, h/week)			
Vigorous physical activity	0.5±0.2	0.4±0.2	0.2±0.1
Moderate physical activity	1.4±0.3	1.1±0.3	0.6±0.4
Walking	2.1±0.4	3.7±1.8	6.9±1.9†
Sitting	45.3±5.7	56.9±5.5	50.4±7.7
MET-minutes per week	986±143	1162±377	1598±370

Data are means±SEM. $^{\dagger}p<0.05$ vs. lean. T2D, type 2 diabetes; IPAQ-SF, International Physical Activity Questionnaire Short Form.

Supplemental Table 2. Exercise duration, intensity, workload, and energy expenditure during HIIT

	Lean	Obese	T2D
n	16	15	13
Total duration per session (min)			
Week 1-2	32	32	32
Week 3-4	45	45	45
Week 5-6	58	58	58
Week 7-8	71	71	71
Training intensity (%HR max)			
Week 1-4: Peak intensity (peak %HRmax)	96±0	96±0	96±0
Week 5-8: Peak intensity (peak %HRmax)	95±1	95±0*	93±1**†‡
Week 1-8: Peak intensity (peak %HRmax)	96±0	96±0	95±1
Week 1-4: HIIT sessions incl. breaks	80±1	82±1	82±1
Week 5-8: HIIT sessions incl. breaks	79±1**	80±1*	80±1**
Week 1-8: HIIT sessions incl. breaks	80±1	81±1	81±1
Week 1-4: Cycling intervals	89±1	88±1	88±1
Week 5-8: Cycling intervals	88±1	87±1*	85±1**†
Week 1-8: Cycling intervals	88±1	87±1	87±1
Week 1-4: Rowing intervals	88±1	88±1	87±1
Week 5-8: Rowing intervals	87±1*	87±1	85±1*
Week 1-8: Rowing intervals	88±1	87±1	86±1
Maximal cycling capacity (%)			
Week 1-4	104±2	111±3†	112±2†
Week 5-8	100±2*	106±2*†	105±3*
Week 1-8	102±2	109±2†	108±2†
Workload (watt)			
Week 1-4: Cycling intervals	278±11	290±12	244±11†‡
Week 5-8: Cycling intervals	286±11*	297±11	252±11*†‡
Week 1-8: Cycling intervals	282±11	294±12	248±11†‡
Week 1-4: Rowing intervals	214±11	221±11	168±8†‡
Week 5-8: Rowing intervals	229±11**	244±13**	185±9**†‡
Week 1-8: Rowing intervals	221±11	230±12	176±8†‡
Energy expenditure (kJ)			
Week 1-4: Total during training intervals	919±38	953±40	766±32‡
Week 5-8: Total during training intervals	1729±71**	1759±91**	1463±65**†‡
Week 1-8: Total during training intervals	1311±54	1365±56	1100±46†‡
Week 1-4: During cycling intervals	473±18	494±20	416±18
Week 4-8: During cycling intervals	873±32**	909±34**	770±33**†‡
Week 1-8: During cycling intervals	669±25	698±103	589±25†‡
Week 1-4: During rowing intervals	446±22	459±23	350±16†‡
Week 5-8: During rowing intervals	855±42**	910±47**	693±35**†‡‡
Week 1-8: During rowing intervals	642±32	667±33	512±24†‡

Data are means±SEM. *p<0.05 and **p<0.001 week 5-8 vs. week 1-4, †p<0.05 and ††p<0.001 vs. lean. ‡p<0.05 and ‡‡p<0.001 vs. obese. T2D, type 2 diabetes; HRmax, heart rate max.

Supplemental Table 3. Morphological characteristics of lipid droplets at baseline

	Lean	Obese	T2D	Lean		Obese		T2D	
	All			Type 1	Type 2	Type 1	Type 2	Type 1	Type 2
Area (μm²)									
SS	0.19 (0.16-0.27)	0.23 (0.17-0.28)	0.32 (0.20-0.47) **a,b**	0.18 (0.12-0.26)	0.24 (0.21-0.29) ‡‡	0.19 (0.11-0.22)	0.30 (0.21-0.39) ‡‡	0.22 (0.16-0.39)	0.40 (0.23-0.50) ‡‡
IMF	0.19 (0.19-0.21)	0.23 (0.15-0.29)	0.21 (0.17-0.23)	0.20 (0.17-0.21)	0.23 (0.15-0.28)	0.24 (0.19-0.28)	0.23 (0.18-0.27)	0.19 (0.17-0.21)	0.20 (0.18-0.25)
Diameter (μm)									
SS	0.47 (0.42-0.54)	0.51 (0.44-0.54)	0.57 (0.46-0.72) **a,b**	0.45 (0.38-0.53)	0.53 (0.48-0.58) ‡‡	0.46 (0.36-0.48)	0.58 (0.47-0.65) ‡‡	0.48 (0.42-0.65)	0.64 (0.50-0.74) ‡‡
IMF	0.47 (0.45-0.49)	0.51 (0.42-0.54)	0.48 (0.42-0.50)	0.47 (0.45-0.49)	0.48 (0.44-0.51)	0.51 (0.46-0.54)	0.50 (0.44-0.55)	0.47 (0.45-0.48)	0.48 (0.45-0.53)
Feret (μm)									
SS	0.57 (0.53-0.64)	0.61 (0.54-0.67)	0.71 (0.58-0.84) **a,b**	0.48 (0.42-0.57)	0.55 (0.51-0.61) ‡‡	0.50 (0.39-0.52)	0.62 (0.49-0.70) ‡‡	0.53 (0.46-0.68)	0.69 (0.54-0.79) ‡‡
IMF	0.57 (0.54-0.58)	0.62 (0.52-0.66)	0.57 (0.53-0.60)	0.50 (0.48-0.52)	0.52 (0.46-0.54)	0.55 (0.49-0.60)	0.55 (0.47-0.58)	0.50 (0.47-0.52)	0.51 (0.48-0.56)
Sphericity									
SS	0.57 (0.56-0.60)	0.58 (0.53-0.61)	0.59 (0.57-0.61)	0.57 (0.54-0.60)	0.57 (0.57-0.58)	0.58 (0.52-0.59)	0.59 (0.55-0.66)	0.61 (0.54-0.65)	0.59 (0.54-0.62)
IMF	0.59 (0.57-0.65)	0.57 (0.53-0.60)	0.58 (0.56-0.62)	0.60 (0.56-0.66)	0.62 (0.58-0.66)	0.56 (0.52-0.61)	0.60 (0.55-0.61)	0.58 (0.55-0.60)	0.59 (0.56-0.62)
Shape factor									
SS	0.78 (0.77-0.80)	0.79 (0.77-0.81)	0.80 (0.76-0.83)	0.78 (0.76-0.79)	0.80 (0.77-0.82)	0.79 (0.75-0.80)	0.80 (0.79-0.83)	0.78 (0.74-0.85)	0.80 (0.77-0.83)
IMF	0.80 (0.79-0.83)	0.80 (0.77-0.81)	0.81 (0.77-0.83)	0.81 (0.79-0.83)	0.83 (0.79-0.84) ‡	0.78 (0.76-0.81)	0.82 (0.81-0.84) ‡	0.80 (0.77-0.82)	0.82 (0.78-0.84) ‡
P:V ratio									
SS	0.86 (0.71-0.94)	0.78 (0.69-0.90)	0.65 (0.54-0.88) **b**	0.92 (0.74-1.12)	0.78 (0.70-0.82) ‡‡	0.90 (0.80-1.15)	0.68 (0.60-0.77) ‡‡	0.81 (0.59-0.94)	0.57 (0.52-0.77) ‡‡
IMF	0.85 (0.84-0.88)	0.79 (0.70-0.97)	0.81 (0.78-0.93)	0.86 (0.82-0.92)	0.84 (0.79-0.92)	0.76 (0.72-0.87)	0.81 (0.72-0.88)	0.88 (0.77-0.91)	0.82 (0.77-0.90)
Convexity									
SS	0.96 (0.96-0.97)	0.96 (0.96-0.98)	0.97 (0.95-0.98)	0.96 (0.95-0.97)	0.97 (0.96-0.98) †	0.96 (0.96-0.98)	0.98 (0.96-0.98) †	0.96 (0.94-0.99)	0.97 (0.95-0.98) †
IMF	0.97 (0.96-0.98)	0.98 (0.96-0.98)	0.98 (0.96-0.98)	0.97 (0.96-0.98)	0.98 (0.97-0.99) ††	0.97 (0.96-0.98)	0.99 (0.97-0.99) ††	0.98 (0.95-0.98)	0.97 (0.96-0.98) ††
Aspect ratio									
SS	1.40 (1.35-1.43)	1.37 (1.33-1.44)	1.36 (1.32-1.41)	1.40 (1.36-1.43)	1.40 (1.35-1.42)	1.37 (1.34-1.44)	1.36 (1.27-1.39)	1.34 (1.27-1.43)	1.38 (1.34-1.43)
IMF	1.34 (1.27-1.41)	1.41 (1.34-1.48) **a**	1.39 (1.32-1.41)	1.36 (1.24-1.41)	1.32 (1.28-1.40)	1.44 (1.34-1.49)	1.35 (1.35-1.41)	1.40 (1.34-1.44)	1.38 (1.32-1.40)
Perimeter (μm)									
SS	1.67 (1.54-1.90)	1.81 (1.56-1.97)	2.08 (1.70-2.47) **a,b**	1.6 (1.38-1.88)	1.80 (1.69-2.03) ‡‡	1.67 (1.30-1.76)	2.06 (1.63-2.38) ‡‡	1.77 (1.53-2.23)	2.29 (1.78-2.61) ‡‡
IMF	1.67 (1.60-1.74)	1.82 (1.51-1.96)	1.67 (1.52-1.75)	1.64 (1.58-1.73)	1.72 (1.53-1.79)	1.82 (1.62-2.01)	1.83 (1.57-1.91)	1.64 (1.55-1.72)	1.67 (1.60-1.82)

Data are medians (IQR). SS, Subsarcolemmal; IMF, Intermyofibrillar; P:V, Perimeter-to-volume. Lean: n=7–14; Obese: n=10–14; T2D: n=8–14. Simple linear mixed-effects model: *P*: **a**<0.05 vs. Lean. *P*: **b**<0.05 vs. Obese. *P*: †<0.05; ††<0.01; ‡<0.001; ‡‡<0.0001 vs. Type 1 fibers.

Appendix II

Papers I–III

sdu.dk/grafiskcenter

februar 2023

SDU
Syddansk Universitet

University of Southern Denmark
Campusvej 55
DK-5230 Odense

Phone: +45 6550 1000
sdu@sdu.dk
www.sdu.dk